UNIVERSITY OF CALIFORNIA
RIVERSIDE

Impact of Targeted Nanomaterials for Chloroplast Bioengineering on *Arabidopsis thaliana*

A Dissertation submitted in partial satisfaction
of the requirements for the degree of

Doctor of Philosophy

in

Botany and Plant Sciences

by

Israel Santana

March 2022

Dissertation Committee:
Dr. Juan Pablo Giraldo, Chairperson
Dr. Linda Walling
Dr. Robert Jinkerson

The Dissertation of Israel Santana is approved by:

Committee chairperson

University of California, Riverside

Acknowledgments

The text of this dissertation in full, is a reprint of the material as it appears in Wu, H., Santana, I., Dansie, J. & Giraldo, J. P. *In Vivo* Delivery of Nanoparticles into Plant Leaves. *Curr. Protoc. Chem. Biol.* 9, 269–284 (2017). This work was supported by the University of California, Riverside and USDA National Institute of Food and Agriculture, Hatch project 1009710. We thank Dr. Jinming Li for his technical help in TGA-QD synthesis.

The text of this dissertation in full, is a reprint of the material as it appears in Santana, I., Wu, H., Hu, P. & Giraldo, J. P. Targeted delivery of nanomaterials with chemical cargoes in plants enabled by a biorecognition motif. *Nat. Commun.* 11, 2045 (2020). In Chapter 2: We thank Jason White and Craig Musante from the Connecticut Agricultural Research Station for providing ICP-MS measurements. Ms. Gail Garcia assisted in biocompatibility assays of nanoparticles in plants. This material is based upon work supported by the National Science Foundation under Grant No. 1817363 to Juan Pablo Giraldo.

Juan Pablo Giraldo, Israel Santana, Hong Hong Wu, and Peiguang Hu conceived and designed the experiments. Israel Santana performed nanoparticle synthesis and *in vivo* experiments. Hong Hong Wu and Peiguang Hu contributed to nano-material characterization and isothermal titration calorimetry analysis. Israel Santana, Hong Hong Wu, and Peiguang Hu, and Juan Pablo Giraldo, analyzed datasets and performed the statistical analysis. All authors contributed to writing the manuscript.

The text of this dissertation in full, is a reprint of the material as it appears in Santana, I. *et al.* Peptide-mediated Targeting of Nanoparticles with Chemical Cargoes to Chloroplasts in *Arabidopsis* Plants. *Bio Protoc* 11, e4060 (2021).

This material is based upon work supported by the National Science Foundation under Grant No. 1817363 to Juan Pablo Giraldo. The National Science Foundation supported students Chris Castillo, Hann Tu, and Peiguang Hu under the Center for Sustainable Nanotechnology, CHE-1503408. The CSN is part of the Centers for Chemical Innovation Program.

The co-authors listed in these publications directed and supervised the research, which forms the basis for this dissertation.

Dedications

As a young child, my dad would tell me stories about working as a farmhand in Romita Guanajuato, a rural farm town, and native lands to the Chichimeca indigenous peoples of central Mexico. He enjoyed talking about the techniques they used in the past to increase yields. My mother has continued practicing her knowledge of ethnobotany, plant-derived medicines, and alternative cures passed down from her ancestors. Plants are involved in every aspect of my life and my ancestors.

My family provided me with a strong support system and a strong work ethic that helped me navigate social-economic issues. Never did I dream that the kid from South Central Los Angeles would be discovering and pushing boundaries in an interdisciplinary field that has the potential to revolutionize agriculture. A special thanks to my brother and sister for their support and love.

I have crossed paths with friends, loved ones, mentors, and professors who have supported me throughout my academic journey and sparked my love for science and answers to the unknown. I am grateful for those who have supported me throughout my life. As I enter the next stage in my career, I am determined to help others by sharing my knowledge and passion for fostering a new generation of scientists from diverse backgrounds.

This dissertation is dedicated to my parents Jose Guadalupe Santana and Virginia Torres Santana. My parents were my first teachers. Their love and support gave me the strength to continue regardless of the circumstances. Thanks to my committee Linda Walling and Robert Jinkerson, for their guidance and support in developing my research

work. Special thanks to Professor Juan Pablo Giraldo for guiding my development in becoming a better scientist and innovator. I joined Dr. Juan Pablo Giraldo's lab because his personality and research ideas stood out across the department and continued to inspire my love for science and plant biology. I knew his plant nano-bionics would present a cutting-edge project at the forefront of future technology in agriculture. I am grateful for his guidance and mentorship in my journey through the Ph.D. and for allowing me to be a part of his lab. I also want to thank the undergraduate mentees Gail Garcia, and Rashi Abashta, who I had the opportunity to work alongside and who aided me in completing experiments and developing methods for this research. They have begun their biotechnology careers due to this research, and I wish them the best. Lastly, thank you to Ariana Firebaugh Ornelas for being there for me. I appreciate you believing in me when I did not and showing me how to love unconditionally.

From the bottom of my heart, thank you all for believing in me and providing me with tools, strength, and knowledge to take on new challenges and grow as a scientist from the bottom of my heart.

ABSTRACT OF THE DISSERTATION

Impact of Targeted Nanomaterials for Chloroplast Bioengineering
on *Arabidopsis thaliana*

by

Israel Santana

Doctor of Philosophy, Graduate Program in Botany and Plant Science
University of California, Riverside, March 2022
Dr. Juan Pablo Giraldo, Chairperson

Plant nanobiotechnology is an emerging field utilizing nanomaterials to study and engineer plant biological functions. The use of nanotechnology on plants can improve the efficacy of plant bioengineering and agriculture tools to improve future food securities. There is immense potential for applying nanomaterials-based tools' physical and chemical properties to chloroplast biotechnology. The chloroplast prokaryotic-like genome makes them excellent targets for genetic engineering application due to their polycistronic gene structure, lack of silencing mechanisms, and ability to isolate genetic markers in parental lines. Current chloroplast transformation techniques are limited to a handful of plant species (<10) due partly to the absence of efficient gene delivery mechanisms to chloroplasts. If appropriately engineered, nanomaterials can overcome plant cell barriers such as walls and internal organelle compartments, making them ideal systems for chemical and gene delivery tools in plant model systems.

In this dissertation, standardized methods to interface nanomaterials into plant tissues in Chapter one. Chapter two designed nanomaterials to localize inside chloroplasts

using biorecognition motifs and deliver biochemicals to modulate chloroplast function in *Arabidopsis thaliana*. Chapter three utilized the targeted strategies implemented in Chapter two to construct two carbon-based nanomaterials (Carbon dots and single-walled carbon nanotubes) complexes for chemical and gene delivery into chloroplasts.

In Chapter Three, we investigated the biological impact of nanomaterials on *Arabidopsis* plants using targeted nanomaterials. We found increased localization and confirmed increased chemical and gene delivery into chloroplasts using cell- and molecular-based assays. Furthermore, no significant difference in cell or chloroplast integrity demonstrated low cell damage. However, the targeted nanomaterials affected the levels of oxidative DNA damage in whole plant cell extracts and increased hydrogen peroxide (H_2O_2) levels at 24 hr of exposure. Photosynthetic measurements showed no significant difference in Fv/Fm dark-adapted photosystem II efficiencies. A decrease in chlorophyll content and photosynthesis in the carboxylation limited region were observed.

Together we demonstrated targeted nanomaterials for chemical and genetic material delivery into the chloroplast. With this information, we can improve the development of biocompatible nanomaterials for a broad range of applications, from improving the understanding of plant biology, enhancing crop yields to transforming plants into technology.

Table of Contents

List of Figures

Supplemental figure list: Chapter 3

Supplemental figure list Chapter 4:

List of Tables

Introduction

Plant Nanotechnology

Nanotechnology is a burgeoning field of science that uses various engineered nanomaterials (ENMs) designed explicitly with unique physical and chemical properties that can be tuned to adjust their attributes such as size, charge, and surface chemistries. ENMs have at least one dimension in the nanometer range (<100 nm). Nanomaterials can be functionalized to have high surface charge and modular surface chemistry, allowing conjugation of biomolecules (Wang et al. 2016; Wang et al. 2013; Tripathi et al. 2017; Sun and Gang 2013).

Nanomaterials used to study biological systems are formed from various starting materials, including metals, metal alloys, polymers, lipids, and carbon-based precursors (Wang et al. 2016). Among the most biocompatible and sustainable are carbon-based ENMs (Hu et al. 2020; Shi Kam et al. 2004; Li et al. 2020; Yang et al. 2009). Some ENMs, such as carbon dots, can exhibit tunable fluorescence that can be monitored with fluorescence microscopy (Vandarkuzhali et al. 2017; Sun et al. 2017; Wang and Chen 2011; Wu et al. 2017; Newkirk et al. 2018). Furthermore, ENMs have been used to act as sensors and probes enabling quantifiable detection of biomolecules and plant metabolites (Wang et al. 2007; Han et al. 2019; Gao et al. 2014; Li et al. 2018; Unnikrishnan et al. 2020; Yang et al. 2009; Newkirk et al. 2018). ENMs have been applied to various biological systems, including bacteria, yeast, algae, mice, human tissues, and more recently, plants (Stark 2011; Monica and Cremonini 2009). Recent studies in plants have demonstrated that ENMs can function as catalytic ROS scavengers, sensors to research

plant salt stress tolerance mechanisms, detect photosynthetic products such as carbohydrates *in vivo*, and improve photosynthetic quantum yield by augmenting the light capturing ability of chloroplasts (Giraldo et al. 2014; Wu et al. 2018; Li et al. 2018; Wu et al. 2017; Giraldo et al. 2019). Developing nanomaterials with different chemical properties such as size charge and surface functionalized ligands (i.e., oligonucleotides, proteins, and chemicals) can lead to novel tools to study plant biology acting as chemical delivery platforms, gene delivery platforms, and developing nanomaterial-based sensors detecting changes in nutrient accumulation and stress.

As demands for food production increase, the need to improve traditional agricultural breeding, genetic engineering, and land management strategies will be pivotal to meet the need for future food security. It is projected that sustainable food production will require radical improvements in fertilizer and nutrient use efficiency, improved breeding, and genetic engineering practices to intensify food production with high-quality outputs (Mba et al. 2012; Baker et al. 2017; Gogotsi 2018). The ability for crop plants to relay their nutritional, water, and stress status to farmers and the use of novel bioengineering nanomaterial platforms onto crops imparts the concept of "smart" agriculture (Figure 1.1). Recent breakthroughs in "smart agriculture" nanotechnology have provided genetic engineering platforms, agrochemical delivery, and nano-sensors, enabling farmers and plant breeders to improve crop yields and land management (Figure 1.1) (Giraldo et al. 2014; Wu et al. 2018; Li et al. 2018; Wu et al. 2017; Giraldo et al. 2019; Hofmann et al. 2020). If applied to scale, nanomaterials on crops could become a primary vessel of environmental hazard (Tripathi et al. 2017; Servin and White 2016).

Thus, this dissertation highlights methods and strategies to interface nanomaterials within plant tissues, engineer nanomaterials to enable targeted chemical delivery into plant cell chloroplasts and investigate the impact that targeted nanomaterials have on the plant cell, molecular and photosynthetic physiology on *Arabidopsis thaliana*.

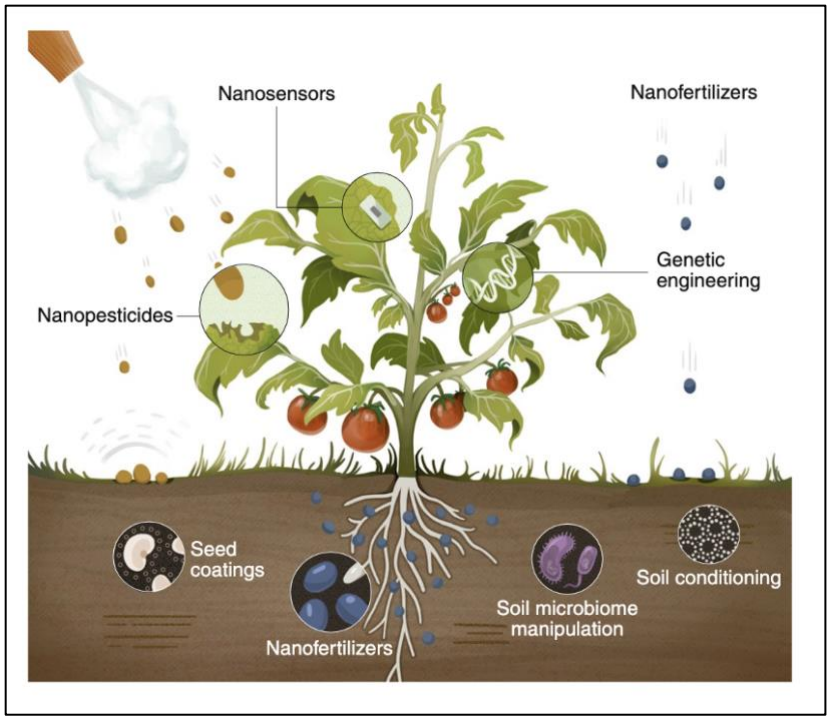

Figure 1.1. Application of plant nanotechnology tools to improve agricure. Excerpt Figure image from (Hofmann et al., 2020) illustrating the potential application of nanotechnology in plant agriculture. Application including genetic engineering platforms, agrochemical delivery, and nano-sensors.

Thesis overview

There is an increase in attention towards developing nanotechnology-based tools to improve sustainable agricultural practices and maintain food securities (Lowry et al. 2019; Clarke and Daniell 2011). One strategy is to bioengineer the photosynthetic machinery inside the chloroplasts through chemical or genetic engineering methods (Kwak et al. 2019; Newkirk et al. 2021). Plant chloroplasts are excellent targets for bioengineering applications due to their function as metabolic hubs. Chloroplasts increased metabolic activity, such as protein production, photosynthetic reactions, and lipid products, to name a few are key processes that can enable improved crop yields (Clarke and Daniell 2011; Siddiqui et al. 2020; Newkirk et al. 2021). However, their

increased metabolic activity produces reactive oxygen species (ROS). These molecules play a dual role in plants acting as a signaling molecules for downstream developmental processes, stress responses and as a harmful chemical agent damaging internal biomolecules and systems (Møller and Sweetlove 2010; Asada 2006). Developing strategies to interface nanomaterials with plants safely and creating tools that can effectively engineer chloroplast function is crucial for improving crop yields and enabling more innovative genetic tools to improve our understanding of plant biology.

My aims and objectives for my Dissertation are to:

1. Develop methods to deliver and image nanomaterials inside plant tissues of *Arabidopsis thaliana*
2. Develop nanomaterials that can localize inside chloroplast in *Arabidopsis thaliana*
3. Bioengineer chloroplasts through the delivery of chemical and genetic materials using carbon-based nanomaterial platforms
4. Assess the molecular, cell, and physiological impact of plants treated with chloroplast-targeted nanomaterials.

The work discussed here will address methods to interface nanomaterials with plants. We also address significant bottlenecks in plant chemical delivery by developing nanomaterials targeted to the chloroplast using transit peptides destined to the chloroplast for chloroplast bioengineering applications. Lastly, we assess target nanomaterials' structures impact on cellular, molecular, and physiology in *Arabidopsis thaliana*.

Ultimately, these aims are critical first steps towards using nanomaterials to study and bioengineer plant chloroplast functions to aid in meeting future food security demands.

Interfacing Nanomaterial in Plants

The second chapter is a detailed protocol on interfacing nanomaterials such as fluorescent quantum dots (QD) into *Arabidopsis thaliana* plant tissues.

The delivery of ENMs such as QDs to plant tissues is a crucial step towards investigating plant nanomaterial interactions and understanding the impact on plant function. In my first objective, three methods were used for delivering QDs into leaves: leaf lamina infiltration, whole shoot vacuum infiltration, and root to leaf translocation (Figure 1.2).

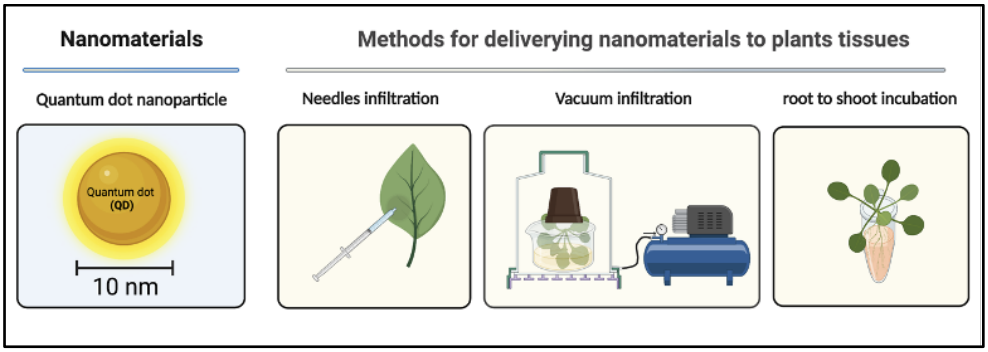

Figure 1.2. Illustration of quantum dot nanoparticles used for *in vivo* tracking inside plant leaf tissues. Methods for delivering quantum dot nanoparticles into leaf tissues in *Arabidopsis thaliana* include needless syringe infiltration, vacuum infiltration, and root to shoot incubation.

The ENMs we synthesized are quantum dot (QD) nanoparticles with a specific size and charge that allows uptake and translocation into various plant tissues (Hu et al. 2020). The fluorescent QDs can be detected using confocal microscopy. The QDs are

nanomaterials made of a cadmium and tellurium metal alloy and can be easily synthesized with basic chemistry lab equipment in our lab (Marmiroli et al. 2020; Wang et al. 2007). Although QDs can be highly toxic, we rationalized using these nanomaterials for fundamental research purposes. Previous studies report ENMs with a high negative charge exhibit improved cellular uptake (Kuhn et al. 2014; Wang et al. 2014; Hu et al. 2020; Rigal et al. 2015; Chithrani et al. 2006). Thus, the QD surface was functionalized with a negatively charged ligand that protects the core of the QD from degradation and improves solubility and biocompatibility (Zhang et al. 2003; Schulz et al. 2016). The maximum cell wall porosity reported is approximately < 20 nm, limiting larger ENMs uptake into plant cells (Carpita et al. 1979; Carpita and Gibeaut 1993; Darvill et al. 2010). Thus, we synthesized the QD with a lower hydrodynamic diameter than the reported cell wall porosity and allowed highly charged particles to pass through the plant cell barriers. This work was published in the Current Protocols in Chemical Biology (Wu et al. 2017).

Targeted Nanomaterials for Chemical Delivery Chloroplast Bioengineering

Chapter three details the synthesis of a nanoparticle able to localize inside chloroplast for targeted chemical delivery and bioengineering of plastid redox chemistry motivated by the increasing need for food security. The tools and nanomaterials were built around the methods and strategies in objective one to develop targeted and controllable chemical delivery platforms to chloroplasts in *Arabidopsis thaliana*. We demonstrated that highly charged nanomaterials with chloroplast targeting peptide

biorecognition motifs attached to their surface could improve localization within the chloroplast of *Arabidopsis thaliana* plants. Furthermore, we showed proof of concept that nanomaterials can carry chemical cargoes using a molecular basket attached to the surface of the nanomaterial (Santana et al. 2020; Santana et al. 2021). The delivered chemical cargoes enabled precise changes in redox status in chloroplasts *in vivo* (Figure 1.3).

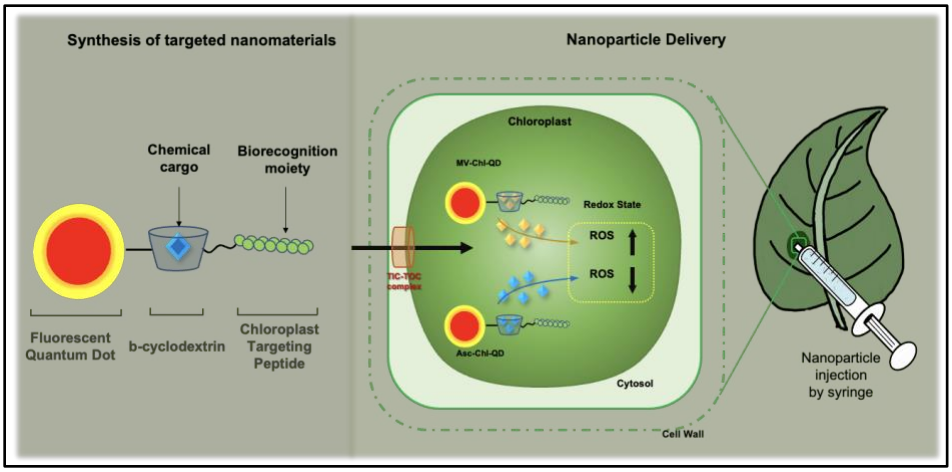

Figure 1.3. Application of targeted nanomaterials for chemical chloroplast bioengineering. Illustration of the designed targeting quantum dot complex containing a fluorescent QD core, attached to its surface a molecular basket that can hold chemical cargoes in its cavity and a chloroplast targeting peptide on its surface. The design can deliver chemicals to the chloroplasts and precisely modulate the chloroplast redox status.

In chapter 3 we highlight strategies to design and synthesize novel ENM platforms that bypass biological barriers in plants. To our knowledge, this is the novel application for in-vivo traceable and targeted delivery of biochemicals to chloroplasts using guiding peptide recognition motifs. The research in this chapter culminated in articles published in *Nature Communications* and a methods paper in *Bio Protocols* (Santana et al. 2020; Santana et al. 2021). Applying these tools can potentially improve

fertilizer use and nutrient use in crops. The strategies to synthesize the targeted nanomaterials with molecular baskets and targeting peptides can be applied to other nanomaterials with increased biocompatibility and biodegradable.

Impact of Targeted Nanomaterials on Plant Cell, Molecular Biology, and Physiology

Demands for food production are increasing, and plant breeding, genetic engineering, and agricultural land management strategies will not meet future food security needs. Sustainable food production will require radical improvements in the later methods to intensify food production with high-quality outputs (Lowry et al. 2019; Mba et al. 2012; Gogotsi 2018). One such strategy gaining momentum is using nanotechnology-based tools (Lowry et al. 2019; Hofmann et al. 2020; Wang et al. 2016). Recent breakthroughs in nanotechnology have provided various technologies that improve upon genetic engineering platforms, agrochemical delivery, and nano-sensors, enabling farmers and plant breeders to improve crop yields and land management (Wang et al. 2016; Giraldo et al. 2019; Newkirk et al. 2021; Hofmann et al. 2020; Lowry et al. 2019; Baker et al. 2017). If applied to scale, these nanotechnology-based crops will be the primary route of human exposure and could become a health and environmental risk (Wang et al. 2016; Baker et al. 2017; Servin and White 2016). Understanding the biological impact of nanomaterials on plants is critical towards engineering safer and more innovative strategies. This chapter provides biological measures and approaches towards developing safe and effective nanotechnology-based tools for smart agriculture in the future.

The fourth chapter utilized the knowledge and engineering design highlighted in Chapters two and three to develop carbon-based nanomaterial for targeted chemical and genetic materials delivery into plants. Furthermore, we developed measures to assess the cell, molecular biology, and physiological response to targeted nanomaterials in *Arabidopsis thaliana*. This chapter developed two nanomaterials for chloroplast-targeted chemical delivery (carbon dots, CDs) and gene delivery platforms for chloroplast genetic engineering (single-walled carbon nanotubes, SWCNT). The engineering of CD and SWCNT nanomaterials for smart agriculture applications are at the forefront of plant nanotechnology strategies to improve agriculture.

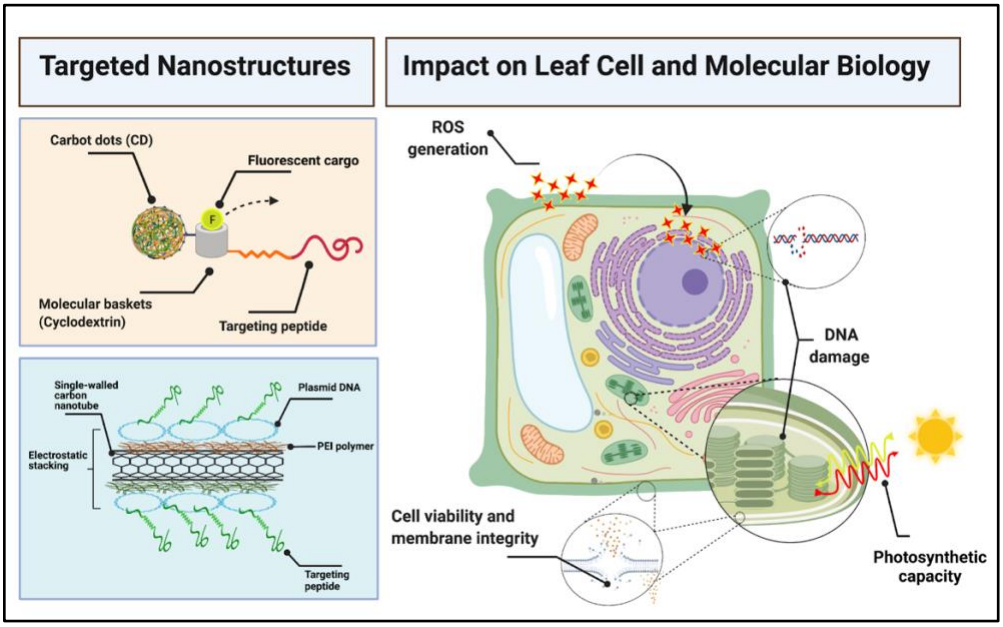

Figure 1.4. Diagram of targeted nanomaterials for chloroplast bioengineering and their impact on the cellular, molecular, and physiological impact on plant mesophyll cells. Diagram Created with BioRender.com.

This chapter shows proof-of-concept of improved chemical and plasmid delivery into chloroplast using targeted nanomaterials functionalized with targeting peptide motifs. Furthermore, we assessed the cell, molecular and photosynthetic carbon assimilation of *Arabidopsis thaliana* plants treated with the targeted nanomaterials described as follows:

1. To enable targeted chemical delivery into chloroplasts, a Carbon dot (CD) was functionalized with a molecular basket and a targeting peptide (TP-β-CD), enabling loading of a fluorescent chemical cargo (carboxy-fluorescein) (Figure 1.4).

2. To enable targeted gene delivery into chloroplasts, a single-walled carbon nanotube (SWCNT) was electrostatically grafted with a cationic polymer, followed by a GFP

plasmid (pATV1) driven by a plastid-specific promoter (TP-pATV1-SWCNT). Next, a fusion peptide containing biorecognition motifs for import into chloroplasts (Figure 1.4). We used confocal microscopy and RT-qPCR to show proof of concept for efficient chemical and molecular cargo delivery into the chloroplast. Next, we used cellular-based assays to determine the effect of the plant cell cellular membrane and chloroplast membrane integrity and DNA damage in whole plant cell DNA and isolated chloroplast DNA and absolute concentration of H_2O_2.

Lastly, we assessed the photosynthetic carbon assimilation rate using an infra-red gas analyzer. Furthermore, we measured the amount of oxidative damage to DNA using an ELISA assay measuring 8-hydroxydeoxyguanosine (8-OHdG) (Yin et al. 1995) and measured the concentration of H_2O_2 in leaf tissues. Lastly, we measured photosynthesis in plants treated with targeted nanomaterials by assessing chlorophyll content levels, a marker for plant stress (Jung 2004; Watanabe et al. 2013; Hörtensteiner and Kräutler 2011; Bieker et al. 2012). Furthermore, we measured the carbon assimilation rates and the maximum quantum yield of photosystem II systems (Fv/Fm) in dark-adapted leaves.

Conclusion

Sustainable food production will require radical improvements in fertilizer and nutrient use efficiency, improved breeding, and genetic engineering practices to intensify food production with high-quality outputs. One such strategy is using nanotechnology-based tools to enhance sustainable agriculture and maintain food security. Recent breakthroughs in nanotechnology (Santana et al. 2020; Li et al. 2018; Giraldo et al. 2019)

have provided various technologies that improve genetic engineering platforms, agrochemical delivery, and nano-sensors, enabling farmers and plant breeders to improve crop yields and land management. If applied to scale, these nanotechnology-based crops will be the primary route of human exposure and could become a health and environmental risk. This work aims to investigate the impact that targeted nanomaterials have on plant cell and chloroplast membrane intactness, hydrogen peroxide (H_2O_2) content in plant cells, and oxidative DNA damage. This work will provide biological measures and approaches towards developing safe and effective nanotechnology-based tools for smart agriculture in the future.

References:

Baker, S., Volova, T., Prudnikova, S. V., Satish, S., & Prasad M N, N. (2017). Nanoagroparticles Emerging Trends And Future Prospects In The Modern Agriculture System. *Environmental Toxicology And Pharmacology*. 53, 10–17.

Bieker, S., Riester, L., Stahl, M., Franzaring, J., & Zentgraf, U. (2012). Senescence-Specific Alteration Of Hydrogen Peroxide Levels In *Arabidopsis Thaliana* And Oilseed Rape Spring Variety *Brassica Napus L.* Cv. Mozart. *Journal Of Integrative Plant Biology*. 54(8), 540–554.

Giraldo, J. P., Wu, H., Newkirk, G. M., & Kruss, S. (2019). Nanobiotechnology Approaches For Engineering Smart Plant Sensors. *Nature Nanotechnology*. 14(6), 541–553.

Gogotsi, Y. (2018). Moving Ions Confined Between Graphene Sheets [Review Of Moving Ions Confined Between Graphene Sheets]. *Nature Nanotechnology*. 13(8), 625–627.

Hofmann, T., Lowry, G. V., Ghoshal, S., Tufenkji, N., Brambilla, D., Dutcher, J. R., Gilbertson, L. M., Giraldo, J. P., Kinsella, J. M., Landry, M. P., Lovell, W., Naccache, R., Paret, M., Pedersen, J. A., Unrine, J. M., White, J. C., & Wilkinson, K. J. (2020). Technology Readiness And Overcoming Barriers To Sustainably Implement Nanotechnology-Enabled Plant Agriculture. *Nature Food*. 1(7), 416–425.

Hörtensteiner, S., & Kräutler, B. (2011). Chlorophyll Breakdown In Higher Plants. *Biochimica Et Biophysica Acta*. 1807(8), 977–988.

Jung, S. (2004). Effect Of Chlorophyll Reduction In *Arabidopsis thaliana* By Methyl Jasmonate Or Norflurazon On Antioxidant Systems. *Plant Physiology And Biochemistry: Ppb / Société Française De Physiologie Vegetale.* 42(3), 225–231.

Li, J., Wu, H., Santana, I., Fahlgren, M., & Giraldo, J. P. (2018). Standoff Optical Glucose Sensing In Photosynthetic Organisms By A Quantum Dot Fluorescent Probe. *ACS Applied Materials & Interfaces*. 10(34), 28279–28289.

Lowry, G. V., Avellan, A., & Gilbertson, L. M. (2019). Opportunities And Challenges For Nanotechnology In The Agri-Tech Revolution. *Nature Nanotechnology*.14(6), 517–522.

Mba, C., Guimaraes, E. P., & Ghosh, K. (2012). Re-Orienting Crop Improvement For The Changing Climatic Conditions Of The 21st Century. *Agriculture & Food Security.* 1(1), 1–17.

Newkirk, G. M., De Allende, P., Jinkerson, R. E., & Giraldo, J. P. (2021). Nanotechnology Approaches For Chloroplast Biotechnology Advancements. *Frontiers In Plant Science.* 12, 691295.

Santana, I., Wu, H., Hu, P., & Giraldo, J. P. (2020). Targeted Delivery Of Nanomaterials With Chemical Cargoes In Plants Enabled By A Biorecognition Motif. *Nature Communications.* 11(1), 2045.

Servin, A. D., & White, J. C. (2016). Nanotechnology In Agriculture: Next Steps For Understanding Engineered Nanoparticle Exposure And Risk. *Nanoimpact*, 1, 9–12.

Wang, P., Lombi, E., Zhao, F.-J., & Kopittke, P. M. (2016). Nanotechnology: A New Opportunity In Plant Sciences. *Trends In Plant Science.* 21(8), 699–712.

Watanabe, M., Balazadeh, S., Tohge, T., Erban, A., Giavalisco, P., Kopka, J., Mueller-Roeber, B., Fernie, A. R., & Hoefgen, R. (2013). Comprehensive Dissection Of Spatiotemporal Metabolic Shifts In Primary, Secondary, And Lipid Metabolism During Developmental Senescence In *Arabidopsis*. *Plant Physiology.* 162(3), 1290–1310.

Yin, B., Whyatt, R. M., Perera, F. P., Randall, M. C., Cooper, T. B., & Santella, R. M. (1995). Determination Of 8-Hydroxydeoxyguanosine By An Immunoaffinity Chromatography-Monoclonal Antibody-Based Elisa. *Free Radical Biology & Medicine*. 18(6), 1023–1032.

Chapter 2: *In Vivo* Delivery of Nanoparticles into Plant Leaves

Hong hong Wu[1,2,] Israel Santana[1,2,] Joshua Dansie[1], Juan P. Giraldo [1,3]

1, Department of Botany and Plant Sciences, University of California, Riverside, CA, U.S. 92521

2, These authors contributed equally to this work.

3, Corresponding author: juanpablo.giraldo@ucr.edu

Abstract

Plant nanobiotechnology is an interdisciplinary field at the interface of nanotechnology and plant biology that aims to utilize nanomaterials as tools to study, augment or impart novel plant functions. The delivery of nanoparticles to plants *in vivo* is a crucial step to investigate plant nanoparticle interactions and their impact on plant function. Quantum dots are smaller than plant cell wall pores, have versatile surface chemistry, bright fluorescence, and do not photobleach, making them ideal for studying nanoparticle uptake, transport, and distribution in plants by widely available confocal microscopy tools. Herein, we describe three different methods for quantum dot delivery into leaves of living plants: leaf lamina infiltration, whole shoot vacuum infiltration, and root to leaf translocation. The methods in this chapter can be extended to other nanomaterials, including nanosensors, drug delivery nanoparticles, and gene delivery nanoparticles.

Introduction

Plant nano-biotechnology aims to utilize nanomaterials as tools to study and manipulate plant function. Mesoporous silica nanoparticles have been shown to deliver DNA and chemicals into plant leaves (Torney et al. 2007) enhance seed germination, increase plant biomass, total protein, and chlorophyll content (Sun et al. 2016). Negatively charged rods of cerium oxide nanoparticles significantly improve wheat growth and shoot biomass (Rico et al. 2014). Multi-walled carbon nanotubes increase the growth of tobacco cell culture (Khodakovskaya et al. 2012), flowers, and fruit production (Khodakovskaya et al. 2013). In contrast, silver nanoparticles inhibit photosystem II (PSII) function in *Arabidopsis thaliana* (Sosan et al. 2016); zinc oxide and copper oxide nanoparticles reduce the net rate of photosynthesis and leaf stomatal conductance in *Arabidopsis* (Wang and Wink 2016) and rice plants (Da Costa and Sharma 2016), respectively. Recently, using a plant nano bionics approach, nanoparticles augmented or imparted novel functions to plants (Giraldo et al. 2014; Wong et al. 2016). Giraldo et al. (2014) found that interfacing DNA-coated single-walled carbon nanotubes with chloroplasts enhances electron transport rates both *ex vivo* and *in vivo*. Embedding single-walled carbon nanotube-based sensors into spinach plants transforms them into detectors of explosives or pollutants in the environment that communicate the presence of an analyte to electronic devices in real-time (Wong et al. 2016).

Herein, we used quantum dots (QD) as a model system for studying the delivery of nanoparticles into plants *in vivo*. QD are nanoparticles with small size (sub-10 nm), versatile surface chemistry, and outstanding optical properties, e.g., narrow emission

profile, bright fluorescence, and no photobleaching (Probst et al. 2013). Unlike animal cells, plants have a cell wall to prevent interfacing nanoparticles with plant cells. The maximum cell wall porosity reported is approximately 13 nm (Darvill et al. 2010), limiting the use of several types of nanoparticles. The small size of QD allows them to easily pass through the intricate matrix formed by cellulose microfibrils, hemicellulose, and pectin in the plant cell wall. The QD can also be imaged by confocal microscopy tools widely available to most research laboratories. The narrow emission profile of QD enables simultaneous imaging of multiple QD and colocalization with fluorescently labeled cellular structures. Another advantage of QD is their bright fluorescence and that they do not photobleach, allowing long-term and single particle tracking in confocal imaging experiments. QD has been widely used as a drug delivery vehicle in nanomedicine research (Delehanty et al. 2009; Probst et al. 2013; Wang and Chen 2011; Zhao and Zhu 2016). QD systems for drug delivery have allowed real-time monitoring and localized treatment at specific disease sites, improved drug stability, lengthened drug circulation time *in vivo* (Zhao and Zhu 2016), and enhanced drug uptake and retention(Al-Jamal et al. 2008). QD has been used in plant biology research for *in situ* hybridization in plant chromosome analysis (Müller et al. 2006), the study of nanoparticle uptake in plants (Al-Salim et al. 2011), imaging of plant volatile precursors (Tu et al. 2014), and investigating the proteomic response of *Arabidopsis thaliana* (Marmiroli et al. 2015).

The first critical step is to standardize the delivery method of the nanoparticles into plants. QD's small size, versatile surface chemistry, and outstanding optical

properties make them ideal nanoparticles for plant nanobiotechnology research. We describe three protocols for delivering QD to plant leaves *in vivo*: leaf lamina infiltration, whole shoot vacuum infiltration, and root to leaf translocation. These delivery methods can be potentially extended to other nanomaterials, such as nanosensors or drug delivery carriers, having at least one dimension smaller than the plant cell wall porosity.

Materials and Methods

Quantum Dot Nanoparticle Synthesis

This protocol describes the synthesis of thioglycolic acid (TGA)-coated quantum dots TGA-QD with cadmium telluride (CdTe) core and cadmium sulfide (CdS) shell, capped by thioglycolic acid (TGA-QD) (Sun and Gang 2013, Yuan et al. 2012). The quantum dots used in this study were coated with TGA to increase shell stability, serve as stabilizing agents (Freitas et al. 2014, Peng et al. 2009), and provide a free carboxyl group site for covalently attaching biomolecules. Furthermore, the TGA-coating increased solubility in an aqueous solution and controlled the QD size and fluorescence emission (Yuan et al. 2012; Freitas et al. 2014; Yuan et al. 2012; Gao et al. 1998). As shown in Figure 2.1, we prepared a sodium hydrogen telluride (NaHTe) solution (Solution A) under an oxygen-free environment with nitrogen gas. Meanwhile, a colloidal solution of cadmium chloride ($CdCl_2$) and TGA (Solution B) was dissolved in molecular grade water (Catalog no. 46000CV Corning) and placed on a stir plate for 30 min. The pH was adjusted to pH at 11 with 1 M sodium hydroxide. Then, NaHTe (Solution A) solution was added to the dissolved $CdCl_2$ and TGA solution (Solution A).

The resulting mixture was heated for 1 hr at 100°C to achieve desired TGA-QD size and photoluminescence emission peak.

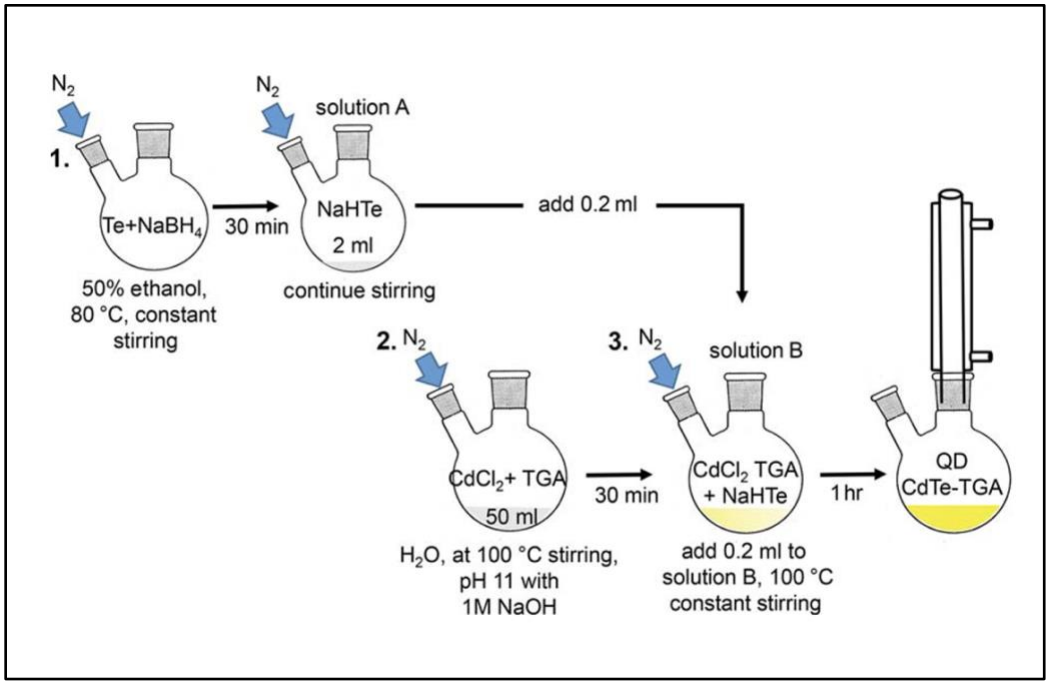

Figure 2.1. Step-by-step synthesis of CdTe/CdS-TGA quantum dots (TGA-QD).

Characterization of Nanoparticles

The QD nanoparticles were characterized by measuring their absorbance spectra, hydrodynamic diameter, and fluorescence emission spectra. It is important to characterize nanomaterials to ensure reproducibility of biological studies, and to understand how the properties of the nanomaterials affect biological systems (Powers et al. 2006). Characterization of nanomaterials was performed by measuring the UV-vis absorption spectrum using a 500-µl sample placed in a plastic cuvette (Eppendorf UV cuvette 220-1600 nm) and measured using a UV-2600 spectrophotometer (Shimadzu).

The size and fluorescence emission spectrum of a 1-ml sample placed in a disposable cuvette (Malvern, cat. no. DTS0012) was measured using a dynamic light scattering (DLS) Zetasizer (Nano-S, Malvern) and Quanta Master 400 fluorometer, respectively. A fluorescence spectrophotometer was used to determine the TGA-QD fluorescence emission peak and excitation peak for setting imaging parameters of a confocal microscope. Figure 2.2 shows the characterization data of synthesized TGA-QD.

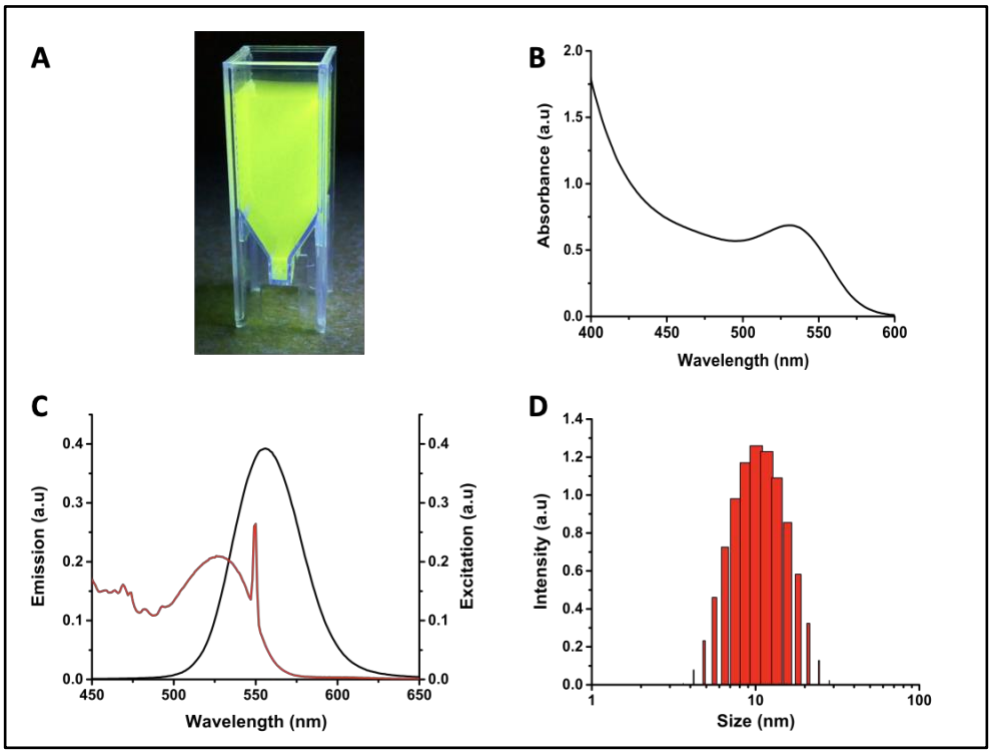

Figure 2.2. Characterization of TGA-QD. (A) TGA-QD fluorescence image upon excitation with UV light (365 nm). (B) UV-vis absorption spectrum of synthesized TGA-QD. (C) Fluorescence excitation spectra (Red line) and emission spectra (Black line) of TGA-QD. (D) Size distribution of TGA-QD measured by Dynamic Light Scattering (DLS).

Infiltration of TGA-Quantum Dots Through Leaf Lamina

Stomatal pores in leaves play a key role in regulating gas exchange between plants and the environment (Buckley and Mott 2013; Hetherington and Woodward 2003). Plants have stomatal apertures usually ranging from 300 to 700 μm^2 (Drake et al. 2013; Fanourakis et al. 2015; Gu et al. 2005). Leaf lamina infiltration of biological and chemical solutions through stomatal pores is commonly used in plant biology research (Mousavi et al. 2013; Sparkes et al. 2006; Wroblewski et al. 2005). Leaf lamina infiltration is also a practical and efficient way to deliver nanoparticles directly into the leaves of living plants (Giraldo et al. 2014; Giraldo et al. 2015; Wong et al. 2016). Herein, we describe a method for leaf lamina infiltration of TGA-QD into living plants. Briefly, a solution of 5.18 nM QDs was added to 10 mM Tris, 10mM ethylenediaminetetraacetic acid, 0.5 % sodium dodecyl sulfate buffer, 10 mM $MgCl_2$, pH 7.5 (TES buffer), and vortexed to make a final 1 ml solution. A solution of 10 mM TES infiltration buffer was used as a control. The infiltration solution was immediately transferred to a 1-ml sterile needleless syringe (NORM-JECT®) (tapped to remove air bubbles). Leaves (four-week-old *Arabidopsis thaliana* plants) were infiltrated with approximately 200 μL of the solution by gently pressing the tip of the syringe against the bottom of the leaf lamina. The excess solution that remained on the surface of the leaf lamina was wiped out using Kimwipes (Kimtech Science®). The eaves infiltrated with TGA-QDs were kept on the lab bench for leaf incubation and adaptation for 3 hr. Figure 2.3 illustrates the workflow of the leaf lamina infiltration protocol.

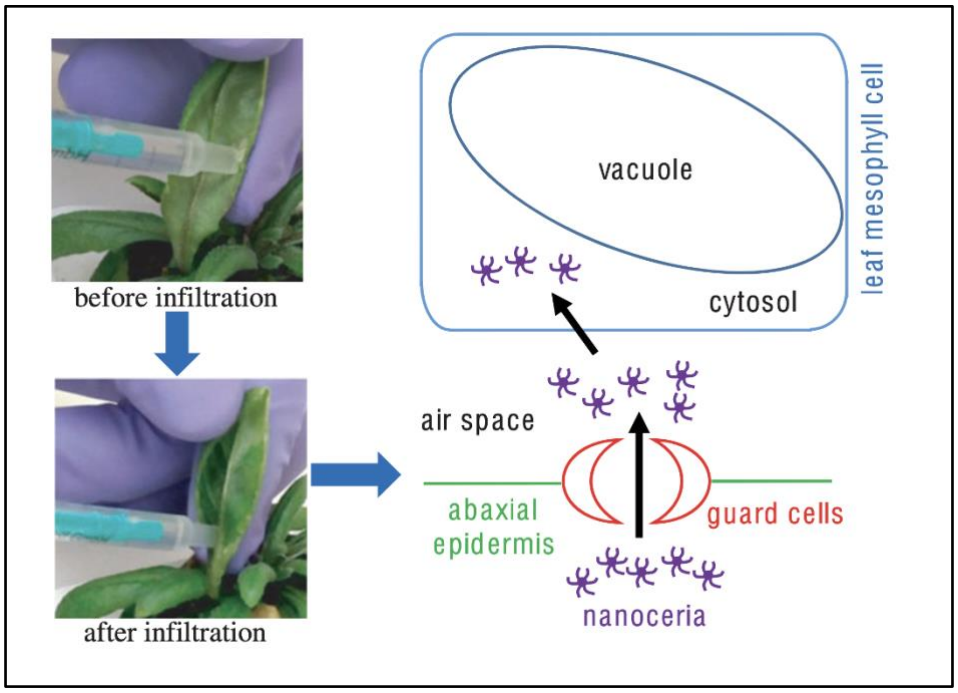

Figure 2.3. Workflow for leaf lamina infiltration of TGA-QD into living plants.

TGA-Quantum Dot Delivery to Leaves via Vacuum Infiltration

Vacuum-assisted infiltration can efficiently deliver nanoparticles to whole shoots or plants (Hussain et al. 2013). Although this technique is commonly used for *Agrobacterium tumefaciens* transformation or virus delivery, vacuum infiltration appears suitable for homogenous plant leaves with nanoparticles (Clough and Bent 1998). A homogenous application of nanoparticles can be applied to many leaves simultaneously, eliminating the need to infiltrate whole plants by hand and possibly lowering the risk of damaging leaves with the varying pressure of syringe-aided approaches. In this modified protocol, a vacuum chamber is utilized to create a momentary disruption of the stomata air layer, subsequently allowing a buffered dilute QD solution into the leaf mesophyll through the stomata. Briefly, the dilute QD solution is sonicated, filtered, and

characterized before being applied to *Arabidopsis thaliana* seedlings through inverted immersion within a depressurized vacuum environment. Figure 2.4 illustrates the workflow of the vacuum infiltration protocol.

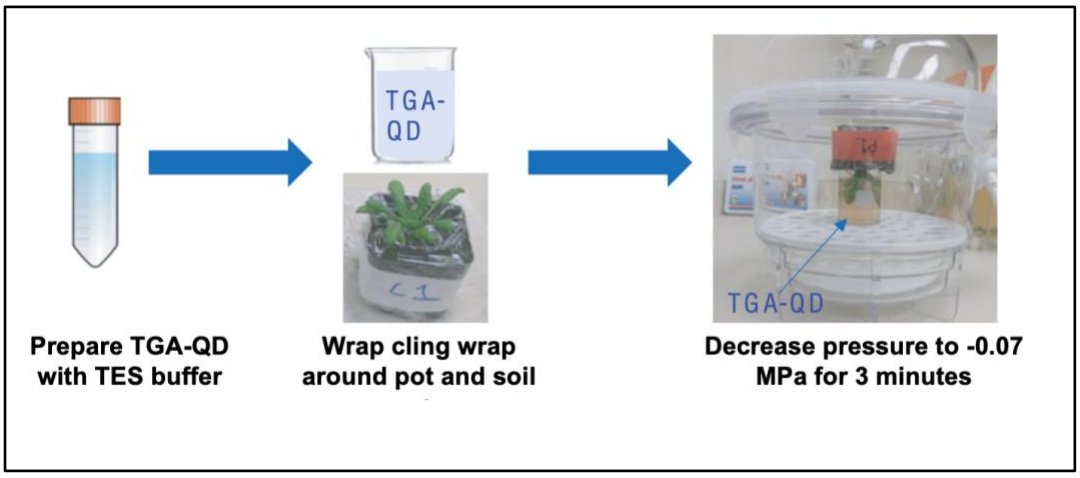

Figure 2.4. Workflow for vacuum infiltration of TGA-QD into plant leaves.

Root-to-Leaf Delivery of TGA-Quantum Dots

This protocol demonstrates a detailed method for root-to-leaf delivery of QD functionalized with thioglycolic acid (TGA) stabilizing agent. Here, we used 8-day-old *Arabidopsis thaliana* Col-0 line seedlings. The *Arabidopsis thaliana* seeds were germinated on agar medium gel. This soft semi-solid gel helps in providing a moist germinating surface and decreases damage during transplantation to the tube during treatment. Figure 2.5 illustrates the workflow of the root-to-leaf delivery of nanoparticles method.

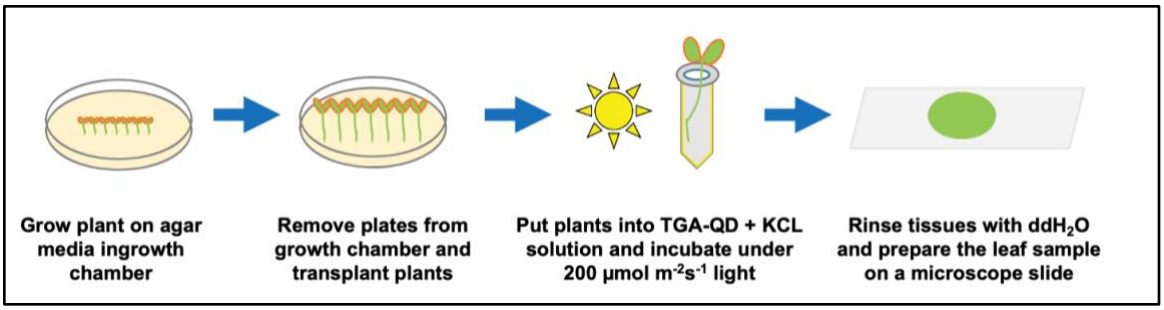

Figure 2.5. Workflow for root to leaf delivery of TGA-QD.

In Vivo Imaging of TGA-Quantum Dots in Plant Leaves by Confocal Imaging

Dissected leaf tissues were analyzed on a Zeiss 510 confocal microscope after infiltration with TGA-QD using the approaches mentioned above. The leaf samples were mounted on a slide inside a hand-made gel chamber filled with perfluorodecalin (PFD) to increase confocal image resolution of living mesophyll (Littlejohn et al. 2014). To determine the appropriate emission and excitation parameters for confocal analysis, the absorption spectra and emission spectra of TGA-QD were characterized as explained in Basic Protocol 1. In this protocol, we excited TGA-QD with an Argon laser set at 488 nm, and a TGA-QD emission signal was detected using a 535-590 nm bandpass filter. Chloroplast pigments in leaves absorb at visible wavelengths with absorption peaks in the blue (near 428 and 453 nm for chlorophyll a and b extracted by diethyl ether, respectively) and red (near 661 and 642 nm for chlorophyll a and b extracted by diethyl ether, respectively) (Lichtenthaler and Buschmann 2001). The chlorophyll pigments autofluorescence was detected using a bandpass filter set at 600 to 800-nm. Figure 2.6 shows TGA-QD's fluorescence signal, and chloroplast pigments in plant leave infiltrated by the methods mentioned above.

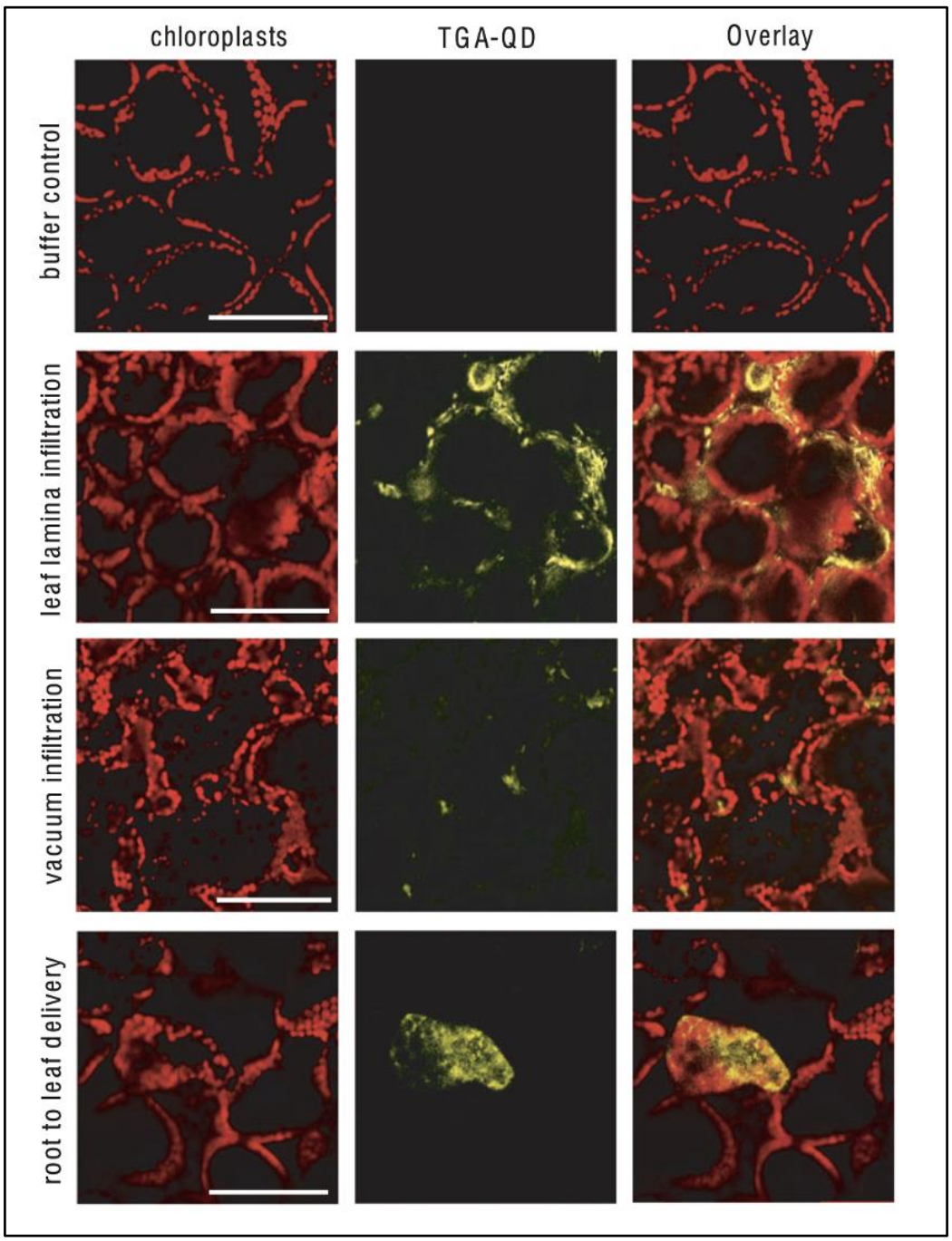

Figure 2.6. Confocal images of TGA-QD delivered into plant leaves via leaf lamina infiltration, whole shoot vacuum infiltration, and root to leaf translocation. Scale bar represents 100 μm.

Results

These methods published in the *Journal of Chemical Biology* describe applying and imaging fluorescent quantum dot nanomaterials inside live plant tissues. Here we developed nanoparticles smaller than the reported cell wall (<20 nm) (Figure 2.2) porosity that can overcome the cell wall matrix and a higher charge that enabled internalization into cell membranes (Carpita et al. 1979; Carpita and Gibeaut 1993; Lew et al. 2018; Wong et al. 2016; Hu et al. 2020). The fluorescence spectra of the QD enabled tracking of the nanomaterials with minimal overlap with autofluorescence and background fluorescence associated with plant cell tissues during confocal imaging (Park et al. 2011; Walling et al. 2009; Marmiroli et al. 2015; Santos et al. 2010). Fluorescent quantum dots were detected in leaf mesophyll tissues using three different methods of infiltration, including leaf lamina infiltration, whole shoot vacuum infiltration, and root to leaf translocation (Figure 2.6).

Among these methods, we observed that needless syringe infiltration exhibited the most direct and controlled method for delivering nanoparticles into plants. The needless syringe infiltration method allowed us to infuse the entire leaf mesophyll space where photosynthesis occurs. The cells located in the vegetative leaves, such as mesophyll and palisade cells, are essential to target bioengineering tools and applications (Poddar et al. 2020; Newkirk et al. 2021). These cells contain organelles and metabolic systems involved in photosynthesis. The strategies described in this Chapter are a vital first step to safely creating tools that can effectively engineer chloroplast function, improve crop yields, and meet future food security demands.

Conclusion

The delivery of engineered nanomaterials into live plant tissues is crucial to investigate plant nanoparticle interactions and the impact on plant function. This Chapter describes three different methods for *in vivo* delivery and imaging of quantum dots in plant leaves: leaf lamina infiltration, whole shoot vacuum infiltration, and root to leaf translocation. These methods provide ways to study nanoparticle uptake, transport, and distribution in plants and understand the impact of nanoparticles on plant function. The protocols described in this manuscript can potentially be applied to other nanoparticles such as nanosensors and drug delivery nanoparticles.

References

Al-Jamal, W. T., Al-Jamal, K. T., Tian, B., Lacerda, L., Bomans, P. H., Frederik, P. M., & Kostarelos, K. (2008). Lipid−Quantum Dot Bilayer Vesicles Enhance Tumor Cell Uptake And Retention *In Vitro* And *In Vivo*. *ACS Nano*, *2*(3), 408–418.

Al-Salim, N., Barraclough, E., Burgess, E., Clothier, B., Deurer, M., Green, S., Malone, L., & Weir, G. (2011). Quantum Dot Transport In Soil, Plants, And Insects. *The Science Of The Total Environment*, *409*(17), 3237–3248.

Buckley, T. N., & Mott, K. A. (2013). Modelling Stomatal Conductance In Response To Environmental Factors. *Plant, Cell & Environment*, *36*(9), 1691–1699.

Carpita, N. C., & Gibeaut, D. M. (1993). Structural Models Of Primary Cell Walls In Flowering Plants: Consistency Of Molecular Structure With The Physical Properties Of The Walls During Growth. *The Plant Journal*, *3*(1), 1–30.

Carpita, N., Sabularse, D., Montezinos, D., & Delmer, D. P. (1979). Determination Of The Pore Size Of Cell Walls Of Living Plant Cells. *Science*, *205*(4411), 1144–1147.

Clough, S. J., & Bent, A. F. (1998). Floral Dip: A Simplified Method For Agrobacterium-Mediated Transformation Of *Arabidopsis thaliana*. *The Plant Journal*, *16*(6), 735–743.

Da Costa, M. V. J., & Sharma, P. K. (2016). Effect Of Copper Oxide Nanoparticles On Growth, Morphology, Photosynthesis, And Antioxidant Response In Oryza Sativa. *Photosynthetica*, *54*(1), 110–119.

Darvill, A., Albersheim, P., Roberts, K., Sederoff, R., & Staehelin, A. (2010). Cell Walls And Plant Anatomy. *Plant Cell Walls*, 430, 19–60.

Delehanty, J. B., Boeneman, K., Bradburne, C. E., Robertson, K., & Medintz, I. L. (2009). Quantum Dots: A Powerful Tool For Understanding The Intricacies Of Nanoparticle-Mediated Drug Delivery. *Expert Opinion On Drug Delivery*, *6*(10), 1091–1112.

Drake, P. L., Froend, R. H., & Franks, P. J. (2013). Smaller, Faster Stomata: Scaling Of Stomatal Size, Rate Of Response, And Stomatal Conductance. *Journal Of Experimental Botany*, *64*(2), 495–505.

Fanourakis, D., Giday, H., Milla, R., Pieruschka, R., Kjaer, K. H., Bolger, M., Vasilevski, A., Nunes-Nesi, A., Fiorani, F., & Ottosen, C.-O. (2015). Pore Size Regulates Operating Stomatal Conductance, While Stomatal Densities Drive The Partitioning Of Conductance Between Leaf Sides. *Annals Of Botany*, *115*(4), 555–565.

Freitas, D. V., Dias, J. M. M., Passos, S. G. B., De Souza, G. C. S., Neto, E. T., & Navarro, M. (2014). Electrochemical Synthesis Of TGA-Capped CdTe And CdSe Quantum Dots. *Green Chemistry: An International Journal And Green Chemistry Resource. Green Chem*, *16*(6), 3247–3254.

Gao, M., Kirstein, S., Möhwald, H., Rogach, A. L., Kornowski, A., Eychmüller, A., & Weller, H. (1998). Strongly Photoluminescent CdTe Nanocrystals By Proper Surface Modification. *The Journal Of Physical Chemistry. B*, *102*(43), 8360–8363.

Giraldo, J. P., Landry, M. P., Faltermeier, S. M., Mcnicholas, T. P., Iverson, N. M., Boghossian, A. A., Reuel, N. F., Hilmer, A. J., Sen, F., Brew, J. A., & Strano, M. S. (2014). Plant Nanobionics Approach To Augment Photosynthesis And Biochemical Sensing. *Nature Materials*, *13*(4), 400–408.

Giraldo, J. P., Landry, M. P., Kwak, S.-Y., Jain, R. M., Wong, M. H., Iverson, N. M., Ben-Naim, M., & Strano, M. S. (2015). A Ratiometric Sensor Using Single Chirality Near-Infrared Fluorescent Carbon Nanotubes: Application To *In Vivo* Monitoring. *Small* , *11*(32), 3973–3984.

Gu, X. F., Yang, A. F., Meng, H., & Zhang, J. R. (2005). In Vitro Induction Of Tetraploid Plants From Diploid *Zizyphus Jujuba* Mill. Cv. Zhanhua. *Plant Cell Reports*, *24*(11), 671–676.

Hetherington, A. M., & Woodward, F. I. (2003). The Role Of Stomata In Sensing And Driving Environmental Change. *Nature*, *424*(6951), 901–908.

Hu, P., An, J., Faulkner, M. M., Wu, H., Li, Z., Tian, X., & Giraldo, J. P. (2020). Nanoparticle Charge And Size Control Foliar Delivery Efficiency To Plant Cells And Organelles. *ACS Nano*. *14*(7), 7970–7986

Hussain, H. I., Yi, Z., Rookes, J. E., Kong, L. X., & Cahill, D. M. (2013). Mesoporous Silica Nanoparticles As A Biomolecule Delivery Vehicle In Plants. *Journal Of Nanoparticle Research: An Interdisciplinary Forum For Nanoscale Science And Technology*, *15*(6), 1676.

Khodakovskaya, M. V., De Silva, K., Biris, A. S., Dervishi, E., & Villagarcia, H. (2012). Carbon Nanotubes Induce Growth Enhancement Of Tobacco Cells. *ACS Nano*, *6*(3), 2128–2135.

Khodakovskaya, M. V., Kim, B.-S., Kim, J. N., Alimohammadi, M., Dervishi, E., Mustafa, T., & Cernigla, C. E. (2013). Carbon Nanotubes As Plant Growth Regulators: Effects On Tomato Growth, Reproductive System, And Soil Microbial Community. *Small* , *9*(1), 115–123.

Lew, T. T. S., Wong, M. H., Kwak, S.-Y., Sinclair, R., Koman, V. B., & Strano, M. S. (2018). Rational Design Principles For The Transport And Subcellular Distribution Of Nanomaterials Into Plant Protoplasts. *Small*, *14*(44), E1802086.

Lichtenthaler, H. K., & Buschmann, C. (2001). Chlorophylls And Carotenoids: Measurement And Characterization By Uv-Vis Spectroscopy. *Current Protocols In Food Analytical Chemistry*, *1*(1), F4.3.1–F4.3.8.

Marmiroli, M., Imperiale, D., Pagano, L., Villani, M., Zappettini, A., & Marmiroli, N. (2015). The Proteomic Response Of *Arabidopsis thaliana* To Cadmium Sulfide Quantum Dots, And Its Correlation With The Transcriptomic Response. *Frontiers In Plant Science*, *6*, 1104.

Mousavi, S. A. R., Chauvin, A., Pascaud, F., Kellenberger, S., & Farmer, E. E. (2013). Glutamate Receptor-Like Genes Mediate Leaf-To-Leaf Wound Signalling. *Nature*, *500*(7463), 422–426.

Müller, F., Houben, A., Barker, P. E., Xiao, Y., Käs, J. A., & Melzer, M. (2006). Quantum Dots-A Versatile Tool In Plant Science? *Journal Of Nanobiotechnology*, *4*, 5.

Newkirk, G. M., De Allende, P., Jinkerson, R. E., & Giraldo, J. P. (2021). Nanotechnology Approaches For Chloroplast Biotechnology Advancements. *Frontiers In Plant Science*, *12*, 691295.

Park, J., Nam, J., Won, N., Jin, H., Jung, S., Jung, S., Cho, S.-H., & Kim, S. (2011). Compact And Stable Quantum Dots With Positive, Negative, Or Zwitterionic Surface: Specific Cell Interactions And Non-Specific Adsorptions By The Surface Charges. *Advanced Functional Materials*, *21*(9), 1558–1566.

Peng, J., Liu, S., Wang, L., Liu, Z., & He, Y. (2009). Study On The Interaction Between CdSe Quantum Dots And Chitosan By Scattering Spectra. *Journal Of Colloid And Interface Science*, *338*(2), 578–583.

Poddar, K., Sarkar, D., & Sarkar, A. (2020). Nanoparticles On Photosynthesis Of Plants: Effects And Role. In J. K. Patra, L. F. Fraceto, G. Das, & E. V. R. Campos (Eds.), *Green Nanoparticles: Synthesis And Biomedical Applications*, 273–287. Springer International Publishing.

Powers, K. W., Brown, S. C., Krishna, V. B., Wasdo, S. C., Moudgil, B. M., & Roberts, S. M. (2006). Research Strategies For Safety Evaluation Of Nanomaterials. Part Vi. Characterization Of Nanoscale Particles For Toxicological Evaluation. *Toxicological Sciences: An Official Journal Of The Society Of Toxicology*, *90*(2), 296–303.

Probst, C. E., Zrazhevskiy, P., Bagalkot, V., & Gao, X. (2013). Quantum Dots As A Platform For Nanoparticle Drug Delivery Vehicle Design. *Advanced Drug Delivery Reviews*, *65*(5), 703–718.

Rico, C. M., Lee, S. C., Rubenecia, R., Mukherjee, A., Hong, J., Peralta-Videa, J. R., & Gardea-Torresdey, J. L. (2014). Cerium Oxide Nanoparticles Impact Yield And Modify Nutritional Parameters In Wheat (*Triticum Aestivum L.*). *Journal Of Agricultural And Food Chemistry*, *62*(40), 9669–9675.

Santos, A. R., Miguel, A. S., Tomaz, L., Malhó, R., Maycock, C., Vaz Patto, M. C., Fevereiro, P., & Oliva, A. (2010). The Impact Of CdSe/ZnS Quantum Dots In Cells Of Medicago Sativa In Suspension Culture. *Journal Of Nanobiotechnology*, *8*, 24.

Sosan, A., Svistunenko, D., Straltsova, D., Tsiurkina, K., Smolich, I., Lawson, T., Subramaniam, S., Golovko, V., Anderson, D., Sokolik, A., Colbeck, I., & Demidchik, V. (2016). Engineered Silver Nanoparticles Are Sensed At The Plasma Membrane And Dramatically Modify The Physiology Of *Arabidopsis thaliana* Plants. *The Plant Journal: For Cell And Molecular Biology*, *85*(2), 245–257.

Sparkes, I. A., Runions, J., Kearns, A., & Hawes, C. (2006). Rapid, Transient Expression Of Fluorescent Fusion Proteins In Tobacco Plants And Generation Of Stably Transformed Plants. *Nature Protocols*, *1*(4), 2019–2025.

Sun, D., & Gang, O. (2013). DNA-Functionalized Quantum Dots: Fabrication, Structural, And Physicochemical Properties. *Langmuir: The ACS Journal Of Surfaces And Colloids*, *29*(23), 7038–7046.

Sun, D., Hussain, H. I., Yi, Z., Rookes, J. E., Kong, L., & Cahill, D. M. (2016). Mesoporous Silica Nanoparticles Enhance Seedling Growth And Photosynthesis In Wheat And Lupin. *Chemosphere*, *152*, 81–91.

Torney, F., Trewyn, B. G., Lin, V. S.-Y., & Wang, K. (2007). Mesoporous Silica Nanoparticles Deliver DNA And Chemicals Into Plants. *Nature Nanotechnology*, *2*(5), 295–300.

Tu, V. A., Kaga, A., Gericke, K.-H., Watanabe, N., Narumi, T., Toda, M., Brueckner, B., Baldermann, S., & Mase, N. (2014). Synthesis And Characterization Of Quantum Dot Nanoparticles Bound To The Plant Volatile Precursor Of Hydroxy-Apo-10'-Carotenal. *The Journal Of Organic Chemistry*, *79*(15), 6808–6815.

Walling, M. A., Novak, J. A., & Shepard, J. R. E. (2009). Quantum Dots For Live Cell And *In Vivo* Imaging. *International Journal Of Molecular Sciences*, *10*(2), 441–491.

Wang, E., & Wink, M. (2016). Chlorophyll Enhances Oxidative Stress Tolerance In *Caenorhabditis Elegans* And Extends Its Lifespan. *Peerj*, *4*, E1879.

Wang, Y., & Chen, L. (2011). Quantum Dots, Lighting Up The Research And Development Of Nanomedicine. *Nanomedicine: Nanotechnology, Biology, And Medicine*, *7*(4), 385–402.

Wong, M. H., Misra, R. P., Giraldo, J. P., Kwak, S.-Y., Son, Y., Landry, M. P., Swan, J. W., Blankschtein, D., & Strano, M. S. (2016). Lipid Exchange Envelope Penetration (Leep) Of Nanoparticles For Plant Engineering: A Universal Localization Mechanism. *Nano Letters*, *16*(2), 1161–1172.

Wroblewski, T., Tomczak, A., & Michelmore, R. (2005). Optimization Of Agrobacterium-Mediated Transient Assays Of Gene Expression In Lettuce, Tomato And *Arabidopsis*. *Plant Biotechnology Journal*, *3*(2), 259–273.

Yuan, Z., Yang, P., & Cao, Y. (2012). Time-Resolved Photoluminescence Spectroscopy Evaluation Of CdTe And CdTe/CdS Quantum Dots. *International Journal Of Spectroscopy.* 2012, 1-8.

Yuan, Z., Zhang, A., Cao, Y., Yang, J., Zhu, Y., & Yang, P. (2012). Effect Of Mercaptocarboxylic Acids On Luminescent Properties Of CdTe Quantum Dots. *Journal Of Fluorescence*, *22*(1), 121–127.

Zhao, M.-X., & Zhu, B.-J. (2016). The Research And Applications Of Quantum Dots As Nano-Carriers For Targeted Drug Delivery And Cancer Therapy. *Nanoscale Research Letters*, *11*(1), 207.

Chapter 3: Targeted delivery of nanomaterials with chemical cargoes in plants enabled by a biorecognition motif

Israel Santana, Honghong Wu, Peiguang Hu & Juan Pablo Giraldo

Nature Communications 11: Article number: 2045 (2020)

Abstract:

Current approaches for nanomaterial delivery in plants cannot target specific subcellular compartments with high precision, limiting our ability to engineer plant function. We demonstrate a nanoscale platform that targets and delivers nanomaterials with biochemicals to plant photosynthetic organelles (chloroplasts) using a guiding peptide recognition motif. Quantum dot (QD) fluorescence emission in a low background window allows confocal microscopy imaging and quantitative detection by elemental analysis in plant cells and organelles. QD functionalization with β-cyclodextrin molecular baskets enables loading and delivery of diverse chemicals, and nanoparticle coating with a rationally designed and con-served guiding peptide targets their delivery to chloroplasts. Peptide biorecognition provides high delivery efficiency and specificity of QD with chemical cargoes to chloroplasts in plant cells *in vivo* (74.6 ± 10.8%) and more specific tunable changes of chloroplast redox function than chemicals alone. Targeted delivery of nanomaterials with chemical cargoes guided by biorecognition motifs has a broad range of nanotechnology applications in plant biology and bioengineering, nanoparticle-plant interactions, and nano-enabled agriculture.

Introduction

The limited ability to target the delivery of biochemicals to specific plant tissues and organelles leads to inefficiencies of chemical inputs in agriculture and unintended alterations in plant function (Smith and Gilbertson 2018; Lowry et al. 2019). Only a fraction of agrochemicals, including nutrients and pesticides, reach the intended target in crops (Smith and Gilbertson 2018), leading to environmental pollution (Sebilo et al. 2013), low resource use efficiency in plants (Baligar et al. 2001), and inhibition of key plant physiological and developmental processes (Li et al. 2014). Although genetically modified organisms have proven to be of high value to understand plant function at the subcellular level, genome mutations or editing is accompanied by confounding effects including abnormal organ and tissue development (Ohno et al. 2004) and even leading to non-viable organisms (Sparkes et al. 2003). Furthermore, the number of crop plants amenable for organelle genetic engineering is limited (Bock 2014). Nanomaterials are emerging as delivery vehicles for biomolecules in plants (Torney et al. 2007; Wang et al. 2019; Demirer et al. 2019; Kwak et al. 2019; Kwak et al. 2017) that can be tuned to control their translocation and distribution to plant cells and organelles.

Plant nanobiotechnology is a burgeoning field, which aims to develop and apply engineered nanomaterials (ENMs) for engineering and studying plant function (Lowry et al. 2019; Wang et al. 2019; Giraldo et al. 2019; Kah et al. 2019; Wang et al. 2016). Interfacing ENMs with plants is leading to significant advances towards addressing crucial challenges in plant genetic element delivery (Demirer et al. 2019), biochemical sensing (Giraldo et al. 2014; Wong et al. 2017; Giraldo et al. 2015), and nutrient and

pesticide delivery (Borgatta et al. 2018; Gogotsi 2018). The broad potential for engineering plants utilizing ENMs with unique physical and chemical properties rely on circumventing plant barriers including cell walls and membranes and improving the targeting to specific tissues and organelles (Wang et al. 2016). Surface functionalization of ENMs with guiding moieties has enabled targeted biochemical delivery in non-plant eukaryotic cells (Mangadlao et al. 2018). Although the *in vivo* delivery efficiencies of nanoparticles coated with biorecognition ligands to target cancer cells are not higher than 2% (Dai et al. 2018), localization in the nuclei of gold nanoparticles coated with SV40 large T antigen in HeLa cell cultures *in vitro* has been reported to be up to 60% (Ryan et al. 2007). Previous studies have reported the non-targeted delivery of DNA and biochemicals into plant cells and organelles by mesoporous silica nanoparticles through particle bombardment of leaf sections *in vitro* (Torney et al. 2007) or by interfacing carbon nanotubes and their cargoes with isolated tobacco cells (Liu et al. 2009). However, the destructive and invasive application of these approaches is not suitable for targeted delivery of nanoparticles to plant subcellular compartments in intact plants *in vivo*.

Current approaches to improve *in vivo* nanoparticle delivery efficiency to specific plant cells or organelles are based on modifying nanoparticle properties such as size and charge but do not reach high levels of subcellular localization specificity (Wu et al. 2017). For example, we have reported that negatively charged cerium oxide nanoparticles delivered into plant leaves have about 45% colocalization rates with chloroplasts (Wu et al. 2017). However, most chloroplasts do not contain nanoparticles. Targeted

nanomaterials guided by biorecognition ligands such as transit peptides have not been reported in plants to date because they cannot be directly translated from non-plant systems. Unlike mammalian cells, plant cells have a wall that acts as an additional barrier for nanoparticle translocation (Mccann et al. 1990). Nanoparticle uptake across plant cell walls is limited by the size of nanomaterials and cell wall pores (Schwab et al. 2016). Although the permeability of plant cell walls to nanomaterials has not been systematically characterized, it is expected to be dependent on plant species and nanoparticle properties, including size and hydrophobicity (Avellan et al. 2019). For instance, amphiphilic nanoparticles (~40 nm) have been reported to translocate across leaf cells but not hydrophilic nanoparticles of similar or larger size. Furthermore, strong leaf background fluorescence from chloroplast pigments impairs our ability to easily track and colocalize nanomaterials in plants, thus requiring a specific design of fluorescent nanomaterials for both targeted and traceable biochemical delivery in plants in low fluorescent background windows.

Chloroplasts are key organelles for plant bioengineering. These semi-autonomous organelles are essential for plant photosynthesis, act as signaling organelles, and play important roles in metabolite synthesis (Bobik and Burch-Smith 2015; Jin and Daniell 2015; Pierella Karlusich et al. 2017). Thus, chloroplasts are essential for improving crop growth, stress tolerance, biopharmaceutical production, and developing synthetic biology tools (Jin and Daniell 2015). Manipulating chloroplast function through biomolecule or chemical delivery in plants is crucial for understanding the role of these plastids in plant biology and developing approaches for chloroplast bioengineering. However, chloroplast

studies are limited to the need of targeted delivery platforms for specifically engineering plant organelle function *in vivo*. Instead, chloroplast research mainly relies on the generation of transgenic or mutant plants with altered development and function in a handful of model species amenable for genetic transformation (Bock 2014). Herein, we demonstrate approaches for designing novel ENM platforms guided by a peptide recognition motif that targets the delivery of chemicals to chloroplasts in wild type *Arabidopsis thaliana* (Col-0) plants. Using these nanoscale platforms, we enabled the capability to specifically manipulate chloroplast function and redox state *in vivo* (Figure 3.1a).

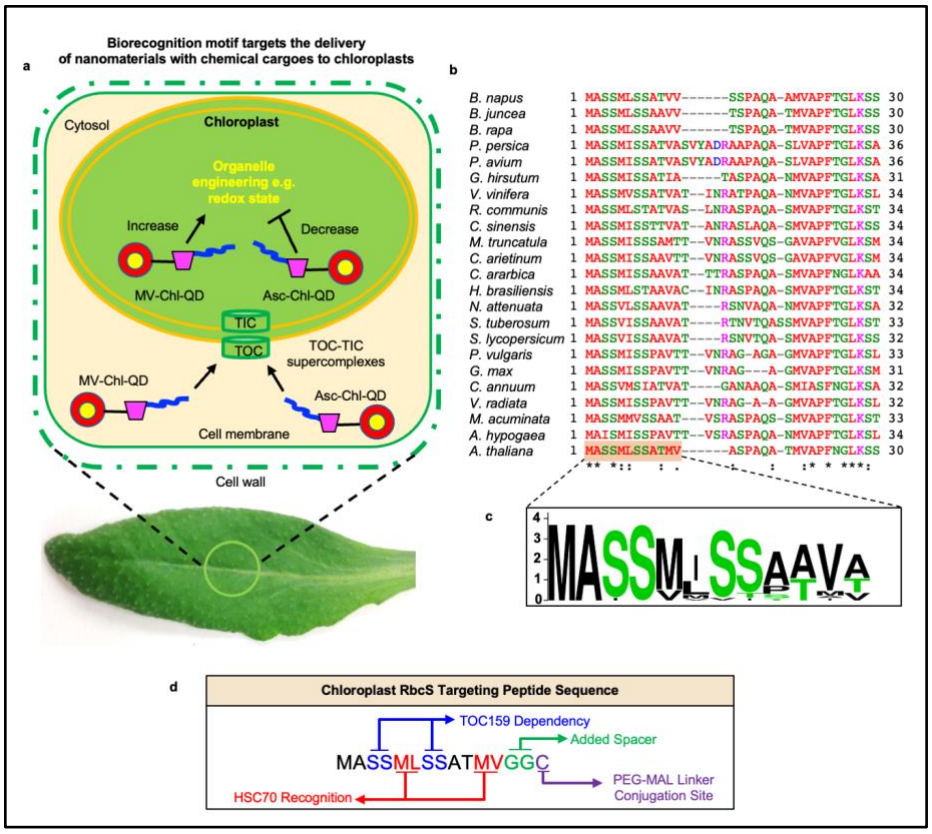

Figure 3.1 Targeted delivery of nanomaterials with chemical cargoes in plants enabled by a biorecognition motif. a, Quantum dots coated with a chloroplast guiding peptide (in blue) and a β-cyclodextrin (β-CD) molecular basket (in magenta) enable loading of methyl viologen (MV-Chl-QD) or ascorbic acid (Asc-Chl-QD) and targeted modification of the redox state of chloroplasts in plants. The Rubisco small subunit (RbcS) targeting peptide is designed to bind to the translocon supercomplex on the chloroplast outer membrane (TOC). b, Multiple sequence alignment analysis (Clustal Omega) of RbcS 1A chloroplast transit peptide sequences in common dicot crops and *Arabidopsis thaliana.* '*' indicates the identical amino acids among all the aligned sequences. ":" and "." suggest conserved substitutions in which another one replaces an amino acid with similar properties. Empty space represents a non-conserved substitution. Dash lines are introduced for optimal alignment and maximum similarity between all compared sequences. c, Frequency logo plot of RbcS 1A targeting peptide consensus sequence across selected dicot species. A score of 4 on y-axis means 100% conserved. d, Rational design of chloroplast guiding peptide based on RbcS peptide biorecognition motif for targeting and translocation across chloroplast membranes. The chloroplast targeting peptide includes recognition sites for chloroplast import machinery by TOC, a cysteine residue at the C-terminus for conjugation with SM-PEG linker, and two glycine (G) amino acids as spacers and for increasing the peptide solubility.

This study highlights approaches to design and synthesize novel ENM platforms that bypass biological barriers in plants such as cell walls, membranes, and organelle envelopes, while avoiding leaf background fluorescence for *in vivo* traceable and targeting the delivery of biochemicals chloroplasts using guiding peptide recognition motifs. To enable this targeted nanoparticle delivery and tracking approach in plants, we designed hydrophilic quantum dots coated with β-cyclodextrin molecular baskets with size that facilitates translocation through leaf cell wall pores, RbcS guiding peptides to recognize organelle membranes, high zeta potential to translocate across lipid bilayers, and optimal fluorescence emission range avoiding leaf background for *in vivo* imaging.

Materials and Methods

Plant Growth

Plants were grown in Adaptis 1000 growth chambers (Conviron) as described in our previous publications (Wu et al. 2017). Growth chamber conditions were 200 μmol m^{-2} s^{-1} PAR, 24 ±1 °C, 60% humidity, and 14/10 h day/night regime. *Arabidopsis* plants were watered once every three days. Four-week-old *Arabidopsis thaliana* (Col-0) was used for this study.

Synthesis of Quantum Dots Functionalized with Chloroplast Targeting Peptide

The CdTe/CdS quantum dots were prepared by the reaction between $CdCl_2$ and NaHTe solution in the presence of mercaptopropionic acid solution (MPA) as the stabilizing agent (Rodrigues et al. 2014; Li et al. 2016; Zhou et al. 2011; Jia et al. 2010). First, 0.01 g of $CdCl_2$ and 50 uL of mercaptopropionic acid were dissolved in 50 mL of

ddH_2O, forming a colloidal solution. The resulting Cd/MPA colloidal solution was adjusted to pH 11 with NaOH solution (0.1 M) and stirred for 15 min under reflux. Meanwhile, NaHTe solution was prepared by dissolving 0.05 g of $NaBH_4$ and 0.02 g of tellurium powder in 0.6 mL of 50% ethanol in a 20 ml glass vial. NaHTe was allowed to react at 70 °C with gentle stirring for 5 min. The reaction vial was lightly capped to avoid excess oxygen from oxidizing the reaction. The $NaBH_4$ and tellurium mixture exhibited a color change as the reaction progressed, turning black-blue to pink-purple in color. Immediately after the color change, 150 µL of freshly prepared NaHTe was added to the Cd/MPA colloidal solution under reflux conditions. Following reflux, an increase in fluorescence of the solution could be monitored when excited under UV light. Aliquots of quantum dot solution were collected in 5 min. The emission of QD could be tuned to a specific wavelength by adjusting the reaction time. The resultant MPA-QD absorbance, size, zeta potential, and emission (under 405 nm excitation) were characterized accordingly. QD for targeted delivery of biochemicals to chloroplasts (Chl-QD) were designed and synthesized for their application to plants including size that facilitates translocation across leaf cell walls, fluorescence within the low background optical window for leaves, and coated with a truncated RbcS guiding peptide to target chloroplasts as described in multiple steps outlined below and in Figure 3.1. RbcS peptide was randomized by using http://www.bioinformatics.org/sms2/shuffle_protein.html javascript suite (Stothard 2000). All chemicals were purchased from Sigma Aldrich unless otherwise stated.

Preparation of p-Aminophenylboronic Acid-Capped QD (APBA-QD)

The MPA-QD terminal carboxyl group was functionalized by 1-ethyl-3-(3-dimethylaminopropyl) carbodiimide (EDC) and N-hydroxysuccinimide (NHS) activated reaction (Li et al. 2016). Briefly, NHS (2000 nmol) and EDC/HCl (2000 nmol) was added to the 1 nmol of the MPA-capped QD in 10 mM Tris, 10mM ethylenediaminetetraacetic acid, 0.5 % sodium dodecyl sulfate buffer pH 7.4 (TES buffer). Then, the mixture was gently stirred (500 rpm) for 15 min at room temperature. Next, 80 μL of a 25 mM APBA solution was added to the activated MPA-QD solution to generate aminophenyl boronic acid-functionalized quantum dots (APBA-QD). The reaction was stirred (500 rpm) for 3 hr at room temperature. Finally, the excess of APBA was removed by washing at least twice through a 10 K (molecular weight cutoff, MWCO) Amicon filter with ddH_2O. The APBA-QD solution was sonicated for 30 min at 80% power at 37 hz to break down any agglomerated particles.

Preparation of β-CD-Capped QD

The APBA-QD were dissolved in a 10 mM TES buffer (pH 10.4). Then 1 μmol of β-cyclodextrin (β-CD, Cavcon) in water was added to the APBA-QD solution, and the resulting mixture was reacted overnight at room temperature with gentle stirring (500 rpm) (Ai et al. 2012). The excess of β-cyclodextrin was removed by washing with a 10 K Amicon filter followed by sonication for 30 min at 80% power at 37 hz. The resulting β-cyclodextrin coated quantum dots (CD-QD) were suspended in 10mM TES (pH 7.5).

Peptide-Conjugated β-CD-Capped QD

After preparing CD-QD, 1 μmol SM-PEG linker (succinimidyl-[(N-maleimidopropionamido)-tetraethyleneglycol] ester, Thermo Fisher Scientific, USA) was added to the surface of CD-QD by reacting with its terminal amine to form a covalent bond (Li et al. 2016; Ai et al. 2012). The mixture was incubated at ambient temperature for 1 hr with gentle stirring (500 rpm). The excess SM-PEG was removed by washing the mixture through a 10 K Amicon column with ddH_2O, and the product was suspended in 10 mM TES (pH 8.0). Finally, 1 μmol of RbcS chloroplast targeting peptide purchased from GeneScript® biotech was added to SM-PEG-QD and allowed to react for 1 hr at room temperature with gentle stirring (500 rpm). The RbcS peptide dissolved in DMSO was diluted with a TES buffer to adjust the pH to 8.0. The resulting chloroplast targeting quantum dot (Chl-QD) was pulse centrifuged for 30 seconds at 3,500 rpm to remove large agglomerates of the non-conjugated peptide. Chl-QD can be stored for up to one week without significant aggregation.

Methyl Viologen and Ascorbic Acid Loading to Quantum Dots

Loading of methyl viologen and ascorbic acid were loaded into β-CD conjugated onto Chl-QD by adding MV and Asc in excess (0.1 mM) to an aqueous solution of 200 nM (0.17 mg mL^{-1}) Chl-QD in 10 mM TES buffer pH 7.0. The mixture of MV-Chl-QD or Asc-Chl-QD was vortexed and incubated for 0.5 hr and washed once through an Amicon 10 K filter with ddH_2O to remove excess molecules. MV and Asc exhibit the maximum absorbance at 260 and 265.5 nm, respectively. The inclusion complex

concentration of chemicals loaded onto nanomaterials (MV-Chl-QD and Asc-Chl-QD) was calculated based on the absorbance at 260 or 265.5 nm of reference to unloaded Chl-QD (Saha et al., 2016; Q. Wang et al., 2013). The resultant MV-Chl-QD or Asc-Chl-QD concentration was extrapolated using a standard curve (Supplementary Figure. S3.2b–d). The final dosage of chemicals infiltrated into plants with 200 nM of Chl-QD was 60 μM MV or 60 μM Asc in 100 μL TES buffer (pH 7.0) (Supplementary Figure. S3.2c, d). To compare with chemicals alone, the same concentration of chemicals was applied to plants, 60 μM MV or 60 μM Asc in 100 μL TES buffer (pH 7.0).

Isothermal Titration Calorimetry (ITC) of Quantum Dots with Chemical Cargoes

ITC of cyclodextrin functionalized QD (CD-QD) or MPA-QD with chemical cargoes (Asc or MV) was performed using a MicroCal ITC200 instrument (GE Healthcare). QD and Asc or MV were dissolved in 10 mM TES buffer, pH 7.3 at 25 °C. The concentrations of QD were set at 0.5 μM, and the concentration of injected Asc and MV was 25 mM. The volume of each injection was 2 μL, and a total of 21 injections were performed at 180 s intervals with a reference power of 5 μcal s^{-1}. The ITC curves were analyzed with Origin (MicroCal) using a one-set-of-sites fitting model. The bound fractions of Asc and MV on QD in the final solution (with initial Asc or MV loading of 60 μM) injected into leaves was calculated based on the following equation (Bisswanger 2017):

$$[A_{bound}] = n[QD]_0[A]K_d + [A]$$

where [Abound] and [A] are the concentration of bound and unbound chemicals in solution, respectively, n is the number of binding sites on QD, $[QD]_0$ is the initial QD concentration, and Kd is the dissociation constant between QD and chemicals.

Nanomaterial Characterization

All nanomaterials were characterized for their absorbance in the UV-vis, hydrodynamic size, zeta potential, and fluorescence emission. Surface functional groups were analyzed by FTIR. Zeta potential and hydrodynamic sizes of nanomaterials were measured in DI water (pH 7) using a Malvern Zetasizer (Nano ZS) and sizer (Nano S), respectively. UV-vis absorption spectra were collected using a UV-2600 Shimadzu spectrophotometer. The sample was prepared in a quartz cuvette filled with 1 mL of a 1:10 fold dilution of nanoparticles. The concentration of the nanomaterials (mol L^{-1}) was determined using Lambert-Beer's law (Eq. 1) where Abs is absorbance, ϵ is the extinction coefficient, L is the path length, and c is concentration. Equation 2 refers to the extinction coefficient (ϵ), calculated based on the QD hydrodynamic diameter (d) (Yu et al. 2003). The QD absorbance at 465 nm was used to determine the QD concentration in the solution (Eq. 1).

Eq.1 $$\mathbf{Abs = \epsilon \times L \times c,}$$

$$\mathbf{\epsilon = 10043 \times (Diameter)^{2.12}}$$

Transmission electron microscopy (TEM) was performed on a Philips FEI Tecnai 12 microscope operated at an accelerating voltage of 120 kV. The TEM samples were prepared by placing one drop of particle solution (0.5 μM) onto the grid (ultrathin carbon

film on lacey carbon support film, 400 mesh, Cu, Ted Pella) followed by drying naturally. The surface coatings and functional groups on nanomaterials were characterized by Fourier transform infrared spectroscopy (FTIR) from Bruker (Alpha I). Samples from each step in the synthesis of Chl-QD were taken to analyze functional groups on the nanoparticle surface (Figure 3.2e).

Nanoparticle delivery into plant leaves

All nanoparticles infused through the *Arabidopsis* leaf lamina were suspended in a 10 mM TES buffer (pH 7.0). The Chl-QD solution was diluted to 200 nM (0.17 mg mL^{-1}) and loaded with 60 μM methyl viologen or ascorbic acid. Nanoparticle solution was infused through the abaxial side of the leaf using a 1-mL syringe plunger (Wu et al. 2017; Newkirk et al. 2018). Approximately 100 μL solution was perfused into each plant leaf by gently pressing the tip of the syringe against the bottom of the leaf lamina and depressing the plunger. The excess solution was gently removed from the leaf surface by Kimwipes.

Confocal fluorescence microscopy imaging of nanoparticles and ROS in leaves

Arabidopsis leaf samples were imaged by a Leica laser scanning confocal microscope TCS SP5 (Leica Microsystems, Germany) (Wu et al. 2017; Wu et al. 2018). Each leaf was infused with 200 nM (0.17 mg mL^{-1}) Chl-QD, MV-Chl-QD or Asc-Chl-QD and incubated for 3 hr. After incubation, a leaf punch was excised and incubated in 10 μM DHE (Thermo Fisher Scientific, USA) in 10 mM TES buffer (pH 7.0) for 30 min. The leaf was immediately placed on a glass slide equipped with Carolina observation gel

for confocal analysis. A pea-size amount of observation gel (Carolina) was placed on a glass slide and pressed to about 1 mm thin on slides. A cork borer was used to cut a circular section of gel roughly twice the size of the leaf discs at the center of the observation gel and a leaf disc was placed within the cavity. The imaging settings were as follows: ×40 wet objective (Leica Microsystems, Germany); 405 nm laser excitation for QD; 514 nm for DHE; z-stack section thickness = 2 μm; line average = 4. The PMT detection range was set 500–550 nm for QD; 580−615 nm for DHE; and 720−780 nm for chloroplast autofluorescence. The confocal imaging of QD and DHE signals was conducted separately to avoid the overlap between excitation of DHE dye and emission detection range of QD. Three to eight individuals (4 leaf discs for each plant) in total were used. The z-stacks ("xyz") of two different regions were taken per leaf disc.

All confocal microscopy images were analyzed using FIJI (ImageJ) in which QD, DHE, and chloroplast images were evenly divided by drawing six lines of the region of interest (ROI), with the same length and distance between each ROI line (Wu et al. 2017; Li et al. 2018). The corresponding fluorescence intensity profiles of QD and DHE fluorescence and chloroplast autofluorescence were then measured across the six ROI line sections and reported as a subset of the image showing signal intensity plot. The percentage of chloroplasts colocalized with QD was counted as the overlapped peaks of fluorescence emission of chloroplast pigments and QD or DHE fluorescence signals. For DHE intensity analysis in chloroplasts, the pixel intensity of DHE fluorescence was measured (FIJI) in an ROI enclosing chloroplast and reported as mean DHE intensity.

Chloroplast isolation

Chloroplasts were isolated through a centrifugation gradient method (Giraldo et al. 2014; Weise et al. 2004). Intact chloroplasts were isolated from plants treated with 500 nM of Chl-QD, or buffer (10 mM TES pH 7.3). Approximately 100 µL of the solution was infiltrated into the primary leaf whorl of 3–4-week-old *Arabidopsis thaliana* plants. Approximately 8 g of leaf tissue with or without nanoparticles was collected from 5–6 plants per treatment. Leaf tissue was macerated in 1X chilled sucrose buffer (28 mM Na_2HPO_4, 22 mM KH_2PO_4, 2.5 mM $MgCl_2$, 400 mM sucrose, and 10 mM KCl at pH 7.3) by two cycles of centrifugation at 4000 RCF for 10 min. Immediately following chloroplast isolation, a sample of intact chloroplasts was placed on a glass slide to confirm and detect quantum dot fluorescence within extracted chloroplasts using confocal microscopy.

Elemental analysis of isolated chloroplasts by inductively coupled plasma mass spectrometry (ICP-MS)

Following chloroplast isolation, sample pellets (~0.1 g) were air-dried for 48 h, placed in 50 mL polypropylene digestion tubes, and digested with a solution of 5% HNO_3/1% HCl/1% H_2O_2 v/v. Samples were first digested in 1 mL of HNO_3/ 0.4 mL of HCl and heated at 115 °C for 5 min using a hot block (DigiPREP System; SCP Science, Champlain, NY). Then, 0.4 mL of H_2O_2 was added and incubated for an additional 10 min. The solution was further diluted and analyzed by ICP-MS (Agilent 7700x ICP-

MS) to quantify the content of Cd and Te. Individual element concentrations were calculated in μg g^{-1} (element mass in μg per gram of dry chloroplast mass).

Statistical analysis

All data were represented as mean ± SD (n = biological replicates) and analyzed using SPSS 23.0. One-way ANOVA performed comparisons based on Duncan's multiple range test (two-tailed). All data were subjected to normal distribution tests by using non-parametric tests based on 1-Sample K-S (Kolmogorov-Smirnov test). Different lower-case letters mean significance at $P < 0.05$.

Results

Quantum dots with rationally designed guiding peptide

Multifunctional fluorescent QD acted as traceable chemical delivery platforms by forming inclusion complexes with chemicals such as methyl viologen (MV) and ascorbic acid (Asc) on their surface through conjugated β-cyclodextrins (β-CD) molecular baskets (Supplementary Figure. 3.1). The delivery of MV and Asc by QD allowed tunable changes in chloroplast redox status by inducing or reducing superoxide anion production in this organelle with high specificity (Figure 3.1a). The manipulation of chloroplast redox status has been associated with wide genetic and physiological responses in plants (Pierella Karlusich et al. 2017). A conserved chloroplast targeting peptide, rationally designed from Rubisco small subunit 1 A (RbcS, genbank: OAP15425), was used to functionalize fluorescent QD for targeting chloroplasts in intact leaves of plants *in vivo*

(Figure. 3.1b–d). To our knowledge, this is the first time a nanoparticle has been guided to a specific subcellular compartment in plants (e.g., chloroplasts) by mimicking the biorecognition mechanisms used for protein precursor delivery. An alignment of the peptide amino acid sequence with RbcS-peptide analogs from multiple dicotyledonous plant species indicated a high degree of conservation in its composition and sequence across crop and model plants (Figure. 3.1b, c). The RbcS transit peptide enabled cytosolic recognition of proteins destined for import into plastids by the chloroplast outer membrane translocon TOC159 (Figure. 3.1a) (Lee et al. 2015). TOCs recognize the N-binding domain of most pre-proteins destined to plastids and function in coordination with translocons at the inner membrane of chloroplasts (TICs) to allow the import of pre-proteins into the chloroplast stroma (Richardson et al. 2014). Our ENM targeting sequence was truncated to the first 14 amino acids to minimize the increase in hydrodynamic diameter of functionalized QD and improve the penetration through leaf cell wall pores (Figure. 3.1d) (Mccann et al. 1990) . A short sequence containing GGC was added to the C-terminal of the peptide as a spacer. The terminal cysteine residue was further utilized as a conjugation site to bind with an NHS-PEG4-MAL (succinimidyl-[(N-maleimidopropionamido)-tetraethyleneglycol] ester) linker onto the QD (Figure. 3.1d). The first 14 amino acids from the RbcS peptide sequence used to guide nanoparticles are highly conserved among dicots and contain functional biorecognition motifs allowing translocation across the chloroplast double membranes (Lee et al. 2015; Lee et al. 2009). Thus, this targeted nanoparticle approach using RbcS-peptides is likely to have broad applicability in dicot plant species.

QDs with β-cyclodextrin molecular baskets conjugated with targeting peptides (Chl-QD) allow the targeted delivery of biochemical cargoes into chloroplasts. The β-CD molecular basket composed of seven cyclic oligosaccharides enables "host-guest" formation with ascorbic acid or methyl viologen (Saha et al. 2016; Szejtli 1998) and can form inclusion complexes with a broad range of biomolecules and chemicals including metabolic intermediates (β-carotenes), or herbicides (MCPA and norflurazon) (Supplementary Table 1). At the terminal amine group located on the β-CD, a succinimidyl-dPEG-maleimide linker (NHS-PEG_4-MAL) was added, providing a selective conjugation site for cysteine residues located on the transit peptide. The QD core size of 4.3 ± 0.2 nm (± indicates standard deviation, n = 3) measured by transmission electron microscopy (TEM) (Figure. 3.2a), and the Chl-QD average hydrodynamic diameter of 24.5 ± 2.5 nm (± indicates standard deviation, n = 5) measured by dynamic light scattering (DI water, pH 7) (Figure. 3.2b) were under the maximum size for nanomaterials reported to translocate across leaf cell walls (Mccann et al. 1990; Avellan et al. 2019). The synthesized Chl-QD were negatively charged with a zeta potential of −28.4 ± 3.8 mV (± indicates standard deviation, n = 17) in DI water (pH 7) (Figure. 3.2c) to facilitate translocation across plant lipid membranes. Nanoparticles with high zeta potential have been reported to penetrate through chloroplast envelopes passively and plant cell membranes (Kwak et al. 2019; Giraldo et al. 2014; Wong et al. 2016; Lew et al. 2018). Furthermore, QD has a high and stable fluorescence enabling *in vivo* tracking within plant tissues and cellular compartments (Li et al. 2018). The Chl-QD fluorescence peak was tuned to 540 nm to reduce interference with leaf background and fluorescent

dyes used in this study (Figure. 3.2d). The QD exhibited a characteristic absorption peak at 465 nm in the UV-vis absorption spectrum (Supplementary Figure. 3.2a). In Fourier transmittance infrared spectra (FTIR) (Figure. 3.2e), significant characteristic bands for asymmetric glycosidic vibration (C–O–C) denoting β-cyclodextrin were detected at 1058 cm^{-1}, and bands typical of type I and II amide bonds at 1615 and 1515 cm^{-1} supported successful conjugation of β-cyclodextrin and RbcS peptide on QD surface forming Chl-QD.

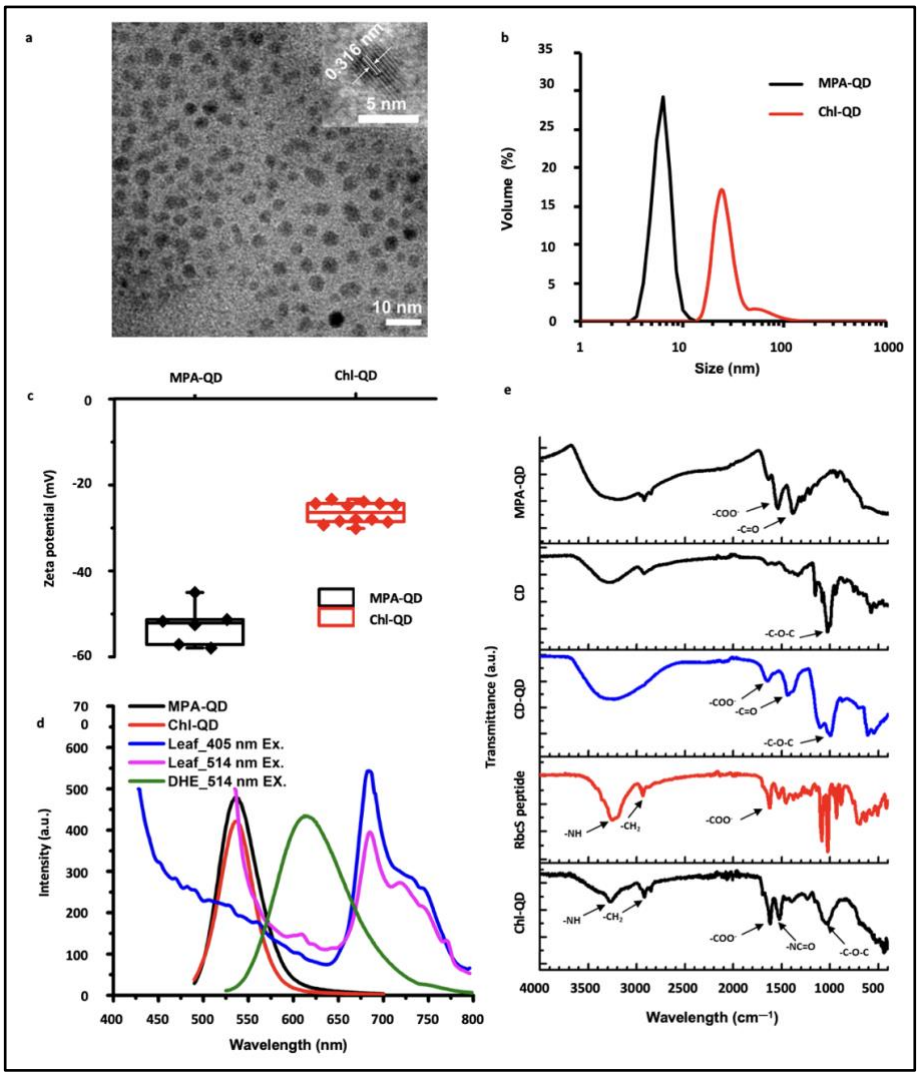

Figure. 3.2 Design and characterization of multifunctional quantum dots with chloroplast guiding peptide. a, Representative transmission electron microscopy image of MPA-QD showing the average diameter of the QD nanoparticle core of 4.3 ± 0.5 nm. b, Hydrodynamic diameter measured by DLS (pH 7) of MPA-QD (6.1 ± 0.5 nm) and Chl-QD (24.8 ± 2.3 nm). c, High zeta potential of MPA-QD (-52.6 ± 4.7 mV) and Chl-QD (-28.4 ± 3.8 mV) allows penetration through lipid bilayers in the cell membrane and chloroplasts. d, Fluorescence emission spectra of MPA-QD and Chl-QD measured in the range of low background fluorescence emission from leaves. e, FTIR spectra of MPA-QD, β-cyclodextrin (β-CD) coated QD (CD-QD) and Chl-QD indicating successful functionalization of QDs with β-CD and guiding peptide. n= 7-12.

Biorecognition Targeted Delivery of Nanoparticles *In Vivo*

The localization between Chl-QD and chloroplasts in leaf mesophyll cells of *Arabidopsis* plants was assessed by confocal fluorescence microscopy. QD lacking the targeting peptide (MPA-QD) and QD functionalized with a randomized RbcS sequence (R-QD, ASLSSMMATSGVGMC) were tested to validate the role of the conjugated chloroplast targeting peptide sequence on Chl-QD localization in plants. We found similar chloroplast colocalization rates between MPA-QD (37.6 ± 4.2 %) and R-QD (38.9 ± 3.9 %) (Figure 3.3a). In contrast, we observed a two times higher percentage of chloroplasts containing Chl-QD coated with the guiding peptide (74.6 ± 10.8 %) (Figure 3.3a-b). No QD fluorescence was detected in buffer-treated plants (Supplemental Figure S3.3). The spatial distribution of QD within chloroplasts was visualized by orthogonal views which are constructed from multiple Z-stack images (Figure 3.3c, supplemental Figure S3.4, Supplementary video 1) collected at 2 μm per scanning layer, which is smaller than *Arabidopsis* chloroplast size (5-10 μm) (Wu et al. 2017). These results demonstrate that our truncated RbcS-peptide guided the QD to chloroplasts with high targeted nanoparticle delivery efficiency and specificity in plants. Interestingly, the zeta potential of Chl-QD is significantly lower than MPA-QD (Figure 3.2c) indicating that models based on increased nanoparticle charge for promoting chloroplast delivery (Kwak et al. 2019; Wong et al. 2016; Lew et al. 2018) are not sufficient to predict plant organelle localization of nanomaterials guided by biomolecule recognition motifs in plants *in vivo*.

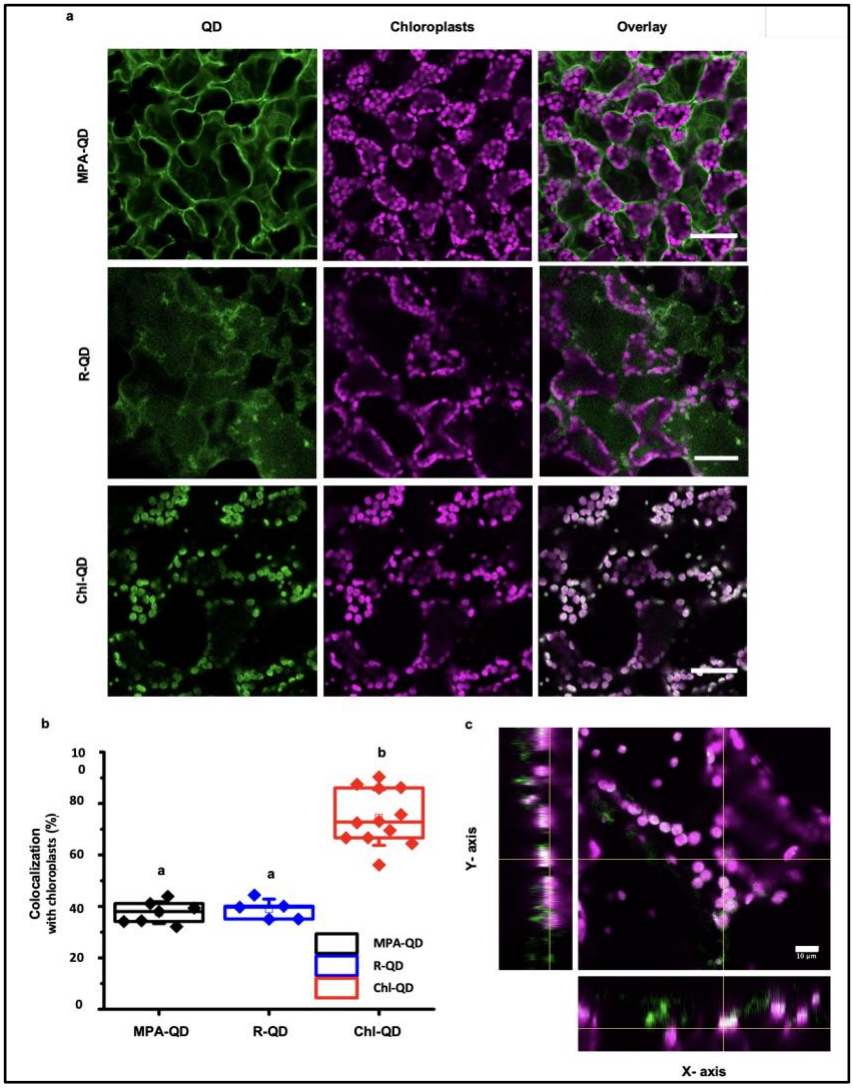

Figure. 3.3 Targeted delivery of quantum dots to chloroplasts of *Arabidopsis* leaf mesophyll cells. a, Confocal microscopy images of chloroplasts in leaf mesophyll cells indicating a higher degree of colocalization of QD coated with guiding peptide (Chl-QD) with chloroplasts compared to QD without targeting peptide (MPA-QD) and QDs coated with a randomized amino acid sequence of the guiding peptide (R-QD). Scale bar, 40 µm. b, Colocalization rates of Chl-QD with chloroplasts compared to MPA-QD and R-QD (n= 5-12). c, Orthogonal views of different planes from confocal images (z-stack) of Chl-QD colocalization within chloroplasts. Scale bar, 10 µm.

Detection of Quantum Dots in Isolated Chloroplasts by Confocal Microscopy and Inductively Coupled Plasma – Mass Spectrometry (ICP-MS)

The presence of QD core elements, Cadmium (Cd) and Tellurium (Te), was confirmed by ion coupled plasma mass spectrometry (ICP-MS) of isolated chloroplasts from leaves treated with Chl-QD and controls. Chloroplasts from *Arabidopsis* plants treated *in vivo* with Chl-QD (500 nM) or 10 mM TES buffer (pH 7.0) controls were isolated and imaged by confocal microscopy to record QD fluorescence (Figure 3.4a). The concentration of Cd and Te measured by ICP-MS in Chl-QD treated samples was 32.8 ± 6.71 ppm and 12.02 ± 3.03 ppm, respectively (Figure 3.4b). In contrast, controls contained negligible amounts of Cd and Te 0.23 ± 12 and 0.36 ± 3.03 ppm, respectively. Together, confocal microscopy and ICP-MS analysis demonstrate that nanomaterials coated with chloroplast transit peptide motifs (Chl-QD) translocate in leaf mesophyll cells and localize within chloroplasts (Figure 3.3 - 3.4). The Chl-QD (200 nM) were also biocompatible in *Arabidopsis* leaves in which we did not observe toxicity effects in mesophyll cells up to 24 hr measured by staining the nuclei of dead cells with PI (propidium iodide) dye (Supplemental Figure 3.5).

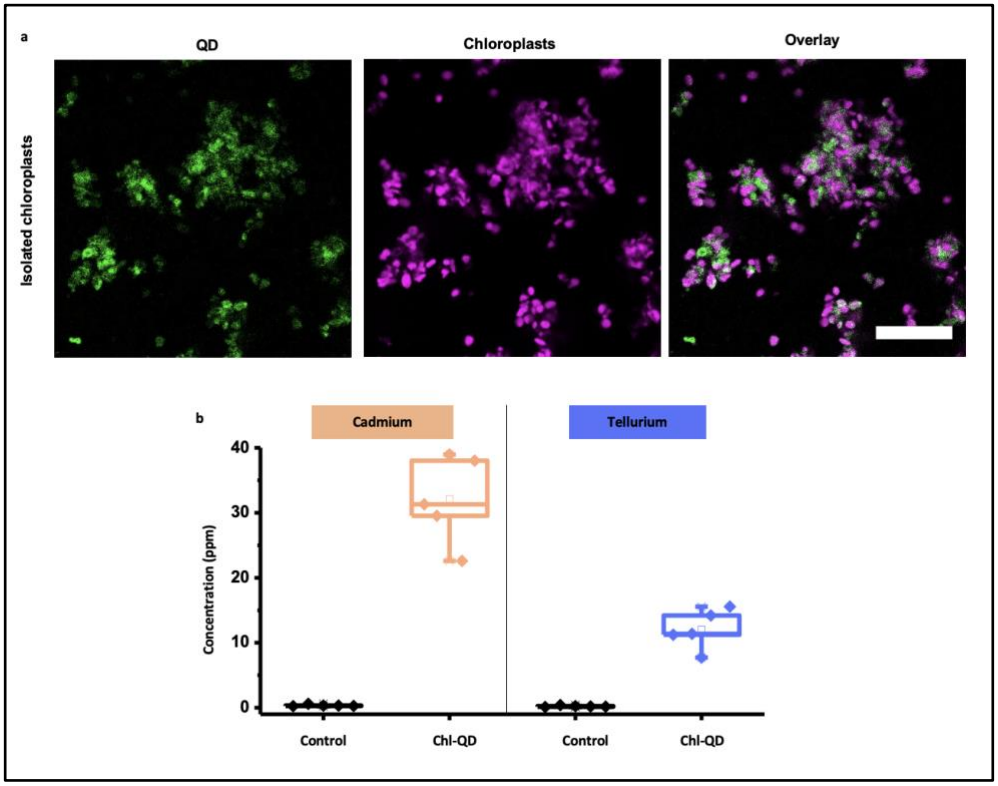

Figure. 3.4 Detection of quantum dots in isolated chloroplasts by confocal microscopy and inductively coupled plasma–mass spectrometry (ICP-MS). a, Confocal fluorescence microscopy images of isolated chloroplasts that were targeted *in vivo* with Chl-QD. b, ICP-MS elemental analysis of cadmium and tellurium in isolated chloroplasts from plant leaves exposed to CdTe quantum dots (Chl-QD) and controls infiltrated with TES buffer. n= 4 – 5. Scale, 50 μm.

Chloroplast Specific Tuning of Oxidative Status by Targeted Delivery of Nanoparticles with Chemical Cargoes

As a proof of concept, we demonstrate that targeted biochemical delivery to chloroplasts using Chl-QD allows tunable changes in the redox status of these organelles. Chloroplast function is intrinsically related to generating reactive oxygen species (ROS) (Foyer and Noctor 2003). ROS plays a dual role in plants as signaling or damaging

molecules (Mittler 2017). ROS accumulation in chloroplasts leads to declines in photosynthesis, plant growth, and yield (Foyer and Shigeoka 2011). However, understanding the role of ROS in chloroplasts has been limited to research in plant model species amenable for genetic engineering and in mutants that often suffer from impaired growth and development (Ohno et al. 2004; Sparkes et al. 2003). To enable the manipulation of ROS levels in chloroplasts of wild-type plants *in vivo*, Chl-QD were loaded either with methyl viologen (MV) to generate superoxide anion in chloroplasts (Hawkes 2014) or ascorbic acid (Asc), a known scavenger of superoxide anion (Akram et al. 2017).

The absorption spectra of MV-Chl-QD and Asc-Chl-QD (Supplementary Figure 3.2b) indicate the initial loading (60 μM) of MV or Asc in Chl-QD solution (Supplementary Figure S3.2c, d). In addition, we assessed the binding between cyclodextrin-coated QD (CD-QD) and MPA-QD to Asc or MV by isothermal titration calorimetry (ITC) (Figure. 3.5a, b, Supplementary Figure S3.6a, b). ITC experimental data and best-fit binding curves of MV and Asc with CD-QD (Figure. 3.5a, b) provided the stoichiometry for calculating the number of binding sites (N), association constants (Ka), dissociation constants (Kd), enthalpy (ΔH), and entropy (ΔS) changes (Table 1).

The ITC analysis yielded that CD-QD has a higher binding affinity to both Asc and MV than MPA-QD as indicated by lower dissociation constants or more binding sites per particle (Table 1, Supplementary Figure S3.6). The Kd of 3.98×10^{-5} M for CD-QD and Asc is lower than that for MPA-QD, and Asc (Kd = 5.52×10^{-5} M), and the number of binding sites on CD-QD for Asc (5130) is 10 times higher than MPA-QD. Although

the Kd for CD-QD and MV (4.76×10^{-5} M) is similar to that for MPA-QD and MV (Kd = 4.81×10^{-5} M), the number of binding sites on CD-QD of 1580 for MV is more than 3 times higher than MPA-QD. The lower dissociation constant of Asc (Kd = 3.98×10^{-5} M) to CD-QD than MV (Kd = 4.76×10^{-5} M) is likely due to the high –OH group association between Asc and the cyclodextrin rim (Saha et al., 2016).

Furthermore, the Kd values for CD-QD are also an order of magnitude lower than that for β-CD reported by previous studies (10^{-4}–10^{-3} M) (Diaz et al., 1988; Mirzoian & Kaifer, 1997; Saha et al., 2016), indicating a higher binding affinity of CD-QD than β-CD to Asc and MV. The increase in the number of binding sites for Asc and MV on CD-QD reflects the ability of cyclodextrin molecules on these particles to act as molecular baskets for the loading and delivery of biomolecules. As a result of either lower dissociation constant or more binding sites of CD-QD to Asc and MV (Table 1), the calculated fraction of bound Asc (96.05%) and MV (84.78%) onto the CD-QD was significantly increased relative to that of MPA-QD lacking cyclodextrins (Asc 54.94%, MV 56.73%) (Table 2). This increase of nanoparticle inclusion complexes with chemicals such as viologens using cyclodextrins (Mirzoian & Kaifer, 1997) enables the loading and subsequent release of chemicals to intended targets in plants.

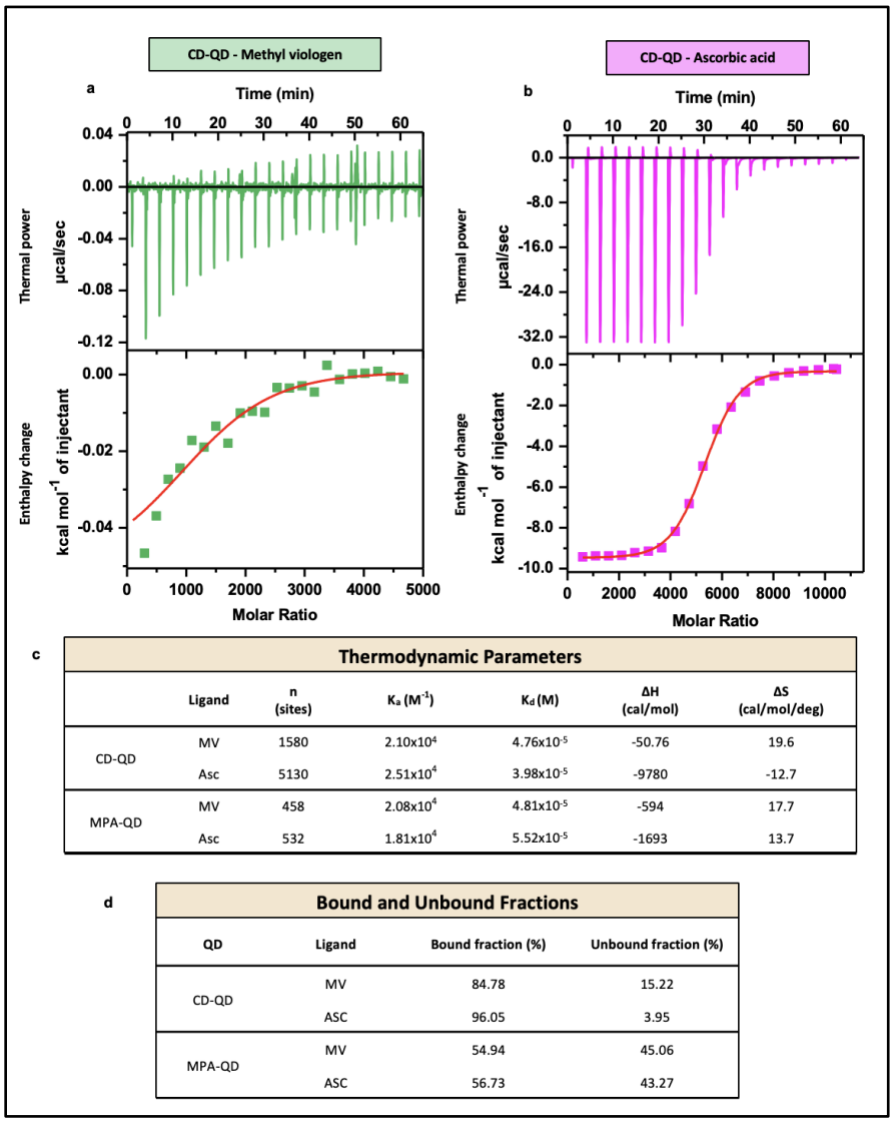

c

Thermodynamic Parameters

	Ligand	n (sites)	K_a (M^{-1})	K_d (M)	ΔH (cal/mol)	ΔS (cal/mol/deg)
CD-QD	MV	1580	2.10×10^4	4.76×10^{-5}	-50.76	19.6
	Asc	5130	2.51×10^4	3.98×10^{-5}	-9780	-12.7
MPA-QD	MV	458	2.08×10^4	4.81×10^{-5}	-594	17.7
	Asc	532	1.81×10^4	5.52×10^{-5}	-1693	13.7

d

Bound and Unbound Fractions

QD	Ligand	Bound fraction (%)	Unbound fraction (%)
CD-QD	MV	84.78	15.22
	ASC	96.05	3.95
MPA-QD	MV	54.94	45.06
	ASC	56.73	43.27

Figure. 3.5 Isothermal titration calorimetry of cyclodextrin coated quantum dot (CD-QD) with chemical cargoes. Thermograms (top) and binding isotherms (bottom) of CD-QD interacted with a, methyl viologen, and b, ascorbic acid. c, Thermodynamic parameters including the number of binding sites (n), association constant (Ka), dissociation constant (Kd), enthalpy change (ΔH), and entropy change (ΔS) of interactions between QD (CD-QD or control MPA-QD) and chemical cargoes (methyl viologen or ascorbic acid). d, The bound and unbound fractions of methyl viologen and ascorbic acid on Chl-QD.

Current methods of MV and Asc delivery in plants rely on foliar or soil absorption in aqueous solutions (Akram et al. 2017; Bromilow 2004). However, MV is a

non-selective herbicide that reacts with NADPH in the apoplast, chloroplasts, mitochondria, and peroxisome, thus non-specifically increasing both intra- and extracellular levels of superoxide anion (Cristóvão et al. 2009; Chung et al. 2008). Through confocal fluorescence microscopy in *Arabidopsis* leaf mesophyll cells, we measured the levels of ROS colocalization with chloroplasts and intensity changes using DHE (dihydroethidium) dye, a superoxide anion indicator (Figure. 3.6a). Leaves treated with MV alone exhibited superoxide anion signals both in chloroplasts and surrounding plant cell membranes and organelles. In contrast, most superoxide anion generation was detected in chloroplasts of leaves infiltrated with MV-loaded Chl-QD (MV-Chl-QD). We observed a significantly higher degree of colocalization between chloroplasts and DHE induced by MV-Chl-QD (78.8 ± 7.0%) (± indicates standard deviation, n = 7) than by MV chemical alone (32.2 ± 11.2%) (± indicates standard deviation, n = 11) ($P < 0.001$) (Supplementary Figure S3.7). In comparison with chemical application of MV (n = 4) alone or MV plus Asc (n = 10) without nanoparticles, the developed MV-Chl-QD (n = 10) and Asc-Chl-QD (n = 9) resulted in precise ROS manipulation within chloroplasts (Figure. 3.6b). Furthermore, the Chl-QD can tune the redox status of chloroplasts by MV-Chl-QD (n = 5) application that generates ROS in chloroplasts followed by Asc-Chl-QD (n = 5) that scavenges ROS in chloroplasts after 6 hr (Figure. 3.6a, c). Control experiments, in which Chl-QD (n = 3) without cargoes were infused into leaves, resulted in no changes of DHE intensity in chloroplasts, indicating that the nanoparticles alone are not responsible for the observed changes in ROS (Figure. 3.6b).

The two-fold increase in targeted delivery of chemicals by nanomaterials, from 32.2% to 78.8%, could have a significant impact on minimizing agricultural inputs in the field and pollution of the environment. It may also allow studies in plant cell biology in wild-type and non-model plants that require specific organelle engineering. For example, ENM targeted delivery of biochemicals to subcellular compartments guided by peptide recognition motifs may improve our understanding of the role of signaling molecules (e.g., ROS) in plants. By specifically manipulating levels of ROS in chloroplasts, we can gain insight into the role of this organelle in regulating redox-sensitive physiological and developmental processes (Suzuki et al. 2012). MV is a widely used herbicide, also named paraquat, that leads to toxic effects to mammalian cells due to its redox activity in mitochondria and has been linked to the development of Parkinson's disease (Berry et al. 2010). Our rational design of targeted biochemical delivery of ENM leveraging the plant molecular machinery could be utilized to create a variety of nanoparticle-targeting approaches for nano-enabled agricultural applications.

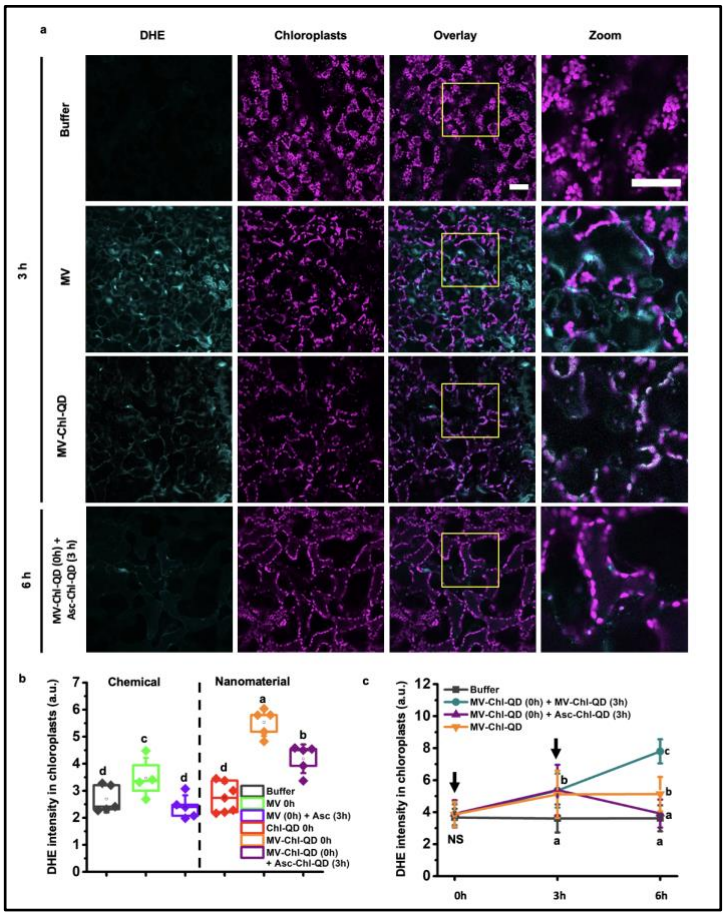

Figure. 3.6 Chloroplast specific subcellular tuning of oxidative status by targeted delivery of nanoparticles with chemical cargoes. a, Confocal microscopy images of *Arabidopsis* leaf mesophyll cells illustrating the targeted generation and scavenging of superoxide anion (detected by DHE fluorescent dye) in chloroplasts by MV-Chl-QD and Asc-Chl-QD guided by peptide recognition motifs, respectively. Scale bar, 40 µm. b, Comparison between chemical and nanotechnology-based approaches for specifically increasing superoxide in chloroplasts. DHE was used as an indicator for superoxide ROS levels after 6 h. Chemicals and nanomaterials were treated at the time points specified in the legend. c, Temporal patterns of DHE fluorescence signal intensity inside chloroplasts in leaf mesophyll cells showing the specific increase and subsequent decrease of chloroplast superoxide anion levels in plants infiltrated with MV-Chl-QD at time 0 hr and subsequently perfused with Asc-Chl-QD at time 3 hr (purple line). A steady increase in DHE intensity was observed in leaves treated with MV-Chl-QD at times 0 hr and 3 hr (cyan line). Leaves infiltrated with MV-Chl-QD at time 0h only (orange line) showed an increase in DHE signal that plateaus. Controls were performed for leaves infiltrated only with a buffer (dark grey line). Mean ± SD (n = 6-10). Lower case letters represent significance at $P < 0.05$. NS, not significant.

Conclusions:

Precise control of nanoparticle location in plants is crucial for applying nanotechnology in plant biology, biotechnology, and nano-enabled agriculture. To date, there are no approaches that leverage the plant molecular recognition machinery for controlling nanoparticle specific location and intended function in plant organelles. The use of guiding peptides provides a molecular tool for targeted nanomaterials to subcellular compartments with a precision not achieved before in plants. We demonstrated that by controlling QD size, zeta potential, and fluorescence emission range, we circumvent plant cell barriers for biochemical delivery, allowing *in vivo* tracking with low interference from leaf background. Although Cd based QD properties make them ideal for detection by multiple advanced analytical tools including confocal fluorescence microscopy and elemental analysis by ICP-MS, chronic or high-level exposure of these nanoparticles can lead to toxic effects in organisms depending on their surface properties (Oh et al. 2016). QD within the non-toxic exposure conditions of this study are useful to model nanoparticle systems for basic research at the interface of plants and nanotechnology, but applications in agriculture would require the use of environmentally friendly Cd-free QD (Brown et al., 2018). However, the QD functionalization with a peptide recognition motif demonstrates an approach to engineer targeted nanomaterials for improved colocalization within organelles and delivery of biochemicals *in vivo*. The high localization efficiency and specificity of nanomaterials enabled by biorecognition surpass that of conventional methods based on nanoparticle size and charge alone. As a result, the nanoparticle-mediated delivery of biochemicals

such as MV and Asc to chloroplasts specifically allows tuning their redox status while significantly minimizing ROS generation or scavenging in other subcellular compartments.

Although we demonstrate that biochemicals including MV and Asc are delivered to chloroplasts with high efficiency (78.8%), further research on modifying guiding peptide properties including spacer amino acids, hydrophilicity, and charge, among others, may allow enhancing the delivery specificity to plant organelles while avoiding unwanted exposure to other plant cell compartments. We expect that increasing the amino acid spacer length would be needed for nanoparticles coated with ligands larger than those used in this study (e.g., plasmid DNA, RNA). Tuning hydrophobicity of the peptide recognition motif is also likely to affect the nanoparticle translocation in plant cells as it was shown by previous studies coating nanoparticles with amphiphilic polymers (Avellan et al. 2019). Models of plant cell and chloroplast uptake based on nanoparticle size and charge alone using polymeric ligands (Wong et al. 2016; Lew et al. 2018) do not explain why Chl-QD coated with biorecognition motifs with lower zeta potential magnitude than MPA-QD exhibit higher colocalization rates with chloroplasts. This indicates that nanoparticle-plant interaction models should incorporate engineered biomolecule coatings and acquired coronas for making accurate predictions of the distribution of nanoparticles in plants.

Our comparative analysis of the designed chloroplast guiding peptide with highly conserved sequence recognition motifs in Rubisco small subunits from other plant species, suggests that biorecognition motif targeted delivery approaches can be translated

to a wide range of dicot plant species. This study highlights strategies to create nanobiotechnology tools that can bypass plant biological barriers for targeted delivery of biomolecules and chemical cargoes to chloroplasts for fundamental research in plant biology and more efficient delivery of agrochemicals to crops. The biorecognition approach of coating nanoparticles with guiding peptides for targeted delivery could be extended to other types of nanomaterials for applications including genetic element delivery and targeted delivery of sensors, nutrients or pesticides to specific plant tissues or subcellular compartments.

References

Ai, X., Niu, L., Li, Y., Yang, F., & Su, X. (2012). A Novel B-Cyclodextrin-QDs Optical Biosensor For The Determination Of Amantadine And Its Application In Cell Imaging. *Talanta*, *99*, 409–414.

Akram, N. A., Shafiq, F., & Ashraf, M. (2017). Ascorbic Acid-A Potential Oxidant Scavenger And Its Role In Plant Development And Abiotic Stress Tolerance. *Frontiers In Plant Science*, *8*, 613.

Avellan, A., Yun, J., Zhang, Y., Spielman-Sun, E., Unrine, J. M., Thieme, J., Li, J., Lombi, E., Bland, G., & Lowry, G. V. (2019). Nanoparticle Size And Coating Chemistry Control Foliar Uptake Pathways, Translocation, And Leaf-To-Rhizosphere Transport In Wheat. *ACS Nano*, *13*(5), 5291–5305.

Baligar, V. C., Fageria, N. K., & He, Z. L. (2001). Nutrient Use Efficiency In Plants. *Communications In Soil Science And Plant Analysis*, *32*(7-8), 921–950.

Berry, C., La Vecchia, C., & Nicotera, P. (2010). Paraquat And Parkinson's Disease. *Cell Death And Differentiation*, *17*(7), 1115–1125.

Bisswanger, H. (2017). *Enzyme Kinetics: Principles And Methods*. John Wiley & Sons. *3*(2), 27.

Bobik, K., & Burch-Smith, T. M. (2015). Chloroplast Signaling Within, Between And Beyond Cells. *Frontiers In Plant Science*, *6*, 781.

Bock, R. (2014). Genetic Engineering Of The Chloroplast: Novel Tools And New Applications. *Current Opinion In Biotechnology*, *26*, 7–13.

Borgatta, J., Ma, C., Hudson-Smith, N., Elmer, W., Plaza Pérez, C. D., De La Torre-Roche, R., Zuverza-Mena, N., Haynes, C. L., White, J. C., & Hamers, R. J. (2018). Copper Based Nanomaterials Suppress Root Fungal Disease In Watermelon (*Citrullus Lanatus*): Role Of Particle Morphology, Composition, And Dissolution Behavior. *ACS Sustainable Chemistry & Engineering*, *6*(11), 14847–14856.

Bromilow, R. H. (2004). Paraquat And Sustainable Agriculture. *Pest Management Science*, *60*(4), 340–349.

Brown, R. P., Gallagher, M. J., Fairbrother, D. H., & Rosenzweig, Z. (2018). Synthesis And Degradation Of Cadmium-Free InP And InPZn/ZnS Quantum Dots In Solution. *Langmuir: The ACS Journal Of Surfaces And Colloids*, *34*(46), 13924–13934.

Chung, J.-S., Zhu, J.-K., Bressan, R. A., Hasegawa, P. M., & Shi, H. (2008). Reactive

Oxygen Species Mediate Na+-Induced *sos*1 mRNA Stability In *Arabidopsis*. *The Plant Journal: For Cell And Molecular Biology*, *53*(3), 554–565.

Cristóvão, A. C., Choi, D.-H., Baltazar, G., Beal, M. F., & Kim, Y.-S. (2009). The Role Of NADPH Oxidase 1-Derived Reactive Oxygen Species In Paraquat-Mediated Dopaminergic Cell Death. *Antioxidants & Redox Signaling*, *11*(9), 2105–2118.

Dai, Q., Wilhelm, S., Ding, D., Syed, A. M., Sindhwani, S., Zhang, Y., Chen, Y. Y., Macmillan, P., & Chan, W. C. W. (2018). Quantifying The Ligand-Coated Nanoparticle Delivery To Cancer Cells In Solid Tumors. *ACS Nano*, *12*(8), 8423–8435.

Demirer, G. S., Zhang, H., Matos, J. L., Goh, N. S., Cunningham, F. J., Sung, Y., Chang, R., Aditham, A. J., Chio, L., Cho, M.-J., Staskawicz, B., & Landry, M. P. (2019). High Aspect Ratio Nanomaterials Enable Delivery Of Functional Genetic Material Without DNA Integration In Mature Plants. *Nature Nanotechnology*, *14*(5), 456–464.

Diaz, A., Quintela, P. A., Schuette, J. M., & Kaifer, A. E. (1988). Complexation Of Redox-Active Surfactants By Cyclodextrins. *The Journal Of Physical Chemistry*, *92*(12), 3537–3542.

Foyer, C. H., & Noctor, G. (2003). Redox Sensing And Signalling Are Associated With Reactive Oxygen In Chloroplasts, Peroxisomes And Mitochondria. *Physiologia Plantarum*, *119*(3), 355–364.

Foyer, C. H., & Shigeoka, S. (2011). Understanding Oxidative Stress And Antioxidant Functions To Enhance Photosynthesis. *Plant Physiology*, *155*(1), 93–100.

Giraldo, J. P., Landry, M. P., Faltermeier, S. M., Mcnicholas, T. P., Iverson, N. M., Boghossian, A. A., Reuel, N. F., Hilmer, A. J., Sen, F., Brew, J. A., & Strano, M. S. (2014). Plant Nanobionics Approach To Augment Photosynthesis And Biochemical Sensing. *Nature Materials*, *13*(4), 400–408.

Giraldo, J. P., Landry, M. P., Kwak, S.-Y., Jain, R. M., Wong, M. H., Iverson, N. M., Ben-Naim, M., & Strano, M. S. (2015). A Ratiometric Sensor Using Single Chirality Near-Infrared Fluorescent Carbon Nanotubes: Application To In Vivo Monitoring. *Small*, *11*(32), 3973–3984.

Giraldo, J. P., Wu, H., Newkirk, G. M., & Kruss, S. (2019). Nanobiotechnology Approaches For Engineering Smart Plant Sensors. *Nature Nanotechnology*, *14*(6), 541–553.

Gogotsi, Y. (2018). Moving Ions Confined Between Graphene Sheets [Review Of *Moving Ions Confined Between Graphene Sheets*]. *Nature Nanotechnology*, *13*(8),

625–627.

Hawkes, T. R. (2014). Mechanisms Of Resistance To Paraquat In Plants. *Pest Management Science*, *70*(9), 1316–1323.

Jia, L., Xu, J.-P., Li, D., Pang, S.-P., Fang, Y., Song, Z.-G., & Ji, J. (2010). Fluorescence Detection Of Alkaline Phosphatase Activity With B-Cyclodextrin-Modified Quantum Dots. *Chemical Communications*, *46*(38), 7166–7168.

Jin, S., & Daniell, H. (2015). The Engineered Chloroplast Genome Just Got Smarter. *Trends In Plant Science*, *20*(10), 622–640.

Kah, M., Tufenkji, N., & White, J. C. (2019). Nano-Enabled Strategies To Enhance Crop Nutrition And Protection. *Nature Nanotechnology*, *14*(6), 532–540.

Kwak, S.-Y., Giraldo, J. P., Wong, M. H., Koman, V. B., Lew, T. T. S., Ell, J., Weidman, M. C., Sinclair, R. M., Landry, M. P., Tisdale, W. A., & Strano, M. S. (2017). A Nanobionic Light-Emitting Plant. *Nano Letters*, *17*(12), 7951–7961.

Kwak, S.-Y., Lew, T. T. S., Sweeney, C. J., Koman, V. B., Wong, M. H., Bohmert-Tatarev, K., Snell, K. D., Seo, J. S., Chua, N.-H., & Strano, M. S. (2019). Chloroplast-Selective Gene Delivery And Expression In Planta Using Chitosan-Complexed Single-Walled Carbon Nanotube Carriers. *Nature Nanotechnology*, *14*(5), 447–455.

Lee, D. W., Lee, S., Oh, Y. J., & Hwang, I. (2009). Multiple Sequence Motifs In The Rubisco Small Subunit Transit Peptide Independently Contribute To Toc159-Dependent Import Of Proteins Into Chloroplasts. *Plant Physiology*, *151*(1), 129–141.

Lee, D. W., Woo, S., Geem, K. R., & Hwang, I. (2015). Sequence Motifs In Transit Peptides Act As Independent Functional Units And Can Be Transferred To New Sequence Contexts. *Plant Physiology*, *169*(1), 471–484.

Lew, T. T. S., Wong, M. H., Kwak, S.-Y., Sinclair, R., Koman, V. B., & Strano, M. S. (2018). Rational Design Principles For The Transport And Subcellular Distribution Of Nanomaterials Into Plant Protoplasts. *Small*, *14*(44), e1802086.

Li, B., Li, G., Kronzucker, H. J., Baluška, F., & Shi, W. (2014). Ammonium Stress In *Arabidopsis*: Signaling, Genetic Loci, And Physiological Targets. *Trends In Plant Science*, *19*(2), 107–114.

Li, J., Lee, W. Y., Wu, T., Xu, J., Zhang, K., Li, G., Xia, J., & Bian, L. (2016). Multifunctional Quantum Dot Nanoparticles For Effective Differentiation And Long-Term Tracking Of Human Mesenchymal Stem Cells In Vitro And In Vivo. *Advanced*

Healthcare Materials, *5*(9), 1049–1057.

Li, J., Wu, H., Santana, I., Fahlgren, M., & Giraldo, J. P. (2018). Standoff Optical Glucose Sensing In Photosynthetic Organisms By A Quantum Dot Fluorescent Probe. *ACS Applied Materials & Interfaces*. *10*(34), 28279–28289.

Liu, Q., Chen, B., Wang, Q., Shi, X., Xiao, Z., Lin, J., & Fang, X. (2009). Carbon Nanotubes As Molecular Transporters For Walled Plant Cells. *Nano Letters*, *9*(3), 1007–1010.

Lowry, G. V., Avellan, A., & Gilbertson, L. M. (2019). Opportunities And Challenges For Nanotechnology In The Agri-Tech Revolution. *Nature Nanotechnology*, *14*(6), 517–522.

Mangadlao, J. D., Wang, X., Mccleese, C., Escamilla, M., Ramamurthy, G., Wang, Z., Govande, M., Basilion, J. P., & Burda, C. (2018). Prostate-Specific Membrane Antigen Targeted Gold Nanoparticles For Theranostics Of Prostate Cancer. *ACS Nano*, *12*(4), 3714–3725.

Mccann, M. C., Wells, B., & Roberts, K. (1990). Direct Visualization Of Cross-Links In The Primary Plant Cell Wall. *Journal Of Cell Science*, *96*(2), 323–334.

Mirzoian, A., & Kaifer, A. E. (1997). Reactive Pseudorotaxanes: Inclusion Complexation Of Reduced Viologens By The Hosts B-Cyclodextrin And Heptakis(2,6-Di-O-Methyl)-B-Cyclodextrin. *Chemistry: A European Journal*, *3*(7), 1052–1058.

Mittler, R. (2017). ROS Are Good. *Trends In Plant Science*, *22*(1), 11–19.

Newkirk, G. M., Wu, H., Santana, I., & Giraldo, J. P. (2018). Catalytic Scavenging Of Plant Reactive Oxygen Species In Vivo By Anionic Cerium Oxide Nanoparticles. *Journal Of Visualized Experiments: JOVE*, *138*, E58373.

Oh, E., Liu, R., Nel, A., Gemill, K. B., Bilal, M., Cohen, Y., & Medintz, I. L. (2016). Meta-Analysis Of Cellular Toxicity For Cadmium-Containing Quantum Dots. *Nature Nanotechnology*, *11*(5), 479–486.

Ohno, C. K., Reddy, G. V., Heisler, M. G. B., & Meyerowitz, E. M. (2004). The *Arabidopsis* Jagged Gene Encodes A Zinc Finger Protein That Promotes Leaf Tissue Development. *Development*, *131*(5), 1111–1122.

Pierella Karlusich, J. J., Zurbriggen, M. D., Shahinnia, F., Sonnewald, S., Sonnewald, U., Hosseini, S. A., Hajirezaei, M.-R., & Carrillo, N. (2017). Chloroplast Redox Status Modulates Genome-Wide Plant Responses During The Non-Host Interaction Of Tobacco With The Hemibiotrophic Bacterium *Xanthomonas Campestris Pv*.

Vesicatoria. *Frontiers In Plant Science*, *8*, 1158.

Richardson, L. G. L., Paila, Y. D., Siman, S. R., Chen, Y., Smith, M. D., & Schnell, D. J. (2014). Targeting And Assembly Of Components Of The TOC Protein Import Complex At The Chloroplast Outer Envelope Membrane. *Frontiers In Plant Science*, *5*, 269.

Rodrigues, S. S. M., Ribeiro, D. S. M., Molina-Garcia, L., Ruiz Medina, A., Prior, J. A. V., & Santos, J. L. M. (2014). Fluorescence Enhancement Of CdTe MPA-Capped Quantum Dots By Glutathione For Hydrogen Peroxide Determination. *Talanta*, *122*, 157–165.

Ryan, J. A., Overton, K. W., Speight, M. E., Oldenburg, C. N., Loo, L., Robarge, W., Franzen, S., & Feldheim, D. L. (2007). Cellular Uptake Of Gold Nanoparticles Passivated With BSA−SV40 Large T Antigen Conjugates. *Analytical Chemistry*, *79*(23), 9150–9159.

Saha, S., Roy, A., Roy, K., & Roy, M. N. (2016). Study To Explore The Mechanism To Form Inclusion Complexes Of B-Cyclodextrin With Vitamin Molecules. *Scientific Reports*, *6*, 35764.

Schwab, F., Zhai, G., Kern, M., Turner, A., Schnoor, J. L., & Wiesner, M. R. (2016). Barriers, Pathways, And Processes For Uptake, Translocation And Accumulation Of Nanomaterials In Plants-Critical Review. *Nanotoxicology*, *10*(3), 257–278.

Sebilo, M., Mayer, B., Nicolardot, B., Pinay, G., & Mariotti, A. (2013). Long-Term Fate Of Nitrate Fertilizer In Agricultural Soils. *Proceedings Of The National Academy Of Sciences Of The United States Of America*, *110*(45), 18185–18189.

Smith, A. M., & Gilbertson, L. M. (2018). Rational Ligand Design To Improve Agrochemical Delivery Efficiency And Advance Agriculture Sustainability. *ACS Sustainable Chemistry & Engineering*, *6*(11), 13599–13610.

Sparkes, I. A., Brandizzi, F., Slocombe, S. P., El-Shami, M., Hawes, C., & Baker, A. (2003). An *Arabidopsis* Pex10 Null Mutant Is Embryo Lethal, Implicating Peroxisomes In An Essential Role During Plant Embryogenesis. *Plant Physiology*, *133*(4), 1809–1819.

Stothard, P. (2000). The Sequence Manipulation Suite: Javascript Programs For Analyzing And Formatting Protein And DNA Sequences. *Biotechniques*, *28*(6), 1102, 1104.

Suzuki, N., Koussevitzky, S., Mittler, R., & Miller, G. (2012). ROS And Redox Signalling In The Response Of Plants To Abiotic Stress: ROS And Redox Signalling

In Plants. *Plant, Cell & Environment*, *35*(2), 259–270.

Szejtli, J. (1998). Introduction And General Overview Of Cyclodextrin Chemistry. *Chemical Reviews*, *98*(5), 1743–1754.

Torney, F., Trewyn, B. G., Lin, V. S.-Y., & Wang, K. (2007). Mesoporous Silica Nanoparticles Deliver DNA And Chemicals Into Plants. *Nature Nanotechnology*, *2*(5), 295–300.

Wang, J. W., Grandio, E. G., Newkirk, G. M., Demirer, G. S., Butrus, S., Giraldo, J. P., & Landry, M. P. (2019). Nanoparticle-Mediated Genetic Engineering Of Plants. *Molecular Plant*, *12*(8), 1037–1040.

Wang, P., Lombi, E., Zhao, F.-J., & Kopittke, P. M. (2016). Nanotechnology: A New Opportunity In Plant Sciences. *Trends In Plant Science*, *21*(8), 699–712.

Wang, Q., Huang, X., Long, Y., Wang, X., Zhang, H., Zhu, R., Liang, L., Teng, P., & Zheng, H. (2013). Hollow Luminescent Carbon Dots For Drug Delivery. *Carbon*, *59*, 192–199.

Weise, S. E., Weber, A. P. M., & Sharkey, T. D. (2004). Maltose Is The Major Form Of Carbon Exported From The Chloroplast At Night. *Planta*, *218*(3), 474–482.

Wong, M. H., Giraldo, J. P., Kwak, S.-Y., Koman, V. B., Sinclair, R., Lew, T. T. S., Bisker, G., Liu, P., & Strano, M. S. (2017). Nitroaromatic Detection And Infrared Communication From Wild-Type Plants Using Plant Nanobionics. *Nature Materials*, *16*(2), 264–272.

Wong, M. H., Misra, R. P., Giraldo, J. P., Kwak, S.-Y., Son, Y., Landry, M. P., Swan, J. W., Blankschtein, D., & Strano, M. S. (2016). Lipid Exchange Envelope Penetration (Leep) Of Nanoparticles For Plant Engineering: A Universal Localization Mechanism. *Nano Letters*, *16*(2), 1161–1172.

Wu, H., Santana, I., Dansie, J., & Giraldo, J. P. (2017). In Vivo Delivery Of Nanoparticles Into Plant Leaves. *Current Protocols In Chemical Biology*, *9*(4), 269–284.

Wu, H., Shabala, L., Shabala, S., & Giraldo, J. P. (2018). Hydroxyl Radical Scavenging By Cerium Oxide Nanoparticles Improves *Arabidopsis* Salinity Tolerance By Enhancing Leaf Mesophyll Potassium Retention. *Environmental Science: Nano*, *5*(7), 1567–1583.

Wu, H., Tito, N., & Giraldo, J. P. (2017). Anionic Cerium Oxide Nanoparticles Protect Plant Photosynthesis From Abiotic Stress By Scavenging Reactive Oxygen Species.

ACS Nano, *11*(11), 11283–11297.

Yu, W. W., Qu, L., Guo, W., & Peng, X. (2003). Experimental Determination Of The Extinction Coefficient Of CdTe, CdDe, And CdS Nanocrystals. *Chemistry Of Materials: A Publication Of The American Chemical Society*, *15*(14), 2854–2860.

Zhou, D., Lin, M., Chen, Z., Sun, H., Zhang, H., Sun, H., & Yang, B. (2011). Simple Synthesis Of Highly Luminescent Water-Soluble CdTe Quantum Dots With Controllable Surface Functionality. *Chemistry Of Materials: A Publication Of The American Chemical Society*, *23*(21), 4857–4862.

Chapter 4: Impact of Chloroplast Targeted Carbon Nanomaterials on Plant Cell Structure and Function And Molecular Biology

Israel Santana[1], Christopher Castillo[1], Gail F. Garcia[1], Gregory M. Newkirk[2], Su-Ji Jeon[1], Juan Pablo Giraldo[1*].

Affiliations:

[1]Department of Botany and Plant Sciences, University of California-Riverside, Riverside, California United States, 92521, [2]Department of Microbiology and Plant Pathology, University of California-Riverside, Riverside, CA, United States, Riverside, 92521, USA.

Corresponding Email: juanpablo.giraldo@ucr.edu; Tel: +1 9518273583

Abstract

The increasing demand for food production requires novel and sustainable technologies for efficient agrochemical and biomolecule delivery into plants. We developed targeted carbon-based nanomaterials as tools for precise chemical delivery (carbon dots, CD) and gene delivery platforms (single-walled carbon nanotubes, SWCNT) to chloroplasts. Chloroplasts are at the forefront of plant nanotechnology applications to improve agriculture due to their main role as a metabolic hub, housing photosynthetic reactions, assimilation of nutrients, and target of agrochemicals to enhance yields. A biorecognition approach of coating the nanomaterials with a rationally designed chloroplast targeting peptide improved the delivery of carbon dots (Targeting

peptide carbon dots with cyclodextrin baskets, TP-β-CD) with molecular baskets that can carry a wide range of agrochemicals, and plasmid DNA coated SWCNT (Targeted single-walled carbon nanotubes with GFP encoding plasmid, TP-pATV1-SWCNT) up to 69.9 ± 9.457 % and 56.85 ± 4.577 % for delivery to chloroplasts in plants, respectively. To engineer biocompatible targeted nanomaterials, we investigated targeted nanomaterial impact on molecular and cell biology in the plant model system *Arabidopsis thaliana* through foliar spraying application. There was no significant difference in the percentage of dead cells in plants treated with 20 mg/L and 2 mg/L of TP-β-CD or TP-pATV1-SWCNT, respectively. To visualize and quantify the percentage of intact chloroplast membranes we used differential interference contrast microscopy. Herein, we showed no significant damage to chloroplast membrane intactness after five days post treatments. However, targeted nanomaterials transiently increased leaf H_2O_2 levels 7-fold above those of controls without nanoparticles at day one but remained within the range reported in land plants (<100 μM). Higher leaf H_2O_2 levels were associated with permanent oxidative damage in whole plant cell DNA but transient damage to chloroplast DNA. The nanomaterials were also observed to decrease chlorophyll content and the carbon reactions of photosynthesis but not the photosystem II quantum yield. This work provides novel targeted delivery approaches for carbon-based nanomaterials mediated by biorecognition motifs. Together this chapter provides a comprehensive understanding of targeted nanomaterial's impact on plant cell and molecular biology for engineering safer and efficient agrochemical and biomolecule delivery tools.

Introduction

Nanotechnology is emerging as a tool to improve sustainable agricultural practices and maintain food security during a rapidly increasing human population and climate change impact on crop yields (Lowry et al. 2019; Gogotsi 2018; Newkirk et al. 2021). Traditional plant breeding, genetic engineering, and land-management strategies will not meet the need for food production in the future (Ray et al. 2013; Kah et al. 2019; Gogotsi 2018). The demands for food production are increasing at a pace straining the earth's ecosystems by increasing greenhouse gases, energy uses, and land use (Willett et al. 2019; Prasad et al. 2014; Mba et al. 2012; Altieri 2011; White and Gardea-Torresdey 2018). The transformation to sustainable food production will require radical improvements in pesticide, herbicide, and nutrient delivery and plant genetic engineering strategies.

Nanotechnology provides approaches for genetic engineering platforms, targeted agrochemical delivery, and nanosensors that can enable farmers to improve monitoring and management of crops (Wang et al. 2019; Santana et al. 2020; Djanaguiraman et al. 2018; Giraldo et al. 2019). The use of engineered nanomaterials (ENMs) in agriculture relies on both advancing our fundamental understanding of nanomaterial–plant interactions and the impact of nanomaterials on plant function. The application of ENMs for improving crops can potentially cause unforeseen plant health and environmental consequences (Miralles et al. 2012; Dietz and Herth 2011; Servin and White 2016). Therefore, studies on the design of nanomaterials should go hand in hand with research on their biocompatibility with plants and humankind.

ENMs have at least one size dimension in the nanoscale (1-100 nm) and exhibit tunable physical and chemical properties such as size, surface charge, amphiphilicity, and biomolecule coatings that enable targeted and controlled delivery of chemicals and biomolecules (Santana et al. 2020; Wang et al. 2016; Hu et al. 2020; Kwak et al. 2019; Avellan et al. 2019). The use of nanotechnology without adequately evaluating the biological impact on plant functions can lead to unforeseen plant health and environmental consequences, causing decreased crop yield and leaching of toxic materials into the environment (Miralles et al. 2012; Dietz and Herth 2011; Servin and White 2016). The use of targeted delivery through nanomaterials in agriculture has gained interest due to its tremendous potential for improving pesticide, herbicide, and fertilizer delivery, while decreasing the environmental impact due to agrochemical runoff (Santana et al. 2020; Newkirk et al. 2021; Kah et al. 2019; Hofmann et al. 2020; Su et al. 2019).

In Chapters 3, we demonstrated that quantum dots functionalized with a highly conserved chloroplast targeting peptide among dicot plants could deliver nanomaterials with their intended cargoes inside chloroplast and enable the delivery of chemicals to modulate chloroplast redox status (Santana et al. 2021; Santana et al. 2020). Although the quantum dot nanomaterials were used for fundamental research purposes, cadmium-based nanomaterials are highly toxic to plants and therefore not suitable for scalable application on crops (Marmiroli et al. 2020; Benavides et al. 2005; Nagajyoti et al. 2010; Al-Salim et al. 2011; Banerjee et al. 2021; Majumdar et al. 2019). In contrast, carbon dots are among the most biocompatible (Li et al. 2020; Li et al. 2016; Swift et al. 2021) and

biodegradable nanomaterials (Swift et al. 2021; Li et al. 2019). Carbon dots have yet to be explored for their use of chloroplast biorecognition motifs for targeted chemical delivery into chloroplast for agricultural applications. This work develops novel carbon dots coated with guiding peptides and molecular baskets to carry agrochemicals to chloroplasts with high specificity.

We build upon our previous work and utilize a carbon-based nanomaterial with increased biocompatibility. Moreover, we assess the biological impact of plant cellular, molecular, and plant photosynthetic capacity in response to nanoparticle treatments. Furthermore, we demonstrate that the chloroplast targeting of Cd-based QD are effective when deployed with carbon dot nanoparticles.

ENMs are also promising genetic engineering platforms due to their ability to bypass plant cell barriers including the cell wall and lipid membranes without mechanical aid in a broad array of plant species and organisms, including some plants that are recalcitrant to traditional genetic engineering strategies (Zhang et al. 2020; Newkirk et al. 2021; Demirer et al. 2018; Wang et al. 2019; Kwak et al. 2019). High aspect ratio nanomaterials (with shorter width than length dimensions) functionalized with highly positively charged polymers enable the delivery of gene constructs into model and crop plants cells and chloroplasts (Wang et al. 2019; Kwak et al. 2019; Demirer et al. 2019). Delivery of a DNA plasmid encoding a green fluorescent protein (GFP) to the plant nuclear genome was mediated by single-walled carbon nanotube (SWCNT) that were covalently modified with a cationic polymer (polyethyleneimine, PEI) (Demirer et al. 2018; Demirer et al. 2019). The surface functionalization with positively charged PEI

allowed electrostatic interactions with the negatively charged plasmid DNA cargoes and transport across plant cell barriers, including the cell wall and membranes. Passive delivery of plasmid DNA without mechanical aid was confirmed by expression analysis of GFP using digital drop PCR and confocal imaging in live plant cells. Furthermore, Kwak et al. reported the delivery of plasmid DNA encoding a yellow fluorescent protein (YFP) into chloroplasts by chitosan coated SWCNT and assessed expression by confocal microscopy analysis (Kwak et al. 2019). These studies investigated plasmid DNA delivery to chloroplasts by tuning the SWCNT surface charge with polymers. However, plant biorecognition approaches for targeting plasmid DNA via SWCNT have not been explored before.

Previously, the impact of CDs and SWCNTs on plants and the environment focused on plant exposure to high doses and short-term exposure to nanomaterials (Servin and White 2016; Sanzari et al. 2019). Investigations focusing on interactions between carbon-based nanomaterials and plants have mainly focused on concentrations greater than 100 mg/L applied to the nutrient solution (e.g., hydroponic systems), soil, and agar substrates (Miralles et al. 2012; Li et al. 2020; Begum and Fugetsu 2012; Lin et al. 2009). Systematic studies are needed to determine the effect of carbon nanomaterials within a range of concentrations intended for plant biotechnology and agricultural systems (Sanzari et al. 2019; Liu et al. 2010; Tripathi et al. 2017). Biological-based studies provide insights into the design and synthesis of nanomaterials that do not negatively affect plant growth and development (Monica and Cremonini 2009; Sanzari et al. 2019). Understanding the impact that targeted nanomaterials have on the plant cell and

molecular biology is critical towards engineering safer and effective chemical and biomolecule delivery strategies.

In this chapter, we developed nanocarriers loaded with fluorescent cargoes as proof of concept of targeted chemical delivery applications using carbon dots (e.g.TP-β-CD) and plasmid DNA delivery by nanotube complexes (e.g., TP-pATV1-SWCNT). We investigated the impact of these nanocarriers on plant cell and molecular biology (Figure 4.1). The carbon dots (TP-β-CD) contained a β-cyclodextrin molecular basket, able to form inclusion complexes with chemical cargos (Santana et al. 2020; Bin et al. 2010; Saha et al. 2016) and a targeting peptide motif from the Rubisco small subunit 1A to improve binding and uptake into chloroplasts (Figure 4.1). An SWCNT complex functionalized with cationic polymers, a plasmid DNA driven by a plastid-specific promoter, and an electrostatically bonded chloroplast targeting peptide, served as a gene delivery platform. Through confocal microscopy, we show proof-of-concept that these nanomaterial platforms can target the delivery of a fluorescent chemical cargo and plasmid DNA into chloroplasts *in vivo*. We used RT-qPCR to measure the fold change expression of the *GFP* gene transcription in the chloroplast. In addition, we assessed the percentage of viable cells in plant leaves treated with targeted nanomaterials and investigated their impact on cell and plastid membrane intactness, leaf cell H_2O_2 levels, oxidative damage to DNA, chlorophyll levels, and photosynthetic capacity. The biocompatibility of nanomaterials with plants was investigated using realistic doses and times of exposure in soil media. This work provides a comprehensive approach towards

understanding the interactions of targeted carbon nanostructures with cargoes in plant cells and their impact on cell and molecular biology.

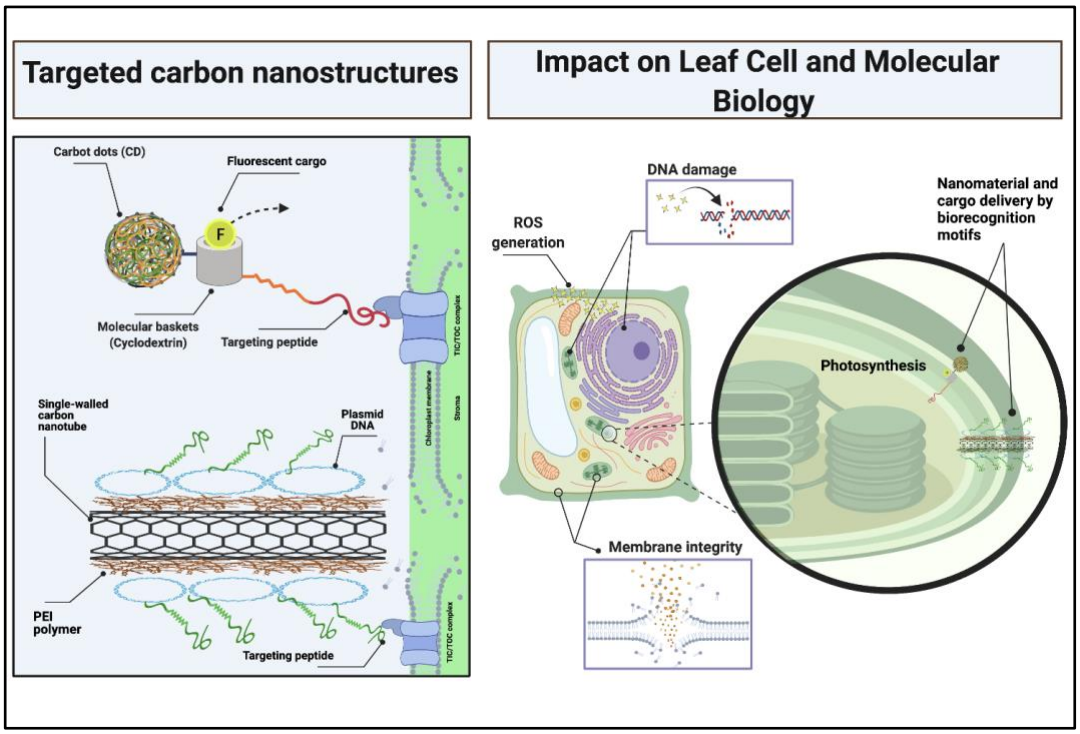

Figure 4.1 Targeted carbon nanostructures for chloroplast bioengineering and their impact on the plant cell and molecular biology. The figure demonstrates nanomaterials developed. Nanomaterials were synthesized for chloroplast targeted chemical delivery (carbon dots, CDs) and gene delivery platforms for chloroplast genetic engineering (single-walled carbon nanotubes, SWCNT). The right panel illustrates the cellular, molecular, and effect of the plant cell cellular membrane and chloroplast membrane integrity and DNA damage in whole plant cell DNA and isolated chloroplast DNA and absolute concentration of H_2O_2. The illustrated figure is created with BioRender.com.

Methods

Plant growth

All plants were grown in Adaptis 1000 growth chambers (Conviron) under the following environmental conditions: 200 µmol $m^{-2}s^{-1}$ PAR, 24 ± 1 and 21 ± 1 °C day/night, 60% humidity, and 14/10 hr (day/night) regime. All plants were grown in (2.5”

x 2.5” x 3”) pots filled with fine sphagnum peat moss soil containing 1% marathon and 1% osmocote. *Arabidopsis* plants were watered once every three days. Three-week-old Columbia ecotype (Col-0) *Arabidopsis thaliana* plants (seed stock source CS60000) in the pre-bolting stage were used for this study.

The onset of leaf senescence was determined by a marked decrease in chlorophyll levels (Supplemental Figure S4.1A). *Arabidopsis* plants younger than 4-weeks old were used to avoid plant senescence symptoms, such as increased programmed cell death rates and decreased chlorophyll content (Jung 2004; Watanabe et al. 2013; Hörtensteiner and Kräutler 2011; Bieker et al. 2012).

Covalent Modification of SWCNT with Polyethyleneimine (PEI) Polymer

Oxidized SWCNTs (>90%, 652490-250MG, Sigma Aldrich) were functionalized using a branched polyethyleneimine polymer (PEI) (10,000 MW, 9002-98-6, Alfa Aesar). The PEI increases the positive charge of the SWCNT surface, allowing the electrostatic grafting of negatively charged DNA and other biomolecules (Ramos-Perez et al. 2013; Demirer et al. 2018; Kwak et al. 2019). First, 20 mg of oxidized SWCNTs were dispersed into 100 mL ultra-purified water and pH adjusted to 12 with NaOH. The SWCNT solution was bath sonicated for 30 min at 80 kHz, 390 watts power at room temperature. The resulting SWCNT solution was slowly poured into a PEI aqueous solution (2 mg/mL) while stirring. The mixture of PEI and SWCNTs was stirred for 30 min before placing in a heat-resistant 25-mL Falcon tube and incubating for 16 hr at 85°C in a research oven (Isotemp, Fisher scientific). The resulting PEI-SWCNT was cooled to room temperature and then resuspended in 15 mL molecular biology grade water

(Catalog no. 46000CV Corning), and bath sonicated. All bath sonication steps were conducted for 30 min at 80 Khz, 390 watts power at room temperature unless stated otherwise. The resulting suspension was centrifuged for 10 min at 4,500 rpm in a benchtop (Allegra X-30R, Beckman Coulter) centrifuge at room temperature to remove large agglomerates. The PEI-SWCNT was further purified with molecular biology grade water to remove excess PEI polymer by washing five times through a 100-kD molecular weight cut-off (MWCO) ultrafiltration microtube (VIVA SPIN 500, Sartorius). After each centrifugation step, PEI-SWCNTs were bath sonicated for 30 min to resuspend the nanomaterial pellet inside the VIVA SPIN 500 100kD column after each washing. Next, the PEI-SWCNT solution was centrifuged six times in a microcentrifuge tube at 13.2 RCF for 1 hr to remove any remaining agglomerates. The lack of a dark pellet after centrifugation steps was an indicator of well-dispersed suspensions of SWCNT.

The resulting PEI-SWCNT suspension was characterized by measuring the absorbance spectra on a UV-Vis absorbance spectrophotometer (UV-2600, Shimadzu). The concentration of the PEI-SWCNT was determined spectrophotometrically using the absorption value at 623 nm and utilizing the equation (absorbance at 632 nm/extinction coefficient of 0.036) = mg L^{-1}(Demirer et al. 2019). The final concentration obtained after purification ranged from 18-30 mg L^{-1}. The zeta potential was measured using a Zetasizer (Nano ZS, Malvern Instruments), and samples were suspended in 10 mM Tris, 10 mM ethylenediaminetetraacetic acid, 0.5 % sodium dodecyl sulfate (TES buffer 7365-44-8, Sigma-Aldrich) pH 7.0 with 0.1 mM NaCl. The hydrodynamic size was measured using

Zetasizer (Nano ZS, Malvern Instruments) with samples suspended in 10 mM TES buffer pH 7.0.

Grafting of Chloroplast Fusion Peptide onto DNA-SWCNT Complex

Electrostatic grafting performed the loading of Chloroplast specific plasmid encoding for GFP (pATV1) onto the PEI-SWCNT, which allows molecules with negative charge to electrostatically interact with positively charged surfaces on the PEI-SWCNT. We used previously reported electrostatic grafting methods (Demirer et al. 2019; Demirer et al. 2019) with some modifications. First, 0.01 mg of PEI-SWCNT (PEI) with a net positive charge of 57.28 ± 1.86 mV was suspended in 1 mL of 10 mM TES buffer (7365-44-8, Sigma-Aldrich) at pH 7.0. Positively charged PEI-SWNTs (0.002 mg) were mixed with negatively charged pATV1 DNA plasmid (0.004 mg) in a 10 mM TES buffer (pH 7.0) to achieve a final concentration of PEI-SWCNT and pATV1 plasmid of 2 mg/L and 4 mg/L, respectively. The PEI-SWCNT coated in pATV1 plasmids was denoted pATV1-SWCNT. The pATV1-SWCNT solution was then bath sonicated at room temperature for 15 min on 80 kHz. The characterization of the pATV1-SWCNT included measuring the change in UV absorbance spectra, hydrodynamic diameter, and zeta potential (Malvern Instruments).

Grafting of Chloroplast Fusion Peptide onto DNA-SWCNT Complex

The pATV1-SWCNT were functionalized with a chloroplast targeting peptide on their outer surface. The targeting peptide amino acid sequence was based on precursors of

the conserved Rubisco small subunit 1A (RbcS, Genbank: OAP15425). Chloroplast targeting peptides have been utilized as a biorecognition motif that allows the import of nanomaterials and other nanoconjugates across the chloroplast membrane (Santana et al. 2020; Shen et al. 2017; Lee et al. 2009). To improve the delivery of pATV1-SWCNT into chloroplasts, we designed a chloroplast targeting peptide with a lysine-histidine (KH_6) polypeptide tail for enabling electrostatic binding to the plasmid DNA grafted onto the PEI-SWCNT (Figures 4.1, 4.4A). The modification of the chloroplast targeting peptide was rationalized to contain a chloroplast biorecognition motif from the RbcS1A transit peptide. The middle section contains a flexible linker of six glycine residues allowing increased stability and interaction between domains (Chen et al. 2013) (Figure 4.4A). Lastly, the terminal end of the fusion peptide contains a lysine histidine (KH_6) polypeptide tail that will allow electrostatic interaction with the DNA backbone grafted onto the PEI-SWCNT (Figure 4.4A). Previous studies have reported lysine-histidine (KH_6) fusion peptides improve the internalization of proteins and DNA into plant cells by destabilizing cell-membranes through electrostatic interaction between the protonated amino acids and the negatively charged cell membrane (Ng et al. 2016; Chen et al. 2000; Lakshmanan et al. 2013). Synthesis of the chloroplast targeting peptide (TP) sequence for plasmid DNA SWCNT (MASSMLSSATMVGGGGGGKHKHKHKHKHKH) was performed by Genscript (Figure 4.4A). A peptide stock solution of 10 mg/L in phosphate-buffered saline (PBS) solution (pH 7.0) was prepared and used immediately. Chloroplast targeting peptide (0.1 mg) was added to 0.002 mg of pATV1-SWCNT suspension. The mass ratio of PEI-SWCNT: DNA: TP was 1:2:50. The resulting TP-pATV1-SWCNT

nanostructure was incubated for 15 minutes while stirring at room temperature, followed by a bath sonication on ice for 15 minutes at 80 kHz, then suspended in a 10 mM TES buffer (pH 7.0) for immediate use in subsequent experiments.

pATV1 GFP-expressing Plasmid

The pATV1 plastid encoding Green fluorescent protein (*GFP*) was obtained from Pal Maliga's lab (UCR-MTA19-0083, Rutgers University) and Giga prepped by Genewiz. The pATV1 vector (Genbank accession MF461355) carries a di-cistronic operon, a *Prrn16* promoter driving expression of the two open-reading frames (ORF): *aadA* spectinomycin-resistance gene and GFP (Figure 4.4A) (Yu et al. 2017; Yu et al. 2019). The pATV1 plasmid contains a homologous recombination site flanking the di-cistronic operon to enable insertion into the inverted repeat region of the plastid genome. The di-cistronic nature of pATV1 and its chloroplast codon optimization of spectinomycin and GFP allow expression in chloroplast genomes of plants treated with plasmid DNA-loaded SWCNTs.

Carbon Dots Synthesis

Carbon dots (CD) are synthesized by a solid-state reaction (Khan et al. 2017; Hu et al. 2020) using citric acid and urea. CDs were further functionalized with a β-cyclodextrin molecular basket that enables chemical cargo loading into its cavity (Flamigni 1993; Saha et al. 2016) and a terminal chloroplast-targeting peptide motif to import the nanomaterial with its chemical cargo into chloroplasts (Santana et al. 2020; Lee et al. 2009). Briefly, 2.40 g of urea (40 mmol) (Cas no. 57-13-6, 99.2%, Fisher

Chemical), 1.92 g of citric acid (10 mmol) (Cas no. 77-92-9, 99.7%, Fisher Chemical), and 1.35 mL of ammonium hydroxide (10 mmol) ($NH_3 \cdot H_2O$, 30−33%, Sigma Aldrich) were added into 2 mL of molecular biology grade water. The mixture was dissolved, placed into a 50-mL beaker, and incubated in a mechanical oven at 180 °C for 1 hr and 20 min. Following this reaction, the resulting CD suspension was allowed to cool down at ambient temperature, dissolved in water, and stirred for 1 hr. This CD solution was bath sonicated for 15 min at 80 kHz with intermittent mixing by pipetting. Then, the solution was centrifuged at 4,000 rpm in a benchtop centrifuge (Allegra X-30R, Beckman Coulter) for 15 min to remove large particles and aggregates. The supernatant was then filtered using a 10 K molecular weight cutoff (MWCO) Amicon filter (Cat no. UFC901024, Amicon ultra, Merch Millipore) at 4500 rpm for 30 min to wash out unreacted precursors and small molecules, repeated five times. Lastly, the solution was filtered through a 0.22-μm filter membrane (Cat no. 229757, CELLTREAT Scientific Products) to obtain the purified CD.

Cyclodextrin Functionalized Carbon Dots

The resulting core CDs were functionalized with molecular baskets with mono-(6-ethanediamine-6-deoxy)-β-cyclodextrin (β-CD, Cavcon). The β-cyclodextrins allowed loading and delivery of chemical cargoes (Santana et al., 2020; Tang et al., 2016). Synthesis of β-CD was adapted from previously reported methods (Santana et al., 2020, 2021; Tang et al., 2016) with some modifications. The CDs were diluted to 2 mg/L in a final volume of 10 mL using 10 mM TES buffer (pH 6.5). The CDs were sonicated for 30

min at 37 kHz and then filtered through a 20-nm filter (6809-1002, Anotop, Whatman). Next, 0.5 mg of N-hydroxysulfosuccinimide (NHS) and 0.2 mg 1-ethyl-3-(3-dimethylaminopropyl) carbodiimide (EDC) were added to the CD solution in 10 mM TES buffer (pH 6.5). The mixture was stirred for 30 min to activate carboxyl groups on the CDs. Following NHS/EDC activation, a total of 0.2 mg of 3-aminophenylboronic acid (APBA) was added dropwise to the reaction mixture and stirred at room temperature. Conjugation of APBA proceeded for 3 hr at room temperature. The resulting APBA-coated CDs were purified by washing three times with molecular biology grade water (Catalog no. 46000CV Corning) through a 10 K (MWCO) Amicon filter (Cat no. UFC901024, Amicon ultra, Merch Millipore). Then, the APBA-coated CDs were sonicated for 30 min and 37 kHz and filtered through a 20-nm filter (6809-1002, Anotop, Whatman). The pH of the resulting solution was adjusted to 10.5 with NaOH (10mg/ml) in the 10 mM TES buffer. Mono-(6-ethanediamine-6-deoxy)-β-cyclodextrin (Cavcon) (0.35 mg) was added to the solution and allowed to react overnight at room temperature while stirring. The resulting β-cyclodextrin functionalized CDs were denoted β-CDs and purified by washing with molecular biology grade water at least twice with a 10 K Amicon filter, then sonicated for 30 min at 37 kHz. The resulting β-CDs were filtered through a 20-nm filter.

β-Cyclodextrin CD Functionalization with Targeting Peptide

Chloroplast targeting peptides were covalently bonded to β-CD by a stepwise conjugation as in Santana et al. (2020, 2021). A double-ended crosslinker was used to attach β-CD to the targeting peptide. The succinimidyl-[(N-maleimidopropionamido)-tetraethyleneglycol]ester (NHS-PEG4-MAL) (Thermo Fisher Scientific, USA) crosslinker contains chemical groups that are reactive with distinct functional groups located on the cyclodextrin molecule of the β-CD (terminal amine) and the targeting peptide's cysteine residue (sulfhydryl). First, 0.75 mg of NHS-PEG_4-MAL linker was added to a solution of β-CD in a 10 mM TES buffer (pH 7.5). The mixture was incubated at room temperature for 1 hr, stirring at 500 rpm. The excess NHS-PEG4-MAL was removed by washing the mixture through a 10 K (MWCO) Amicon filter using molecular biology grade water, and the product was suspended in a 10 mM TES buffer (pH 7.0). Lastly, 0.75 mg of the RbcS chloroplast targeting peptide (MASSMLSSATMVGGC) was added to the NHS-PEG_4-MAL-activated β-CD and allowed to react for 1 hr at room temperature while stirring. The RbcS peptide was dissolved in a 1 mL solution of 0.1% DMSO and 10 mM TES buffer (pH 7.0). The resulting chloroplast targeting carbon dot (TP-β-CD) was washed three times using a 10 K (MWCO) Amicon filter (Cat no. UFC901024, Amicon ultra, Merch Millipore) with molecular biology grade water.

Chemical Cargo Loading in β-Cyclodextrin Molecular Baskets

To show proof of the concept of targeted chemical delivery by TP-β-CD, we utilized a model fluorescent dye, 6-carboxyfluorescein (FDA), that can form inclusion

complexes with β-cyclodextrins (Dong et al. 2013; Flamigni 1993; Angelini et al. 2017; Brittain 1981; Hamada et al. 1996). The loading of FDA fluorescent cargoes onto β-CD nanomaterials was carried out by adding approximately 0.4 mg of FDA to an aqueous solution of 20 mg/L TP-CD (0.2 mg) in 10 mM TES buffer (pH 7.0). The mixture was vortexed and incubated for 0.5 hr and washed to remove unbound molecules through a 10 K (MWCO) Amicon filter (Cat no. UFC901024, Amicon ultra, Merch Millipore) in 10 mM TES buffer (pH 7.0).

Characterization of nanomaterials

All nanomaterials were characterized by absorbance UV-vis spectroscopy (UV-2600 Shimadzu), hydrodynamic size (Nano S), and zeta potential (Nano ZS). The nanomaterial zeta potential and hydrodynamic diameter were measured in a 10 mM TES buffer (pH 7.0). The zeta potential measurements were performed in 0.1 mM NaCl to improve conductivity (Doane et al., 2012). Carbon dot fluorescence emission was collected using a fluorescence spectrometer (Horiba PTI QM-400). The stepwise synthesis of TP-β-CD was analyzed using Fourier-transform infrared spectroscopy (FTIR) (Thermo Nicolet 6700 FTIR). FTIR analysis on TP-β-CD was performed to monitor the stepwise synthesis using a Bruker spectrometer (Alpha I) (Figure S4.2).

Nanomaterial Formulation and Topical Foliar Application

Nanomaterials were suspended in a 10 mM TES buffer (pH 7.0) with 0.1 % Silwet (v/v). The Silwet L-77 (Bio World) surfactant can reduce surface tension allowing rapid uptake into leaf stomata apertures and cuticular pathways (Hu et al. 2020). Each

formulation consisted of 2 mg/L pATV1-SWCNT or TP-pATV1-SWCNT and 20 mg/L 20 β-CD, or TP-β-CD nanomaterials was loaded into a 5-mL spray bottle consisting of 10 mM TES buffer (pH 7.0) with 0.1 % Silwet (v/v). Approximately 0.3 mL of the solution was dispensed with each spritz. For all experiments, each plant replicate was treated with three spritzes of nanomaterials suspended in the formulation mentioned above and left on bench top for 15 min to allow the applied formulation to penetrate tissues. Plants were then placed in an Adaptis 1000 growth chamber set to light levels at 200 μmol $m^{-2}s^{-1}$ PAR, temperature set to 24 ± 1 and 21 ± 1 °C day/night, 60% humidity, and 14/10 hr (day/night) regime.

Confocal Fluorescence Microscopy

Arabidopsis leaf samples were imaged using laser scanning confocal microscopy (TCS SP5, Leica Microsystems, Germany) using an x40 wet objective (Leica Microsystems, Germany). Samples were dissected and mounted on glass slides inside a premade well of observation gel (Carolina, cat no.132700). Confocal imaging of carbon dots (CDs, β-CD, and TP-β-CD) and chloroplast autofluorescence was performed under 405 nm laser excitation (15% power) with an emission detection range set to 500-520 nm and 720-780 nm, respectively. The focal plane depth was set by adjusting the pinhole size to 3 airy units. To visualize the localization of chemical cargoes delivered by targeted carbon dot complexes, a fluorescent 6-carboxyfluorescein dye (FDA, Invitrogen, Cat no. C1360) was loaded into β-CD and TP-β-CD. The loading concentration of FDA to carbon dots was 2:1, as reported previously (Flamigni 1993; Bin et al. 2010; Hamada et al. 1996). The fluorescein dye was excited separately by a 488 nm laser at 40% power

with a Photomultiplier tube detector (PMT) emission detection range of 525-550 nm, and the pinhole size was set to 3 airy units. For confocal analysis of targeted and non-targeted CY3-SWCNT (TP-CY3-SWCNT and CY3-SWCNT), the CY3 covalently linked to the DNA oligo (CY3-GTGTGTGTGTGTGTGTGTGTGTGTGTGT) purchased from (IDT DNA technologies) was excited by a 543 nm laser (40% power) and photomultiplier tube (PMT) emission detection range set to 550-590 nm and the focal plane pinhole size to 3 airy units. Confocal microscopy settings were 488 nm laser excitation and 500-530 nm fluorescence emission detection for imaging GFP in plant leaves. The focal plane pinhole size was set to 3 airy units.

Plant Cell Viability Assays

The percentage of intact cells was determined in *Arabidopsis thaliana* leaf tissues treated with TP-β-CD (20, 100, or 500 mg/L) or TP-pATV1-SWCNT (2, 5 or 10 mg/L) from one to five days. The nuclei of dead cells were visualized by propidium iodide (PI) staining using diluted to 1x concentration from manufactures stock (10x stock) (Plant cell viability assay kit, PA0100, Sigma-Aldrich). PI enters cells with damaged membranes and binds to double-stranded nucleic acids resulting in a bright red fluorescence (puncta) in non-viable cells. Three leaf discs (19.63 mm^2) from each sample were collected (n = 7-12) using a 5 mm cork borer and incubated in PI dye for 15 min before confocal analysis. The leaf disc surface was washed with DI water to remove the residual dye and mounted on a microscope glass slide for imaging by laser scanning confocal microscope (TCS SP5, Leica Microsystems, Germany). Confocal imaging settings were as follows: ×40 wet objective (Leica Microsystems, Germany), propidium iodide dye excitation by a 543

nm laser (40% power), and PMT emission detection range set to 590-630 nm with Pinhole size set to 3 airy units. The % of PI stained nuclei in dead cells vs total number of cells (1727 ± 549 cells per replicate) was determined through confocal microscopy using chloroplast fluorescence and fluorescein dye to identify mesophyll cell boundaries.

Chloroplast Isolation

Chloroplasts were isolated from *Arabidopsis* leaves using a sucrose buffer centrifugation gradient method (Weise et al. 2004; Santana et al. 2020; Santana et al. 2021). Intact chloroplasts were isolated from leaves exposed to targeted and non-targeted CDs and pATV1-SWCNT, and buffer as control (10 mM TES pH 7.3) in 0.1% Silwet (v/v). Following foliar spray with nanomaterials as explained above, 4 g of leaf tissue was collected from a mixture of mature and young leaves of seven plants per treatment. Treated tissue was harvested and ground in ice-cold 1X chilled sucrose buffer (pH 7.3, 28 mM Na_2HPO_4, 22 mM KH_2PO_4, 2.5 mM $MgCl_2$, 400 mM sucrose, and 10 mM KCl). Following maceration of the leaf tissue, the homogenate was condensed to a pellet by two cycles of centrifugation at 4000 rpm for 10 min in a sucrose buffer and the supernatant was discarded. Isolated chloroplast suspension was stored in a 1X sucrose buffer at 4°C for subsequent experiments such as DNA isolation or analysis of intact chloroplast.

Intact Chloroplast Analysis

Identification of intact chloroplast was performed as reported in previous studies (Lilley et al. 1975; Kubis et al. 2008) with some modifications. Following chloroplast isolation, a 100-µL sample of isolated chloroplasts was placed on a glass slide per

treatment (n = 5-7) for examination by differential interference contrast (DIC) microscopy as reported previously with some modifications (Lilley et al. 1975; Kubis et al. 2008). Using a disposable cell counting cytometer slide (InCyto, Cat no. DHC-F01), the total number of chloroplasts per 1 mL was determined to be 32.5 million chloroplasts per mL. Intact chloroplasts were highly reflective with a bright and continuous halo around the envelope, whereas damaged chloroplasts have an opaque with a granular deflated appearance. The number of intact and damaged chloroplasts was determined from ten images from each of seven biological replicates; these values were used to calculate the average percentage of intact chloroplasts.

Leaf H_2O_2 Quantification Assay

We assessed the H_2O_2 levels of *Arabidopsis* in leaves treated with targeted nanomaterials (TP-CD and TP-SWCNT) or buffer controls (Pierce, Thermo Scientific, USA). The leaf discs were collected at one and five days post foliar application treatment of nanomaterials and control samples. Two leaf discs were harvested from each biological replicate (n=6) using a 6-mm cork borer, weighed immediately (60 mg total weight per replicate), and placed in a chilled mortar containing liquid nitrogen. The leaf disks were ground into a fine powder, transferred to a 2-mL microcentrifuge containing 0.5 mL of molecular biology grade water (Catalog no. 46000CV Corning), and centrifuged at 13,000 rpm for 1 min. Following centrifugation, 20 µL of the supernatant was added to a 96-well microtiter plate containing 200 µL of quantitative peroxide assay working reagent (0.25 mM ferrous ammonium sulfate, 100 mM sorbitol, 125 µM xylenol

in 25 mM H_2SO_4). Samples were incubated for 15 min at room temperature, followed by measuring absorbance at 595 nm using an Infinite MPlex plate reader (Tecan).

DNA Extraction from Leaves and Isolated Chloroplasts

DNA was extracted from plant leaf tissue and prepared using a Quick-DNA Plant/Seed DNA Miniprep kit (Zymo) in leaf samples treated with nanomaterials from one to five days. DNA samples were extracted from 150 mg of plant leaf tissue using dissected scissors or from 1 mL of isolated chloroplast suspension collected, as explained above. Samples were placed in liquid nitrogen-filled mortar and pestle, ground, and placed directly into a Zymo Bashing Bead Lysis Tube with 750 µL Bashing Bead Buffer. The mixture was homogenized on a mixer mill (Retsch MM 400) for 10 min at 28 Hz. The DNA extraction was performed according to the manufacturer's instructions (www.zymoresearch.com) and concentrations were measured using a Nanodrop ND-1000 Spectrophotometer. Samples were stored at - 20°C until used for the 8-OHdG DNA damage biomarker assay.

8-OHdG DNA Damage Biomarker Assay

We determined the amount of oxidative DNA damage in plant leaves treated with nanomaterials using an enzyme-linked immunosorbent assay (ELISA) for 8-hydroxydeoxyguanosine (8-OHdG). The OxiSelect™ Oxidative DNA Damage ELISA Kit (Cat no. STA-320, Cell Biolabs, inc.) was used to quantify the amount of 8-OHdG in isolated DNA samples from plant leaf tissue or isolated chloroplast suspensions. The DNA was denatured at 95℃ for 5 min and quenched on ice. Single-stranded DNA was

digested with 20 units of P1 nuclease enzyme (NEB) in 20 mM sodium acetate to convert into single nucleotides. Then, the digested DNA was treated with 10 units of alkaline phosphatase (NEB) in 100 mM Tris (pH 7.5) and incubated for 1 hr at 37ºC to convert into nucleosides for detection by antigen-specific detection by 8-OHdG antibodies. The reaction mixture was placed in a centrifuge and spun down at 6,000 x g for 5 min. The supernatant was collected for subsequent reaction in the 8-OHdG ELISA assay. The DNA Damage ELISA was conducted according to the manufacturer's instructions (Cell Biolabs, inc,).

Real-time Quantitative PCR Analysis

Changes in sentinel gene expression was determined from total RNA extracts performed on 3-week old *Arabidopsis thaliana* leaves treated with 2 mg/L pATV1-SWCNT, TP-pATV1-SWCNT, and buffer controls without nanoparticles in 10 mM TES buffer (pH 7.0). Leaf RNA was extracted after 3 hr and at 3, 5, and 7 days after nanomaterial treatments. The RNA was isolated using the Quick-RNA Plant Miniprep Kit (ZYMO). Residual plasmid DNA in RNA preparations was removed by treating twice with DNase I enzyme (2 units/10 µg of RNA) (Zymo) while on the RNA plant miniprep column prep and after RNA was isolated. Purified RNA (25 ng) was added to the Luna® Universal One-Step RT-qPCR reaction master mix per manufacturer's instructions (catalog no. E3005L, NEB). A quantitative real-time RT-qPCR was performed on a Bio-Rad CFX Connect Real-Time ThermalCycler. The relative levels of *GFP* RNAs were determined by the $2^{-\Delta\Delta CT}$ method (Pfaffl 2001). *Actin2* (At3g18780) was used as internal housekeeping control(Czechowski et al. 2005). *GFP* and *Actin2*

primers were designed with Primer3 (version 4.1.0) using GFP open reading (723bp) as a template (Fig S4.4 A) (Koressaar and Remm 2007; Yu et al. 2017; Yu et al. 2019). The primers set (Table S4.1) were validated for assessing gene expression (Figure S4.3 B).

Chlorophyll Measurements

Three-week-old *Arabidopsis thaliana* Col-0 plants were sprayed with β-CD, TP-β-CD, pATV1-SWCNT, or TP-pATV1-SWCNT r a buffer control (10 mM TES, pH 7.0) formulation, and CCI levels were measured in one- and five-days post-treatments. The CCI measurements were performed using a chlorophyll meter (SPAD-502 plus, Konica Minolta, Tokyo, Japan; CCI readout resolution: 0.1). Each replicate (n=6) was averaged from a subset of 3 leaves per plant, and each leaf was measured 3 times giving an average value for each biological replicate.

Photosynthesis Assays

The photosynthetic capacity of *Arabidopsis* plants was performed using an infrared gas exchange analyzer (GFS-3000, Walz). Leaves from 3-week-old plants were exposed to 20 mg/L TP-β-CD and 2 mg/L TP-pATV1-SWCNTs or 10 mM TES buffer as control through foliar spray and measurements performed after one and five days. Leaves were then placed inside a gas analyzer chamber, ensuring that the leaf lamina was fully expanded to fill the entire chamber area of the gas analyzer (2.5×1 cm^2). CO_2 assimilation in PSII yield light response curves was performed at 1200, 900, 600, 400, 300, 200, 100, 50, and 0 Par (μmol $m^{-2}s^{-1}$). Leaf chamber settings were as follows: relative humidity 50%, CO_2 level 410 ppm, cuvette temperature 25°C, measurement time

interval 210 seconds, and the flow rate was set to 750 μmol/s. Fv/Fm dark-adapted measurements were performed after a 600-second dark interval under the above mentioned conditions.

Results and Discussion

Application of Nanomaterials using Foliar Spray Formulation

The use of a foliar spraying formulation containing nanomaterial was sprayed onto *Arabidopsis thaliana* vegetative tissues. The formulation consisted of The formulation provided an efficient and widely used method to interface targeted nanomaterials to crops at scale (Forster et al. 2015; Hu et al. 2020; Kranjc et al. 2018; Etxeberria et al. 2016; Larue et al. 2014; Su et al. 2019; Djanaguiraman et al. 2018). When combining the nanomaterials with surfactants (Silwet L-77), the surface tension is reduced, allowing uptake and increased wetting area improving uptake into leaf tissues (Hu et al. 2020; Buick et al. 1993; Field and Bishop 1988). The use of a surfactant-based formulation for chemical and nanomaterial delivery on plants has major practical applications. It can improve fertilizer and nutrient nanoparticles' efficacy to enhance plant growth. When combined with nanomaterials with guiding peptides, the foliar application promises efficient delivery methods for plant nanotechnology applications (Su et al. 2019; Hofmann et al. 2020).

Characterization of Targeted Carbon Nanomaterials

The UV-vis absorbance spectra of targeted nanomaterials indicated characteristic peaks for non-targeted carbon dots (β-CD) at 345-350 nm (Wang et al. 2019) and distinct peaks at 230 and 280 nm reported in cyclodextrin functionalized carbon dots (Tang et al. 2016) (Figure 4.2A). The targeted carbon dot (TP-β-CD) complexes exhibited a sharp peak at 215 nm (Santana et al. 2020) (Figure 4.2A). Non-targeted single-walled carbon nanotubes (pATV1-SWCNT) showed a sharp peak at 213 nm and broad shoulders around 260 nm. Broadening of the characteristic peaks in spectra TP-pATV1-SWCNT and TP-β-CD was seen after 250 nm was seen.

The zeta potentials were measured to assess the overall charge of the nanomaterials. A High surface charge of nanomaterials has been reported to improve uptake into plant chloroplast membranes (Hu et al. 2020; Park et al. 2011; Kwak et al. 2019; Giraldo et al. 2014). The zeta potential of β-CDs decreased from -12.07 ± 3.215 mV to -36.42 ± 3.399 mV for TP-β-CD (10 mM TES buffer, pH 7.0) after functionalization with the chloroplast targeting peptide (Figure 4.2B). This targeting peptide (MASSMLSSATMVGGC) has a neutral charge (- 0.1 mV) that, upon covalent bonding to positively charged NH2 groups in β-cyclodextrins, results in the decrease in zeta potential for TP-β-CD. In contrast, the zeta potential for pATV1-SWCNT increased from 27.63 ± 2.827 mV to 33.40 ± 0.764 mV for targeting peptide coated TP-pATV1-SWCNT (10 mM TES and 0.1 mM NaCl, pH 7.0) (Figure 4.2B). The chloroplast targeting peptide for TP-pATV1-SWCNT contains a 12 lysine and histidine residue tail (MASSMLSSATMVGGGGGGKHKHKHKHKH). It has a net positive charge of

(6.6 mV) that, upon electrostatic interaction with pATV1-SWCNT, increases the zeta potential of the resulting TP-pATV1-SWCNT complexes. Both targeted TP-β-CD and TP-pATV1-SWCNT have a highly negative or positive charge, respectively, that have been shown to promote uptake through chloroplast envelopes and plasma membranes *in vitro* (Wong et al. 2016) and leaf surfaces *in vivo* (Hu et al. 2020).

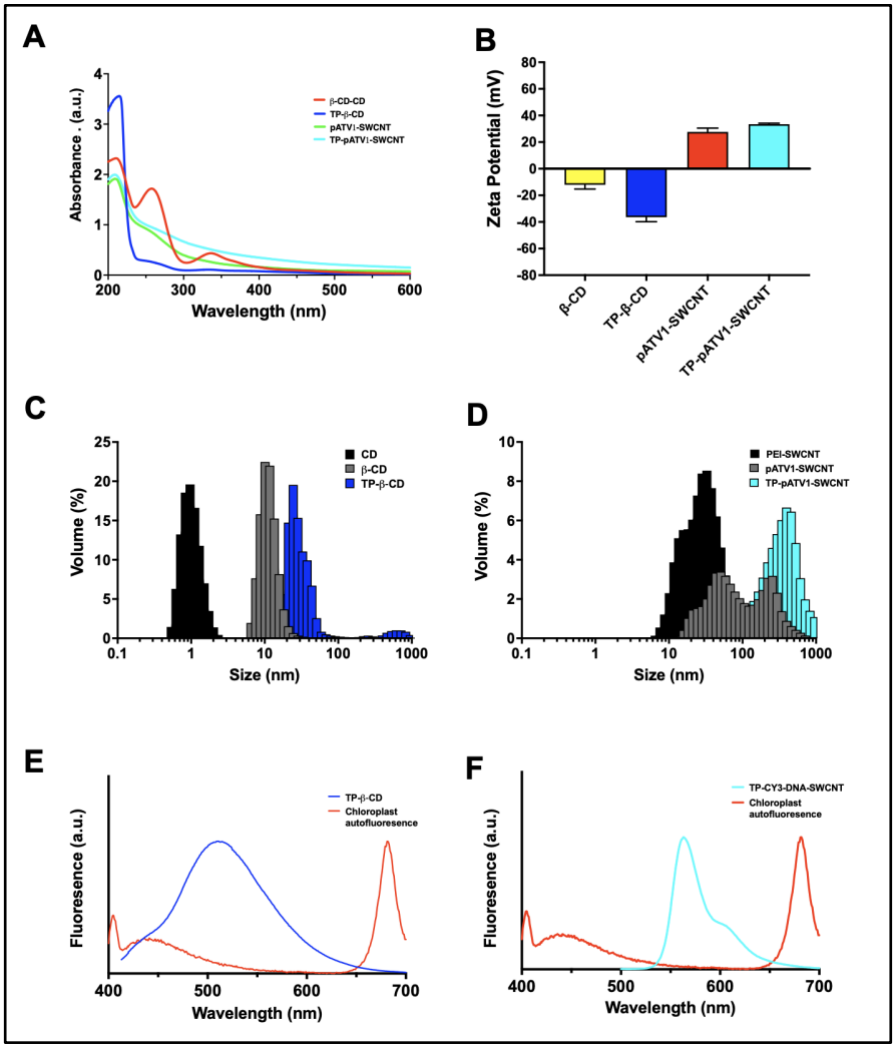

Figure 4.2 Characterization of targeted nanomaterials for chemical and gene delivery. A, UV absorbance targeted nanomaterials (β-CD, TP-β-CD pATV1-SWCNT, and TP-pATV1-SWCNT). **B,** Zeta potential surface charge of targeted nanomaterials. **C,** Hydrodynamic diameter measured by DLS of carbon dots (β-CD, and TP-β-CD), **D,** and SWCNT (pATV1-SWCNT, and TP-pATV1-SWCNT) nanostructures. **E,** Fluorescence

emission of targeted carbon dot (TP-β-CD) nanoparticles and chloroplast autofluorescence, **F**. Fluorescence emission spectra of TP-CY3-DNA-SWCNT complexes and chloroplast autofluorescence (arbitrary units, a.u,).

The hydrodynamic size for β-CD measured by dynamic light scattering (DLS) increased from 10.17 ± 1.491 nm for β-CDs to 27.84 ± 5.806 nm for TP-β-CD (Figure 4.2C). Likewise, the average DLS size for the pATV1-SWCNT and TP-pATV1-SWCNT increased from 49.98 ± 3.450 nm to 382.5 ± 27.0 nm, respectively (Figure 4.2D). The increase in DLS size is associated with the coating of pATV1-SWCNT with a peptide motif (30 residues) containing a terminal tail with KH_6 cationic residues and a G6 spacer (Figure 4.4 A). The KH_6 peptide tail enables the binding of the chloroplast targeting peptide to the negatively charged plasmid DNA in pATV1-SWCNT and, together with the G6 spacer, allows the exposure of the biorecognition motif to membrane receptors (Ng et al. 2016; Yoshizumi et al. 2018; Chen et al. 2000).

FTIR analysis of β-CD and TP- β-CD indicated characteristic bonds for O–H stretching vibrations at 3240 cm^{-1}, C☰C alkyne 2160 cm^{-1}, carboxamides N=C=N at 2010 cm^{-1}. The peaks near 1700 cm^{-1} and 1650 cm^{-1} were attributed to C=O conjugated aldehydes and N–H amine bonds (Li et al. 2021; Khan et al. 2017) (Figure S4.2). The β-CDs exhibited significant characteristic peaks for asymmetric glycosidic vibration bonds (C–O–C) of β-cyclodextrins at 1040 cm^{-1}(Mondal and Purkayastha 2016; Khan et al. 2017) (Figure S4.2). The FTIR of targeted TP-β-CD exhibited peaks at O–H stretching vibrations at 3240 cm^{-1}, asymmetric glycosidic vibration (C–O–C) at 1050 cm^{-1}, and bands typical of type I amide bonds at 1610 cm^{-1} supporting the successful conjugation of β-cyclodextrin and targeting peptides on the carbon dot surface (Figure S4.2). The CD exhibited a fluorescence emission peak at 511 nm and the SWCNT coated in CY3-DNA (CY3-GTGTGTGTGTGTGTGTGTGTGTGTGTGT) a fluorescence emission peak at

564 nm. These nanomaterial fluorescence peaks of emission allowed tracking inside plant cells with minimum overlap with chloroplast autofluorescence background (Figure 4.2F).

In vivo Imaging of Chloroplast Targeted Nanomaterials by Confocal Fluorescence Microscopy

Confocal imaging was used to determine the colocalization rates between chloroplasts in *Arabidopsis* leaves and targeted carbon dots with β-cyclodextrins or DNA-coated SWCNT (Figure 4.3). Confocal images were collected for chloroplast autofluorescence, fluorescence of carbon dots (TP-β-CD, β-CD) (Figure 4.3A), and fluorescence of the double-stranded CY3-tagged $(GT)_{15}$ (CY3-GTGTGTGTGTGTGTGTGTGTGTGTGTGT) electrostatically grafted onto SWCNT complexes (TP-CY3-DNA-SWCNT, CY3-DNA-SWCNT) (Figure 4.3B). The level of colocalization of fluorescent emission from nanocarriers with chloroplasts was analyzed by Manders' coefficients using the COLOC2 analysis package in ImageJ (Figure 4.3 C). The colocalization rates of targeted nanomaterials (TP-β-CD and TP-CY3-DNA-SWCNT) with chloroplasts in leaf mesophyll cells was significantly higher compared to nano-targeted materials lacking the targeting peptide (β-CD and CY3-DNA-SWCNT). The colocalization for TP-β-CD with chloroplasts increased to 70.0 ± 9.46 % from 47.4 ± 9.57 % levels for β-CDs. Similarly, TP-CY3-DNA-SWCNT colocalization rate increased to 56.9 ± 4.58 % from 38.7 ± 6.69 % for non-targeted CY3-DNA-SWCNT nanomaterials (Figure 3C). Previously, we reported an increase in localization of chloroplasts *in vivo* with heavy metal-based quantum dots functionalized with chloroplast

targeting biorecognition peptides (1.9 fold change) (Santana et al. 2020). Collectively, these data indicate the robustness of this approach for a variety of targeted nanomaterials.

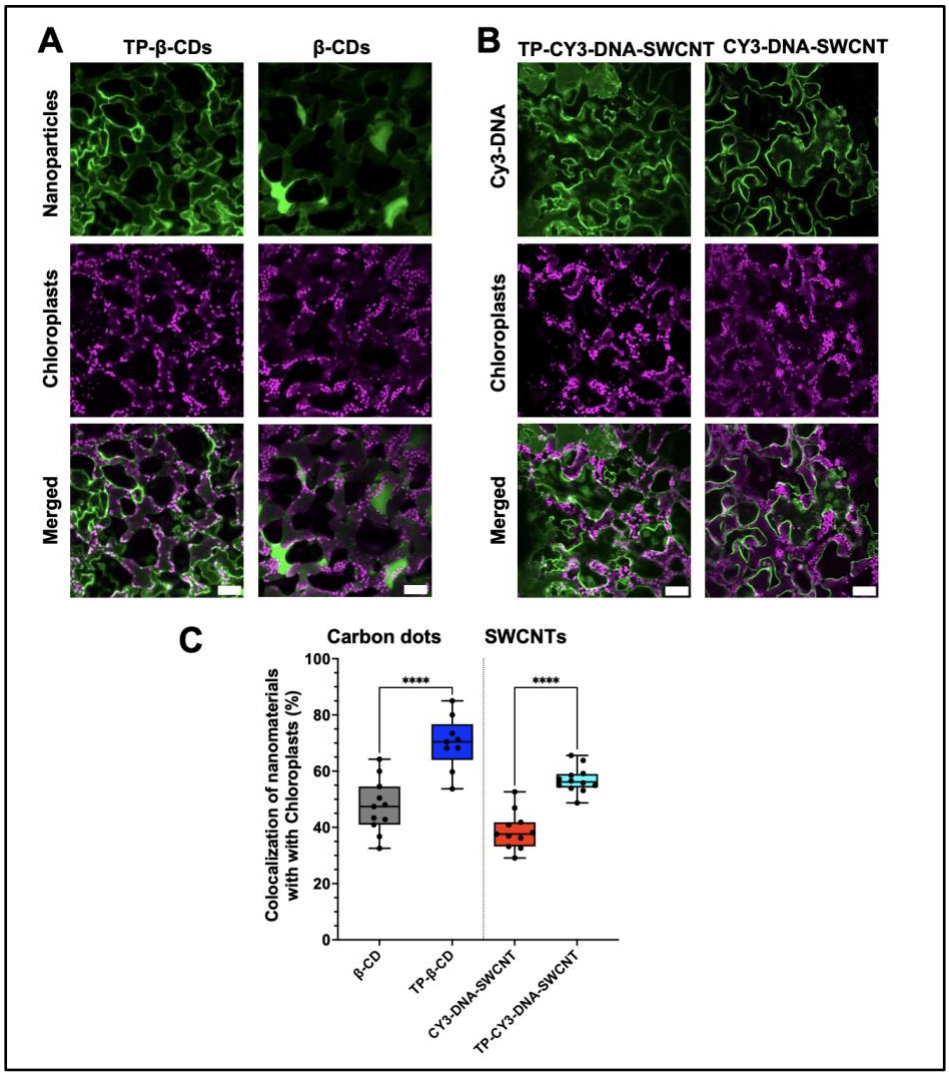

Figure 4.3 Colocalization of targeted nanomaterials with chloroplasts inside plant mesophyll cells. A, Confocal images targeted and non-targeted carbon dots (β-CD, TP-β-CD). **B**, Confocal images of targeted or non-targeted single-walled carbon nanotubes complexes ionically bonded with CY3-double-stranded DNA with and without chloroplast targeting peptide (CY3-DNA-SWCNT, TP-CY3-DNA-SWCNT). Scale bar, 50 microns. **C**, Quantitative analysis of targeted nanostructures are significantly localized with chloroplasts. Statistical analysis using one-way ANOVA based on Tukey test, n=7-12, ****$p < 0.0001$.

Plasmid DNA and Chemical Cargo Delivery to Chloroplasts Mediated by Targeted Nanomaterials

We assessed the targeted delivery and expression in chloroplasts of *Arabidopsis* leaves of pATV1, a plasmid encoding a green fluorescence protein (GFP) gene, mediated by TP-pATV1-SWCNT. The pATV1 is a dicistronic plasmid encoding for codon optimized GFP and spectinomycin resistance genes regulated by the chloroplast plastid rrn promoter, prrn 16, for specific expression in chloroplasts (Figure 4.4 A) (Yu et al. 2017). GFP fluorescence was imaged by confocal microscopy in leaf mesophyll cells, and *RT-qPCR quantified GFP and ACTIN2 RNAs* at 1, 3, 5, and 7 days post-treatment with pATV1-SWCNT, TP-pATV1-SWCNT nanomaterials, and Buffer as control in 3-week-old Col-0 *Arabidopsis thaliana* plants (Figure 4). Confocal analysis of GFP fluorescence emission in plant leaves treated with TP-pATV1-SWCNT exhibits a more robust localized fluorescence within chloroplast *in vivo* (56.66 ± 6.019%) than non-targeted pATV1- SWCNT platforms (37.01 ± 6.291%) (Figure 4 B-D). A 3D rendering of GFP expression and chloroplasts autofluorescence indicated high levels of GFP in these organelles of leaf mesophyll cells in plants treated with targeted TP-pATV1-SWCNT (Figure 4.4 C).

Expression analysis results show the relative *GFP* RNAs levels peaked after five days of exposure to TP-pATV1-SWCNT and pATV1-SWCNT, followed by a decrease in *GFP* RNAs at day seven (Figure 4E). Interestingly, despite greater co-localization of targeted TP-pATV1-SWCNT with chloroplasts, both TP-pATV1-SWCNT and pATV1-SWCNT exhibited similar levels of *GFP* RNA. This could indicate that functionalization

of plasmid DNA-coated SWCNT with targeting peptides increases localization with chloroplasts, but it may lead to reduced accessibility with the plasmid DNA by chloroplasts' expression machinery. Alternatively, the increased localization of TP-pATV1-SWCNT into chloroplast nucleoid structures where primary expression machinery is located could disrupt the level of expression. Alternatively, the increased localization of TP-pATV1-SWCNT into chloroplast and nucleoid structure where primary expression machinery is located could be disrupted the level of expression. Previously, SWCNT functionalized with positively charged chitosan was reported to deliver plasmid DNA to chloroplasts in *Arabidopsis* plant leaves, but GFP expression was only confirmed by confocal fluorescence microscopy (Kwak et al. 2019). Herein, we reported a biorecognition-mediated delivery of transgenes to chloroplasts by targeted SWCNT supported by confocal microscopy and quantitative gene expression molecular level analysis.

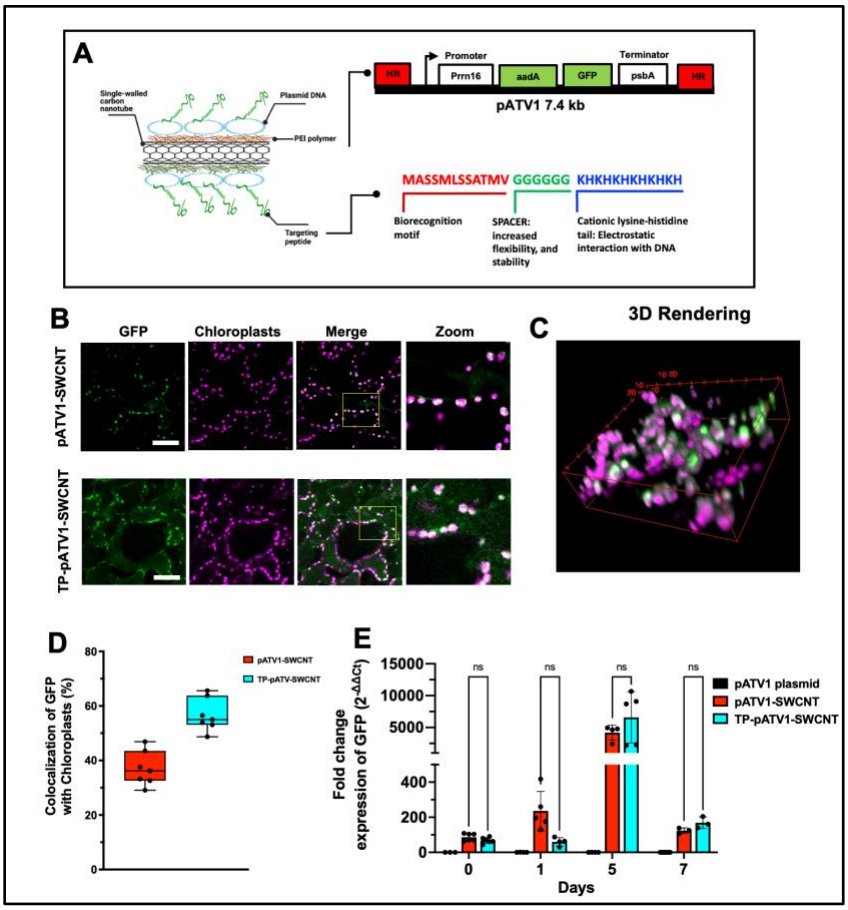

Figure 4.4 Expression analysis of chloroplast-specific GFP plasmid delivered by SWCNT. A, Figure illustrating the gene delivery platforms for chloroplast genetic engineering (single-walled carbon nanotubes, SWCNT). pATV1 plasmid map showing elements for chloroplast gene expression. The rationalized chloroplast targeting peptide fusion sequence. **B,** Confocal images of *Arabidopsis thaliana* plants treated with SWCNT coated in pATV1 plasmid with targeting peptide (TP-pATV1-SWCNT) and without thus peptide (pATV1-SWCNT) after 7 days if exposure to the nanostructures. The yellow box outlining region in the merged image corresponds to zoomed image panels **C.** A 3D image of *GFP* gene expressed in mesophyll cells after treatment with TP-pATV1-SWCNT. **D,** Quantitative colocalization analysis of GFP fluorescence overlapping with chloroplast. Comparison was performed by independent samples t-test (two-tailed) Scale bar 50 micron, (****p=< 0.0001), *n* = 5-7. **E,** RT-qPCR analysis of GFP transcripts in plants treated with targeted (TP-pATV1-SWCNT) and non-targeted (pATV1-SWCNT) nanomaterials. The RT-qPCR analysis of *GFP* mRNA expression was compared to internal housekeeping (Livak & Schmittgen, 2001; Pfaffl, 2001) gene *ACTIN2* (AT3G18780). Statistical analysis of RT-qPCR was analyzed using two-way ANOVA. Not significant (ns). *n* = 5-7.

To assess the delivery of chemical cargoes to chloroplasts mediated by TP-β-CD nanocarriers, we loaded β cyclodextrins with 6-carboxyfluorescein (FDA) (Figure 5). The FDA fluorescent dye binds to the inner cavity of β-cyclodextrins and cyclodextrin derivatives, allowing investigation of chemical delivery by these molecular baskets in non-plant organisms (Brittain 1981; Flamigni 1993; Bin et al. 2010; Li et al. 2015). Plants treated with TP-β-CD-FDA or TP-β-CD were also analyzed for the emission crosstalk of leaf autofluorescence with confocal microscopy under laser excitation with a 488 nm laser (Figure S4.4A). The FDA dye emission spectra exhibited a stronger signal compared to TP-β-CD at 488 nm excitation allowing detection of loaded cargos to chloroplasts with minimal crosstalk from TP-β-CD emission (Figure S4.4A-B).

Plants were treated with TP-β-CD-FDA or β-CDs and the localization of FDA with chloroplasts within leaf mesophyll tissues was determined by confocal microscopy showing a 1.5 fold increase in colocalization (Figure 4.5B-C). The FDA alone localized near the plasma membrane when delivered via CD or within β-CD, observed mainly in the extracellular space. In contrast, when TP-β-CDs were used to deliver FDA, most of the FDA fluorescence signal was detected inside leaf mesophyll cells and highly colocalized with chloroplasts (Figure 4.5B-C). Colocalization rates of FDA fluorescence with chloroplasts were analyzed using the Manders coefficients (COLOC2 in ImageJ). The colocalization rates of TP-β-CD loaded with FDA were compared to FDA dye only, core carbon dots mixed with FDA, and β-CD loaded with FDA (Figure 4.5C). Using 2D plane projections in the XZ and YZ axis from orthogonal Z-stack images, we determined the distribution of FDA in the leaf mesophyll and the localization with chloroplasts

(Figure 4.5 C). The percent colocalization of FDA delivered by TP-β-CD with chloroplasts (62.5 ± 9.22 %) was significantly higher compared to non-targeted β-CD mixtures (40.0% ± 3.42) (ANOVA based Tukey's, *** $p<0.0002$, ****$p<0.0001$) (Figure 4.5B). We previously reported that CdTe quantum dots with molecular baskets coated with chloroplast targeting peptides based on biorecognition motifs from the Rubisco small subunit protein precursors enable the targeted delivery of agrochemicals such as paraquat into chloroplasts increasing colocalization up to 78.4 % an increase of 2.4 fold using paraquat alone (Santana et al. 2020). Herein, the targeted delivery to chloroplasts of a traceable fluorescent chemical cargo (FDA) by TP-β-CD provides increased biocompatibility (Li et al. 2010; Hu et al. 2020; Qian et al. 2014) and biodegradable (Amer Ridha et al. 2020; Alas et al. 2020; Li et al. 2019) platform for agrochemical delivery in plants with subcellular and improved delivery efficiency (Figure 4.5C). Carbon dots are an ideal nanoparticle for application in plants compared to quantum dots nanoparticles, which are highly toxic to biological systems, causing severe damage to respiration, chlorophyll content, and oxidative stress due to their cadmium-rich core (Benavides et al. 2005; Marmiroli et al. 2020).

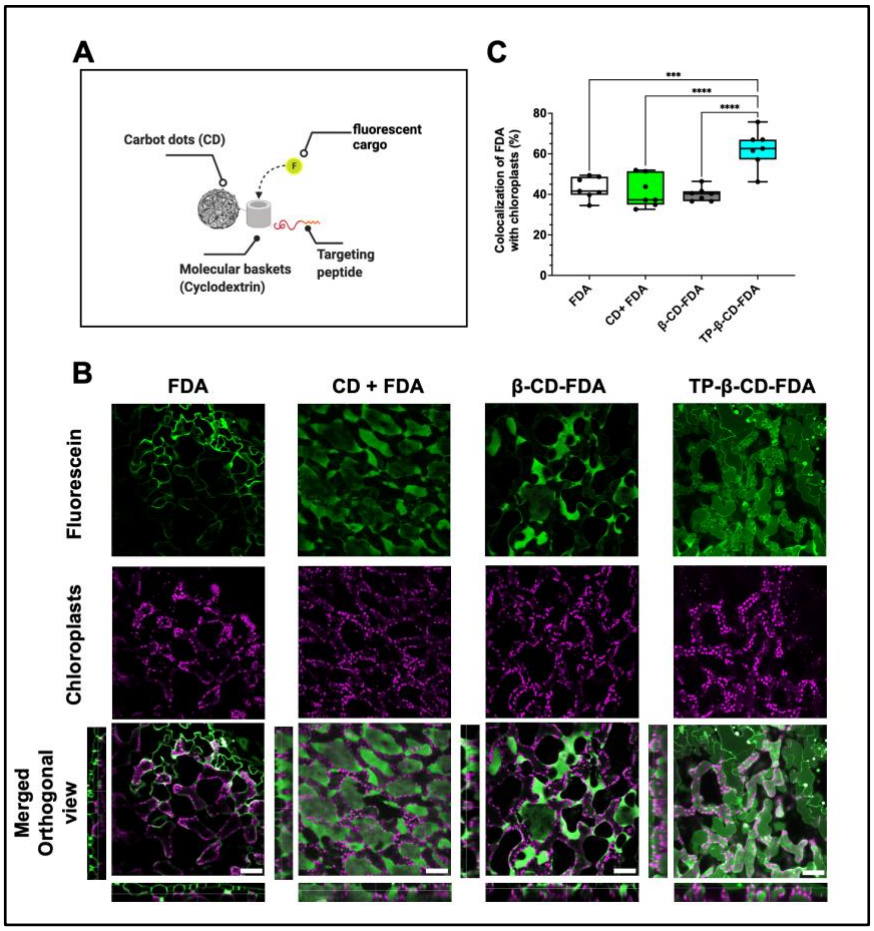

Figure 4.5 Cargo delivery of localization by targeted carbon dot nanostructures. **A,** Figure image engineered targeted carbon dot. Carbon dot is functionalized with a β-cyclodextrin molecular basket for cargo loading and chloroplast targeting peptide for import into chloroplasts. Figure image demonstrates loading of fluorescent chemical cargoes (fluorescein) into cyclodextrin. **B,** Confocal images showing fluorescein localized with chloroplast. Merge image row shows orthogonal views generated from Z-stack images showing the distribution of fluorescent cargoes localizing with chloroplasts along the z-axis. Scale bar 50 microns **C,** quantification of Colocalization of FDA fluorescent cargoes with chloroplast. Significant increase in fluorescent cargoes localizing with chloroplast when loaded onto TP-CD carbon dots functionalized chloroplast targeting. Statistical analysis was performed using a one-way ANOVA based Tukey's test, n=7, *** $p<0.0002$, ****$p<0.0001$.

Plant Cell Viability

Several biocompatibility assays were performed comparing controls and nanoparticle-treated plants. Biocompatibility assessments were performed on plants prior to display of classical senescence phenotypes. The buffer control treated (untreated) *Arabidopsis thaliana* plants experienced the onset of age-related leaf senescence, as marked by significant changes in chlorophyll levels 7 days after treatment (Supplemental Figure S4.4A). For this reason, 3-week-old plants were assessed after 5 days of treatment.

We analyzed the viability of plant cells treated with increasing concentrations of targeted and non-targeted nanomaterials by measuring the percentage of dead plant cells. Fluorescent staining with propidium iodide (PI) allowed the identification of non-viable cells (dead cells). The PI dye enters cells with damaged membranes intercalating into double-stranded nucleic acids enabling quantification of dead cells or damaged cell membranes (Jones et al. 2016; Zhao et al. 2010). Biocompatibility assessments were performed up to five days of nanocarrier exposure before control *Arabidopsis* plants experienced the onset of leaf senescence marked by significant changes in chlorophyll levels (Supplemental Figure S4.1). On day seven significant differences in chlorophyll were detected (Supplemental Figure S4.1). *Arabidopsis* leaves were sprayed with TP-β-CD (20, 100, or 500 mg/L) or TP-pATV1-SWCNT (2, 5, or 10 mg/L) for up to five days post-treat (Figure 4.6). Results show that concentrations above 10 mg/L of TP-pATV1-SWCNT nanomaterials at day 1 significantly increased plant cell death (3.25 ± 8.47 %) compared to controls (0.840 ± 0.498%). On day 5 concentrations of 5 mg/L of TP-

pATV1-SWCNT (8.40 ± 2.891 %) and 10 mg/L concentration compared to controls (Day five, 2.88 ± 1.445 %) exhibited significantly increased plant cell death rates (Figure 4.6 A). The TP-β-CD concentrations of 100 mg/L and 500 mg/L caused significantly higher cell death at day five (7.263 ± 3.620 %, 6.408 ± 1.271 %) compared to control on day one (3.880 ± 2.315%) and day 5 (1.975 ± 0.714) (Figure 4.6B). Therefore, subsequent experiments assessing the impact of targeted nanocarriers on plant cell and molecular biology were focused on concentrations of 2 mg/L and 20 mg/L for TP-pATV1-SWCNTs and TP-β-CD, respectively.

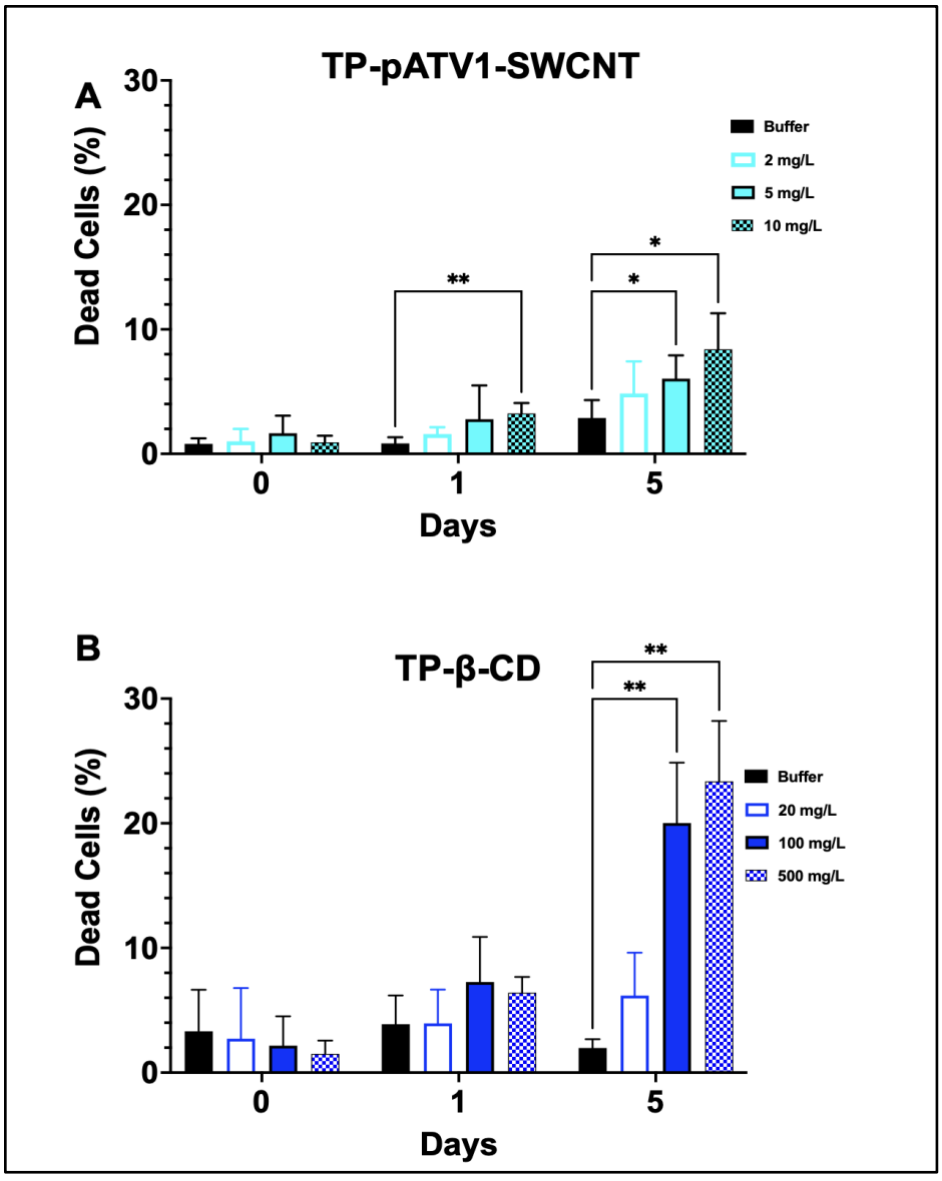

Figure 4.6. Plant cell viability assay in leaves treated with targeted nanomaterials. Percentage of dead cells per (5 mm) leaf discs analyzed using propidium iodide (PI) staining in *Arabidopsis thaliana*. Leaf mesophyll cells infiltrated with increasing concentration of ATP-pATV1-SWCNT or B TP-β-CD. Statistical analysis using one-way ANOVA Dunnett's model test, n=7-12, *p<0.032, **p=<0.0021.

Plant Cell Membrane and Chloroplast Envelope Intactness

Damage to plant lipid membranes causes ion and molecule permeability changes across the membrane, interruption of metabolic processes, intracellular signaling, and trafficking of biomolecules (Liu et al. 2007; Walker 1965; Wang and Dehesh 2018). The application of targeted nanostructures with high charge can penetrate plant cell barriers and localize inside organelles and can cause significant disruption in lipid membrane integrity. Plant cell membrane intactness in leaves treated with TP-β-CD and TP-pATV1-SWCNT was assessed by PI and fluorescein fluorescent dye assays followed by imaging under confocal microscopy. Figure 4.7A shows white arrows pointing to some distinctive stained nuclei puncta detected by confocal microscopy. The overall percentage of intact cells (without PI stained nuclei) was calculated relative to the total number of cells (Figure. 4.7A-B). The targeted nanomaterials did not have a significant impact on plant cell membrane intactness. More than 96% of plant cells had intact membranes in controls and after one and five days of TP-β-CD (20 mg/mL) or TP-pATV1-SWCNT (2 mg/mL) treatment. (Figure. 4.7 B). Intact isolated chloroplasts observed by DIC microscopy have a highly reflective and continuous outer envelope, whereas damaged chloroplasts have a broken envelope with an opaque and granular appearance (Figure 4.7 C). TP-β-CD did not induce significant chloroplast membrane damage during this time frame (Figure 4.7 D).

In contrast, the TP-pATV1-SWCNT induced a significant decrease in chloroplast intactness after one day one of exposure, but no differences were observed on day five (Figure 4.7 D). Lipid exchange between SWCNT and chloroplast envelopes as the

nanomaterials enter these organelles (Wong et al. 2016) could explain a decrease in chloroplast intactness (Wong et al. 2016; Lew et al. 2018). Our results indicate that high aspect ratio carbon nanomaterial SWCNT but not carbon dots disrupt plant lipid membrane structures. However, the damage to chloroplast lipid membranes by SWCNT is overcome by the organelle self-repairing through lipid transfer proteins that maintain chloroplast envelope integrity or chloroplast autophagy mechanisms that remove dysfunctional organelles (Zhang and Sakamoto 2015; Izumi and Nakamura 2017; Ishida et al. 2014; Runk 1983; Nakamura et al. 2018).

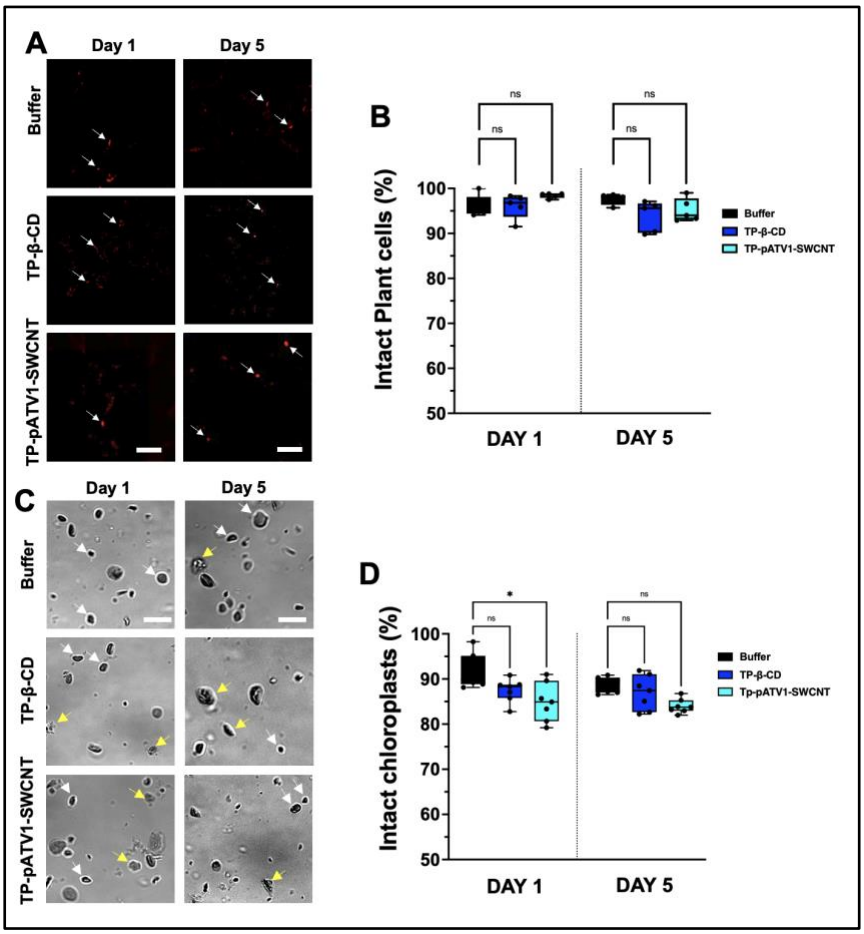

Figure 4.7. Analysis of chloroplast and plant cell membrane intactness. **A,** shows confocal microscopy of propidium iodide-stained plant cells. Damaged cell membranes (non-intact cells) are detected by the ability of PI to enter cells and produce red puncta. White arrows point to some distinctive stained nuclei puncta analyzed. Scale bar: 50 microns. **B,** Quantitative analysis of the percentage of intact plant cells using confocal images. Statistical analysis using a one-way ANOVA-based Bonferroni test. Not significant (ns), n= 5-7. **C,** Light microscopy images of isolated chloroplasts for intact chloroplast analysis. Microscopy analysis utilized differential interference contrast (DIC) optical components to image intact chloroplast membranes. Intact chloroplasts exhibited a highly reflective appearance and the presence of a halo (white arrows). On the other hand, broken or damaged chloroplasts have broken halos, giving a granular appearance (yellow arrows). D. quantitative analysis of the percentage of intact plant chloroplast membrane. Statistical analysis using a one-way ANOVA-based Bonferroni test. *$p<0.032$, n= 5-7. Scale bar for panels A and C is 10 microns.

Leaf H_2O_2 Content

Interactions of nanomaterials with plant cells and organelles have been reported to increase ROS (Kumar et al. 2018; Anjum et al. 2019; Abdal Dayem et al. 2017; Nel et al. 2006; Begum and Fugetsu 2012). ROS levels beyond the plant's antioxidant mechanisms' capacity led to oxidative damage of biomolecules such as lipid membranes, photosystems, and DNA (Das and Roychoudhury 2014; Tripathi et al. 2020; Mignolet-Spruyt et al. 2016). The chloroplast is the main site for ROS evolution (Mignolet-Spruyt et al. 2016; Asada 2006; Liu et al. 2007). However, the impact of targeted nanomaterials on chloroplast ROS levels has not been explored. We used a quantitative peroxide assay to monitor H_2O_2 content in leaves after treatment with targeted nanomaterials (Figure 4.8A). The TP-β-CD and TP-pATV1-SWCNT increased leaf H_2O_2 levels to 28.2 ± 3.269 and 26.4 ± 3.394 μM, respectively, after one day of exposure, whereas control plants exhibited 3.15 ± 1.230 μM H_2O_2. After 5 days, leaf H_2O_2 returned to normal levels of 5.32 μM ± 0.573 TP-β-CD and 4.56 ± 0.517 μM for TP-pATV1-SWCNT after five days of exposure. However, H_2O_2 content values were higher than control treatments without nanoparticles (2.56 μM ± 0.801) (Figure 4.8 A). The transient increase in leaf H_2O_2 could disrupt antioxidant capacity causing DNA damage, chlorophyll pigments, and photosynthetic proteins (Hung and Kao 2004; Bieker et al. 2012; Huff 1982; Tripathi et al. 2020; Das and Roychoudhury 2014; Chi et al. 2013).

For comparison, basal H_2O_2 levels in non-stressed land plants range from 0.1 - 1 μM (Veljovic-Jovanovic et al. 2002; Cheeseman 2006; Černý et al. 2018; Tripathi et al.

2020). Under biotic and abiotic stress, H_2O_2 levels vary depending on plant species and stressors (Cheeseman 2006; Cheeseman 2007; Veljovic-Jovanovic et al. 2002). In stressed plants,> 3 μM of H_2O_2 have been previously reported (Gullner and Tyihák 1991; Maksymiec and Krupa 2006; Drazkiewicz et al. 2004; Cheeseman 2007; Kumar Tewari et al. 2004; He et al. 2005). The values in control treatments fall within the range of H_2O_2 levels found in non-stressed plants, 3.15 μM ± 2.247 μM at day 1 and 2.56 μM ± 0.801 at day five. Leaf H_2O_2 returned to normal levels of 5.32 μM ± 0.573 TP-β-CD and 4.56 ± 0.517 μM for TP-pATV1-SWCNT after five days of exposure. However, H_2O_2 content values were higher than control treatments without nanoparticles (2.56 μM ± 0.801) (Figure 8 A). The transient increase in leaf H_2O_2 could disrupt antioxidant capacity causing DNA damage, chlorophyll pigments, and photosynthetic proteins (Hung and Kao 2004; Bieker et al. 2012; Huff 1982; Tripathi et al. 2020; Das and Roychoudhury 2014; Chi et al. 2013).

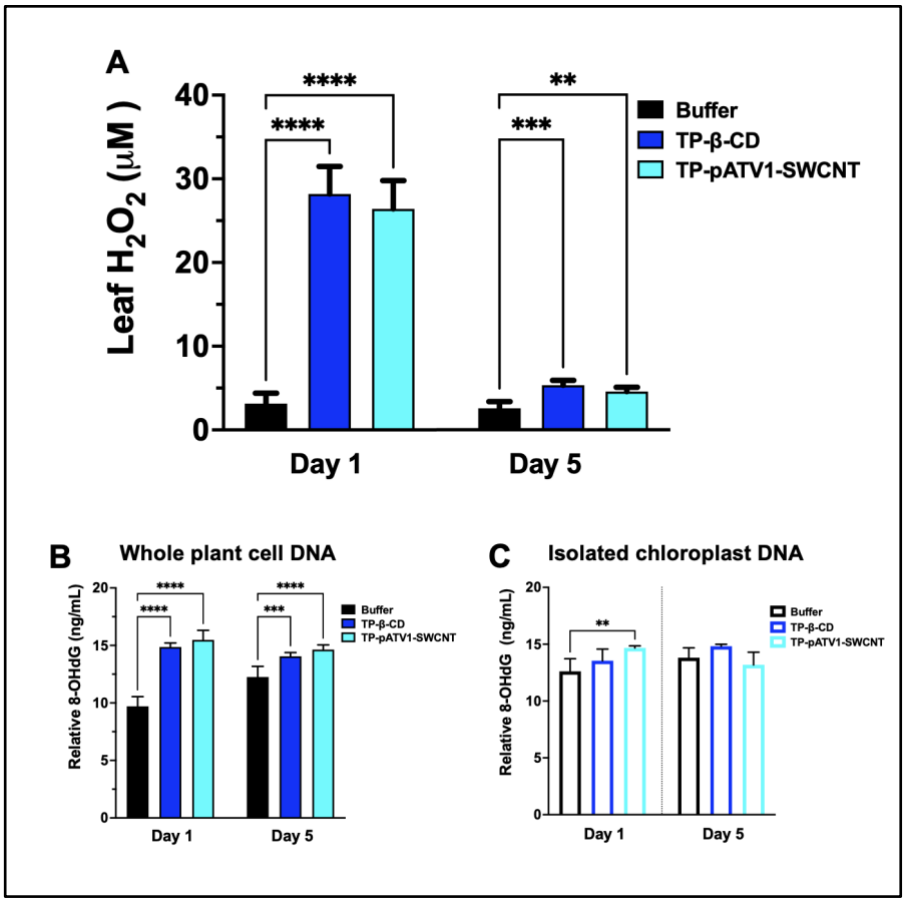

Figure 4.8. Oxidative stress and hydrogen peroxide analysis in plant leaf mesophyll cells treated with targeted nanomaterials. **A.** Plot of absolute H_2O_2 content in leaves treated with targeted nanostructure after one and five days. Statistical analysis using two-way ANOVA-based Tukey's test n=9, * p=<0.05, **p<0.0021, **** p<0.0001, n= 3 **B.** Quantitative assay of DNA damage caused by oxidative stress. ELISA measured the biomarker 8-OHdG. The relative percentages of the 8-OHdG levels were compared to control at one and five days after treatment with targeted and non-targeted nanostructures. **C.** plotted concentration of 8-OHdG measured in isolated chloroplast DNA compared to controls**.** Statistical analysis performed by one-way ANOVA based Tukey's test **p<0.0021, ***p<0.0002, ****p<.0001, n=6.

Oxidative Damage to Cell and Chloroplast DNA

Oxidative stress results in DNA damage and the production of 8-hydroxydeoxyguanosine (8-OHdG), a ubiquitous biomarker in the guanine of nucleic acids (Cabelof et al. 2002; Valavanidis et al. 2009; Yin et al. 1995; Chiou et al. 2003). To gain insight into the impact of increased ROS levels on plant cell and chloroplast genomes, we measured the relative 8-OHdG levels in whole plant cell DNA and chloroplast DNA of leaves treated with targeted nanomaterials. Significantly higher levels of 8-OHdG biomarkers in whole plant cell DNA were observed after one day of leaf exposure to TP-β-CD (14.86 ± 0.3513 ng/mL) and TP-pATV1-SWCNT (15.48 ± 0.8342 ng/mL) relative to controls without nanoparticles (9.703 ± 0.8452 ng/mL) (Figure 4.8B). On day five the levels of 8-OHdG biomarkers remained elevated in treatments with TP-β-CD (14.86 ± 0.3210 ng/mL) and TP-pATV1-SWCNT (14.64 ± 0.4074 ng/mL) relative to controls without nanoparticles (12.26 ± 0.9235 ng/mL) (Figure 4.8B). The increase in control treatments in DNA damage biomarkers could be attributed to symptoms of aging or senescence in plants, causing a slight increase in 8-OHdG biomarker levels (Liguori et al. 2018).

Damage to chloroplast DNA was also assessed at one and five days after targeted nanoparticle treatments and controls. No change in 8-OHdG levels was seen when controls and TP-β-CD samples were compared. However, one day after TP-pATV1-SWCNT treatment, chloroplasts incurred a small but significant amount of damage

(14.67 ± 0.1782 ng/mL) relative. By five days, leaves treated with TP-pATV1-SWCNT, and controls had similar levels of 8-OHdG (Figure 4.8 C).

The differences in damage to the nuclear vs chloroplast genomes are striking. Accumulation of H_2O_2 may inhibit DNA repair mechanisms allowing lesions and DNA damage in the plant nuclear genome to accumulate (Tripathi et al. 2020; Hu et al. 1995). In contrast, plastid genomes are highly dynamic, and each chloroplast contains hundreds of copies relative to the single nuclear genome in plant cells (Bendich 2013; Boesch et al. 2009; Yagi and Shiina 2014). When damaged plastid DNA exceeds the capacity of chloroplast repair machinery, the damaged DNA is fragmented and degraded, and new DNA is replicated (Kumar et al. 2014; Oldenburg and Bendich 2015). On the other hand, plastid's innate increased metabolism can spontaneously evolve high levels of ROS, this has caused an evolutionary adaptation in plastid's antioxidant mechanism to deal with the increased levels of ROS (Das and Roychoudhury 2014; Polle 2001; Asada 2006; Boesch et al. 2009).

Leaf Chlorophyll Content and Photosynthesis

Chlorophyll is a marker for plant health status and photosynthesis (Mukherjee et al. 2019; Kalaji et al. 2016). Oxidative stress can damage chlorophyll pigments and reduce their biosynthesis in chloroplasts (Aarti et al. 2006). We determined the impact of targeted nanomaterials on the chlorophyll content index (CCI) of *Arabidopsis* leaves. Relative to the control, there was a CCI decrease of 99.16 to 99.14 % after one day of exposure to TP-β-CD and TP-pATV1-SWCNT, respectively, and these levels persisted

after five days (Figure 4.9 A,B). The nanomaterials used in this study have physical characteristics attributing light absorbance across a broad range of light and fluorescence. These attributes could interfere with the measurement of chloroplast content using a spad meter that uses fluorescence emission from chlorophyll. Thus, we verified there was no interference in CCI measurement in the targeted nanomaterials treated plants by measuring levels before and after treatment with targeted nanomaterials and found no significant difference (Supplemental Figure S4.4). Previously, we reported no significant changes in chlorophyll content after the treatment with carboxylated, aminated, and amphiphilic carbon dots at concentrations from 500 to 5000 mg/L (Hu et al. 2020) in crop plants and for semiconducting single stranded-DNA-coated SWCNT in *Arabidopsis* plants at concentration 5 mg/L (Giraldo et al. 2014). Targeted delivery of TP-β-CD and TP-pATV1-SWCNT to chloroplasts may reduce leaf chlorophyll content due to the transient increase in ROS generation in leaves reported above.

To assess the impact of TP-β-CD and TP-pATV1-SWCNTs on leaf photosynthetic rates, we measured carbon assimilation rates at varying photosynthetic active radiation levels (PAR). The photosynthesis light response curves provided information on the maximum leaf photosynthetic capacity (Amax) and photosystem II (PSII) quantum yield. The targeted nanomaterials did not influence carbon assimilation rates in the light-limited region (< 400 μmol m^{-2} s^{-1}) at day one or day 5 relative to controls (Figure 4.9 C, D). However, we observed a reduction in Amax in the carboxylation limited region (> 400 μmol m^{-2} s^{-1}) at day one and day five relative to controls without nanoparticles (Figure 4.9 C,D).

Nanomaterials with high surface charge have been reported to form a protein corona in plant cells (Walkey and Chan 2012; Foroozandeh and Aziz 2015; Liu et al. 2013). The localization of nanomaterials in chloroplasts could result in stromal protein adsorption onto the surface of the nanomaterials by electrostatic interactions. The nanomaterial interactions with enzymes and substrates of the carbon reactions of photosynthesis may influence maximum photosynthetic capacity.

In contrast, the quantum yield of PSII was not impacted by targeted nanomaterials within a wide range of PAR levels on day one or five (Figure 4.9 E,F). Furthermore, the maximum quantum yield of photosystem II (Fv/Fm) in dark-adapted leaves was similar between controls (0.74 ± 0.01708) (Figure 4.9 E,F, inset) and targeted nanomaterial treated plants at day one (0.7956 ± 0.0075, 0.801 ± 0.0195) and day five (0.794 ± 0.0273, 0.8043 ± 0.0134) for TP-β-CD and TP-pATV1-SWCNT respectively (Figure 4.9 E, F inset). Fv/Fm is a robust indicator of the maximum quantum yield of PSII chemistry (Kitajima and Butler 1975; Genty et at. 1992; Genty et al. 1989). An Fv/Fm value in the range of 0.79 to 0.84 is optimal for many plant species, with lowered values indicating plant stress (Maxwell and Johnson 2000; Kitajima and Butler 1975). Together these results suggest that targeted nanomaterials do not impact the light-dependent reactions nor damage the photosystems or electron transport chain. Still, their interactions with carboxylation reaction enzymes and biomolecules may limit leaf photosynthetic capacity.

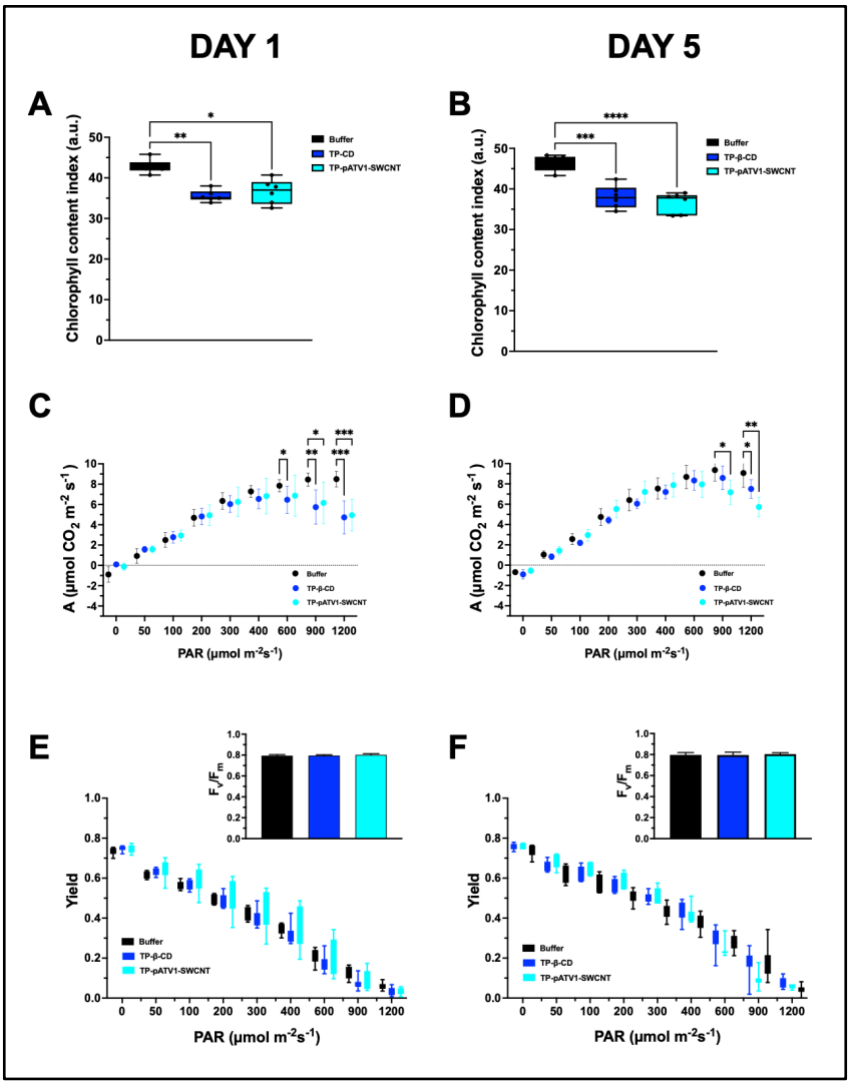

Figure 4.9. Plant photosynthesis measurements. **A,** Chlorophyll content measured by SPAD meter. Comparison of the chlorophyll content index in plants treated with targeted and non-targeted nanomaterials at day 1. **B**. Chlorophyll content index of targeted and non-targeted nanomaterials at day 5. Statistical analysis was performed using a one-way ANOVA-based Tukey's test. * $p<0.02$, **$p<0.0021$, ***$p<0.0002$,**** $p<0.0001$, n= 6. **C-D**, Leaf carbon assimilation rates at varied PAR levels of 3-week-old Col-0 *Arabidopsis* leaves at day 1 (C) and day 5 (D). Two-way ANOVA performed a statistical analysis based on Dunnett's test at each par point. * $p<0.02$, **$p<0.0021$, ***$p<0.0002$,**** $p<0.0001$, n=7-10. **E and F**, Quantum yield of PS II (QY), and inset is the efficiency of photosystem II in a dark-adapted state (Fv/Fm) at day 1 and Day 5, respectively.

Conclusions

We developed novel targeted carbon nanomaterials that plant biorecognition approaches to deliver chemical cargoes (TP-β-CDs) and plasmid DNA (TP-pATV1-SWCNT) into chloroplasts. The application of targeted nanomaterials functionalized with guiding peptides as tools for plant bioengineering and precision agriculture relies on understanding their impact on plant function. Thus, we investigated their effect on plant cell viability, lipid membranes, ROS levels, oxidative DNA damage, and photosynthesis in *Arabidopsis thaliana* plants.

Cell viability assays of plants treated with TP-β-CD (20 mg/L) and TP-pATV1-SWCNT (2 mg/L) indicated no significant differences in the percentage of dead cells compared to control plants after five days of exposure. The TP-β-CD did not affect cell membrane intactness on either day one or five. However, the chloroplast membrane intactness was affected by TP-pATV1-SWCNT treatments, causing an acute disruption at day one, decreasing the chloroplast intactness to 84.92 ± 4.332% compared to 91.66 ± 3.775 % in buffer control treatments. Treatments with TP-pATV1-SWCNT containing high surface charge and chloroplast guiding peptides recognized by membrane translocon TOC159 (Jarvis and Soll 2002; Ng et al. 2016; Lee et al. 2013) resulted in temporary disruption in membrane intactness. As a result, TP-pATV1-SWCNT nanomaterials uptake and penetration through the membrane envelope can displace lipids on the envelope (Wong et al. 2016; Kwak et al. 2019; Lew et al. 2018). Uptake nanomaterials such as SWCNT through endocytic pathways have been reported in plant cell cultures (Liu et al. 2009). Because chloroplasts lack endocytosis-dependent mechanisms,

nanoparticle uptake occurs by disrupting the organelle envelopes and self-healing the lipid bilayers (Lew et al., 2018; Wong et al., 2016).

One-day exposure of plant leaf cells to targeted nanomaterials induced an almost 8-fold transient increase in H_2O_2 levels relative to no-nanoparticle controls but returned to similar levels as controls five days after exposure. The H_2O_2 contents in land plants can vary, in land plant basal levels could range from 0.1 -1 μM (Veljovic-Jovanovic et al. 2002; Cheeseman 2006; Černý et al. 2018; Tripathi et al. 2020). H_2O_2 levels in stress plants have been reported to have H_2O_2 concentration greater than >3 μM Gullner and Tyihák 1991; Maksymiec and Krupa 2006; Drążkiewicz et al. 2004; Cheeseman 2007; Kumar Tewari et al. 2004; He et al. 2005). The transient elevations in H_2O_2 concentrations can lead to damage of biomolecules such as DNA, lipids, and proteins (Nafees et al. 2019; Hu et al. 1995; Watanabe et al. 2006; Das and Roychoudhury 2014) and inhibit photosynthetic carboxylation rates in *Arabidopsis thaliana* plants (Claeys et al. 2014; Veljovic-Jovanovic et al. 2002; Smirnoff and Arnaud 2019). Consistent with the literature, we saw rises in H_2O_2 and inhibition of Amax in the carboxylation range (Robinson et al. 1980; Amory et al. 1992; Desimone et al. 1996; Badger et al. 1980). Increases in oxidation can damage biomolecules such as DNA resulting in modification of the DNA base pairs forming a free radical-induced lesion 8-OHdG (Hu et al. 1995; Watanabe et al. 2006; Boesch et al. 2009; Valavanidis et al. 2009). We observed a 2-fold increase in 8-OHdG levels in whole plant cell DNA, a ubiquitous marker for oxidative damage to DNA, after exposure with TP-β-CD and TP-pATV1-SWCNT. In contrast, isolated chloroplast DNA was not affected by TP-β-CD, while TP-pATV1-SWCNT

induced a temporary increase in 8-OHdG levels on day one of exposure followed by recovery on day five.

A reduction in leaf chlorophyll content index levels after treatment with targeted nanomaterials could be attributed to increasing H_2O_2 levels (Hung and Kao 2004; Bieker et al. 2012; Huff 1982; Tripathi et al. 2020; Das and Roychoudhury 2014; Chi et al. 2013). However, no effect was observed on photosystem II health and quantum yields across a wide range of PAR levels indicating no permanent impact in the light reactions of photosynthesis. Although carbon assimilation rates of leaves exposed to TP-β-CD and TP-pATV1-SWCNT were similar to controls without nanoparticles in the light-limited region, a reduction in maximum photosynthetic capacity was observed in the carboxylation limited region. Interactions between the nanomaterial surface and photosynthetic proteins involved in carbon fixation and assimilation could be responsible for the decline in photosynthetic capacity.

We demonstrate that carbon nanomaterials engineered with targeting peptides increase the delivery efficiency of chemical and plasmid DNA cargoes into chloroplasts by topical application of the leaf surface. The targeted nanomaterials overcome plant cell barriers including the cell wall, and lipid membranes, without mechanical aid, guided to chloroplasts by plant biorecognition. However, targeting nanomaterials to the chloroplasts can induce transient increases in H_2O_2 levels that result in whole leaf cell DNA, chlorophyll, and photosynthesis. The results from this study will guide the use of targeted nanomaterials for precise agrochemical delivery to chloroplasts and plant biotechnology applications. They also provide insights on future directions for improving

the development of more biocompatible nanomaterials for plant research, agriculture, and environmental applications.

References

Aarti, P. D., Tanaka, R., & Tanaka, A. (2006). Effects Of Oxidative Stress On Chlorophyll Biosynthesis In Cucumber (*Cucumis Sativus*) Cotyledons. *Physiologia Plantarum*, *128*(1), 186–197.

Abdal Dayem, A., Hossain, M. K., Lee, S. B., Kim, K., Saha, S. K., Yang, G.-M., Choi, H. Y., & Cho, S.-G. (2017). The Role Of Reactive Oxygen Species (ROS) In The Biological Activities Of Metallic Nanoparticles. *International Journal Of Molecular Sciences*, *18*(1),120.

Alas, M. O., Alkas, F. B., Aktas Sukuroglu, A., Genc Alturk, R., & Battal, D. (2020). Fluorescent Carbon Dots Are The New Quantum Dots: An Overview Of Their Potential In Emerging Technologies And Nanosafety. *Journal Of Materials Science*, *55*(31), 15074–15105.

Al-Salim, N., Barraclough, E., Burgess, E., Clothier, B., Deurer, M., Green, S., Malone, L., & Weir, G. (2011). Quantum Dot Transport In Soil, Plants, And Insects. *The Science Of The Total Environment*, *409*(17), 3237–3248.

Altieri, M. (2011). Modern Agriculture: Ecological Impacts And The Possibilities For Truly Sustainable Farming. *Agroecology In Action.*

Amer Ridha, A., Pakravan, P., Hemati Azandaryani, A., & Zhaleh, H. (2020). Carbon Dots; The Smallest Photoresponsive Structure Of Carbon In Advanced Drug Targeting. *Journal Of Drug Delivery Science And Technology*, *55*, 101408.

Amory, A. M., Ford, L., Pammenter, N. W., & Cresswell, C. F. (1992). The Use Of 3-Amino-1,2,4-Triazole To Investigate The Short-Term Effects Of Oxygen Toxicity On Carbon Assimilation By Pisum Sativum Seedlings. *Plant, Cell & Environment*, *15*(6), 655–663.

Angelini, G., Campestre, C., Boncompagni, S., & Gasbarri, C. (2017). Liposomes Entrapping B-Cyclodextrin/Ibuprofen Inclusion Complex: Role Of The Host And The Guest On The Bilayer Integrity And Microviscosity. *Chemistry And Physics Of Lipids*, *209*, 61–65.

Anjum, N. A., Gill, S. S., Duarte, A. C., & Pereira, E. (2019). Oxidative Stress Biomarkers And Antioxidant Defense In Plants Exposed To Metallic Nanoparticles. In *Nanomaterials And Plant Potential*. *17*(1), 427–439.

Asada, K. (2006). Production And Scavenging Of Reactive Oxygen Species In Chloroplasts And Their Functions. *Plant Physiology*, *141*(2), 391–396.

Avellan, A., Yun, J., Zhang, Y., Spielman-Sun, E., Unrine, J. M., Thieme, J., Li, J., Lombi, E., Bland, G., & Lowry, G. V. (2019). Nanoparticle Size And Coating Chemistry Control Foliar Uptake Pathways, Translocation, And Leaf-To-Rhizosphere

Transport In Wheat. *ACS Nano*, *13*(5), 5291–5305.

Badger, M. R., Andrews, T. J., Canvin, D. T., & Lorimer, G. H. (1980). Interactions Of Hydrogen Peroxide With Ribulose Bisphosphate Carboxylase Oxygenase. *The Journal Of Biological Chemistry*, *255*(16), 7870–7875.

Banerjee, R., Goswami, P., Chakrabarti, M., Chakraborty, D., Mukherjee, A., & Mukherjee, A. (2021). Cadmium Selenide (Cdse) Quantum Dots Cause Genotoxicity And Oxidative Stress In Allium Cepa Plants. *Mutation Research. Genetic Toxicology And Environmental Mutagenesis*, *865*, 503338.

Begum, P., & Fugetsu, B. (2012). Phytotoxicity Of Multi-Walled Carbon Nanotubes On Red Spinach (*Amaranthus Tricolor L*) And The Role Of Ascorbic Acid As An Antioxidant. *Journal Of Hazardous Materials*, *243*, 212–222.

Benavides, M. P., Gallego, S. M., & Tomaro, M. L. (2005). Cadmium Toxicity In Plants. *Revista Brasileira De Fisiologia Vegetal*, *17*(1), 21–34.

Bendich, A. J. (2013). DNA Abandonment And The Mechanisms Of Uniparental Inheritance Of Mitochondria And Chloroplasts. *Chromosome Research: An International Journal On The Molecular, Supramolecular And Evolutionary Aspects Of Chromosome Biology*, *21*(3), 287–296.

Bieker, S., Riester, L., Stahl, M., Franzaring, J., & Zentgraf, U. (2012). Senescence-Specific Alteration Of Hydrogen Peroxide Levels In *Arabidopsis Thaliana* And Oilseed Rape Spring Variety *Brassica Napus L*. Cv. Mozart. *Journal Of Integrative Plant Biology*, *54*(8), 540–554.

Bin, G., Juqin, H., & Huaiyou, W. (2010). Study On Inclusion Reaction Of B-Cyclodextrin With Fluorescein And Neutral Red. *Chemical Analysis And Meterage*. Https://En.Cnki.Com.Cn/Article_en/Cjfdtotal-Hxfj201002004.Htm

Boesch, P., Ibrahim, N., Paulus, F., Cosset, A., Tarasenko, V., & Dietrich, A. (2009). Plant Mitochondria Possess A Short-Patch Base Excision DNA Repair Pathway. *Nucleic Acids Research*, *37*(17), 5690–5700.

Brittain, H. G. (1981). Excited-State Optical Activity Of A Cyclodextrin Inclusion Compound. *Chemical Physics Letters*, *83*(1), 161–164.

Buick, R. D., Buchan, G. D., & Field, R. J. (1993). The Role Of Surface Tension Of Spreading Droplets In Absorption Of A Herbicide Formulation Via Leaf Stomata. *Pesticide Science*, *38*(2-3), 227–235.

Cabelof, D. C., Raffoul, J. J., Yanamadala, S., Guo, Z., & Heydari, A. R. (2002). Induction Of DNA Polymerase Beta-Dependent Base Excision Repair In Response To Oxidative Stress In Vivo. *Carcinogenesis*, *23*(9), 1419–1425.

Černý, M., Habánová, H., Berka, M., Luklová, M., & Brzobohatý, B. (2018). Hydrogen Peroxide: Its Role In Plant Biology And Crosstalk With Signalling Networks. *International Journal Of Molecular Sciences*, *19*(9), 2812.

Cheeseman, J. M. (2006). Hydrogen Peroxide Concentrations In Leaves Under Natural Conditions. *Journal Of Experimental Botany*, *57*(10), 2435–2444.

Cheeseman, J. M. (2007). Hydrogen Peroxide And Plant Stress: A Challenging Relationship. *Plant Stress*. *1*(1), 4-15.

Chen, Q. R., Zhang, L., Stass, S. A., & Mixson, A. J. (2000). Co-Polymer Of Histidine And Lysine Markedly Enhances Transfection Efficiency Of Liposomes. *Gene Therapy*, *7*(19), 1698–1705.

Chen, X., Zaro, J. L., & Shen, W.-C. (2013). Fusion Protein Linkers: Property, Design And Functionality. *Advanced Drug Delivery Reviews*, *65*(10), 1357–1369.

Chiou, C.-C., Chang, P.-Y., Chan, E.-C., Wu, T.-L., Tsao, K.-C., & Wu, J. T. (2003). Urinary 8-Hydroxydeoxyguanosine And Its Analogs As DNA Marker Of Oxidative Stress: Development Of An ELISA And Measurement In Both Bladder And Prostate Cancers. *Clinica Chimica Acta; International Journal Of Clinical Chemistry*, *334*(1), 87–94.

Chi, Y. H., Paeng, S. K., Kim, M. J., Hwang, G. Y., Melencion, S. M. B., Oh, H. T., & Lee, S. Y. (2013). Redox-Dependent Functional Switching Of Plant Proteins Accompanying With Their Structural Changes. *Frontiers In Plant Science*, *4*, 277.

Claeys, H., Van Landeghem, S., Dubois, M., Maleux, K., & Inzé, D. (2014). What Is Stress? Dose-Response Effects In Commonly Used In Vitro Stress Assays. *Plant Physiology*, *165*(2), 519–527.

Czechowski, T., Stitt, M., Altmann, T., Udvardi, M. K., & Scheible, W.-R. (2005). Genome-Wide Identification And Testing Of Superior Reference Genes For Transcript Normalization In *Arabidopsis*. *Plant Physiology*, *139*(1), 5–17.

Das, K., & Roychoudhury, A. (2014). Reactive Oxygen Species (ROS) And Response Of Antioxidants As ROS-Scavengers During Environmental Stress In Plants. *Frontiers Of Environmental Science & Engineering In China*, *2*, 53.

Demirer, G. S., Zhang, H., Goh, N. S., González-Grandío, E., & Landry, M. P. (2019). Carbon Nanotube-Mediated DNA Delivery Without Transgene Integration In Intact Plants. *Nature Protocols.14*, 2954–2971.

Demirer, G. S., Zhang, H., Matos, J. L., Goh, N. S., Cunningham, F. J., Sung, Y., Chang, R., Aditham, A. J., Chio, L., Cho, M.-J., Staskawicz, B., & Landry, M. P. (2019). High Aspect Ratio Nanomaterials Enable Delivery Of Functional Genetic Material Without DNA Integration In Mature Plants. *Nature Nanotechnology*, *14*(5), 456–464.

Desimone, M., Henke, A., & Wagner, E. (1996). Oxidative Stress Induces Partial Degradation Of The Large Subunit Of Ribulose-1,5-Bisphosphate Carboxylase/Oxygenase In Isolated Chloroplasts Of Barley. *Plant Physiology*, *111*(3), 789–796.

Dietz, K.-J., & Herth, S. (2011). Plant Nanotoxicology. *Trends In Plant Science*, *16*(11), 582–589.

Djanaguiraman, M., Nair, R., Giraldo, J. P., & Prasad, P. V. V. (2018). Cerium Oxide Nanoparticles Decrease Drought-Induced Oxidative Damage In Sorghum Leading To Higher Photosynthesis And Grain Yield. *ACS Omega*, *3*(10), 14406–14416.

Doane, T. L., Chuang, C.-H., Hill, R. J., & Burda, C. (2012). Nanoparticle Z -Potentials. *Accounts Of Chemical Research*, *45*(3), 317–326.

Dong, H., Li, Y., Yu, J., Song, Y., Cai, X., Liu, J., Zhang, J., Ewing, R. C., & Shi, D. (2013). A Versatile Multicomponent Assembly Via B-Cyclodextrin Host-Guest Chemistry On Graphene For Biomedical Applications. *Small* , *9*(3), 446–456.

Drazkiewicz, M., Skórzyńska-Polit, E., & Krupa, Z. (2004). Copper-Induced Oxidative Stress And Antioxidant Defence In *Arabidopsis thaliana*. *Biometals: An International Journal On The Role Of Metal Ions In Biology, Biochemistry, And Medicine*, *17*(4), 379–387.

Etxeberria, E., Gonzalez, P., Bhattacharya, P., Sharma, P., & Ke, P. C. (2016). Determining The Size Exclusion For Nanoparticles In Citrus Leaves. *Hortscience: A Publication Of The American Society For Horticultural Science*, *51*(6), 732–737.

Field, R. J., & Bishop, N. G. (1988). Promotion Of Stomatal Infiltration Of Glyphosate By An Organosilicone Surfactant Reduces The Critical Rainfall Period. *Pesticide Science*, *24*(1), 55–62.

Flamigni, L. (1993). Inclusion Of Fluorescein And Halogenated Derivatives In .Alpha.-, .Beta.-, And .Gamma.-Cyclodextrins: A Steady-State And Picosecond Time-Resolved Study. *The Journal Of Physical Chemistry*, *97*(38), 9566–9572.

Foroozandeh, P., & Aziz, A. A. (2015). Merging Worlds Of Nanomaterials And Biological Environment: Factors Governing Protein Corona Formation On Nanoparticles And Its Biological Consequences. *Nanoscale Research Letters*, *10*, 221.

Forster, W. A., Alison Forster, W., & Kimberley, M. O. (2015). The Contribution Of Spray Formulation Component Variables To Foliar Uptake Of Agrichemicals. In *Pest Management Science*. *71*(9), 1324–1334.

Genty, & B. (1992). Modulation Of Efficiency Of Primary Conversion In Leaves, Mechanisms Involved At Photosystem II. *Research In Photosynthesis*, *1*, 603–610.

Genty, B., Briantais, J.-M., & Baker, N. R. (1989). The Relationship Between The Quantum Yield Of Photosynthetic Electron Transport And Quenching Of Chlorophyll Fluorescence. *Biochimica Et Biophysica Acta (Bba) - General Subjects*, *990*(1), 87–92.

Giraldo, J. P., Landry, M. P., Faltermeier, S. M., Mcnicholas, T. P., Iverson, N. M., Boghossian, A. A., Reuel, N. F., Hilmer, A. J., Sen, F., Brew, J. A., & Strano, M. S. (2014a). Plant Nanobionics Approach To Augment Photosynthesis And Biochemical Sensing. *Nature Materials*, *13*(4), 400–408.

Giraldo, J. P., Landry, M. P., Faltermeier, S. M., Mcnicholas, T. P., Iverson, N. M., Boghossian, A. A., Reuel, N. F., Hilmer, A. J., Sen, F., Brew, J. A., & Strano, M. S. (2014b). Plant Nanobionics Approach To Augment Photosynthesis And Biochemical Sensing. *Nature Materials*, *13*(4), 400–408.

Giraldo, J. P., Wu, H., Newkirk, G. M., & Kruss, S. (2019). Nanobiotechnology Approaches For Engineering Smart Plant Sensors. *Nature Nanotechnology*, *14*(6), 541–553.

Gogotsi, Y. (2018). Moving Ions Confined Between Graphene Sheets [Review Of *Moving Ions Confined Between Graphene Sheets*]. *Nature Nanotechnology*, *13*(8), 625–627.

Gullner, G., & Tyihák, E. (1991). Measurement Of Formaldehyde, Hydrogen Peroxide And Non-Protein Thiols In Tobacco Leaves During Ageing. In *Biochemie Und Physiologie Der Pflanzen*. *187*, (2), 131–138.

Hamada, F., Ishikawa, K., Higuchi, Y., Akagami, Y., & Ueno, A. (1996). Strong Binding Between Acidic Guests And Fluorescein Modified -Cyclodextrin Via Hydrogen Bonding. *Journal Of Inclusion Phenomena And Molecular Recognition In Chemistry*, *25*(4), 283–294.

He, Y., Liu, Y., Cao, W., Huai, M., Xu, B., & Huang, B. (2005). Effects Of Salicylic Acid On Heat Tolerance Associated With Antioxidant Metabolism In Kentucky Bluegrass. *Crop Science*, *45*(3), 988–995.

Hofmann, T., Lowry, G. V., Ghoshal, S., Tufenkji, N., Brambilla, D., Dutcher, J. R., Gilbertson, L. M., Giraldo, J. P., Kinsella, J. M., Landry, M. P., Lovell, W., Naccache, R., Paret, M., Pedersen, J. A., Unrine, J. M., White, J. C., & Wilkinson, K. J. (2020). Technology Readiness And Overcoming Barriers To Sustainably Implement Nanotechnology-Enabled Plant Agriculture. *Nature Food*, *1*(7), 416–425.

Hörtensteiner, S., & Kräutler, B. (2011). Chlorophyll Breakdown In Higher Plants. *Biochimica Et Biophysica Acta*, *1807*(8), 977–988.

Huff, A. (1982). Peroxidase-Catalysed Oxidation Of Chlorophyll By Hydrogen Peroxide. *Phytochemistry*, *21*(2), 261–265.

Hu, J. J., Dubin, N., Kurland, D., Ma, B. L., & Roush, G. C. (1995). The Effects Of Hydrogen Peroxide On DNA Repair Activities. *Mutation Research*, *336*(2), 193–201.

Hung, K. T., & Kao, C. H. (2004). Hydrogen Peroxide Is Necessary For Abscisic Acid-Induced Senescence Of Rice Leaves. *Journal Of Plant Physiology*, *161*(12), 1347–1357.

Hu, P., An, J., Faulkner, M. M., Wu, H., Li, Z., Tian, X., & Giraldo, J. P. (2020a). Nanoparticle Charge And Size Control Foliar Delivery Efficiency To Plant Cells And Organelles. *ACS Nano*. *14*(7)*,* 7970–7986.

Hu, P., An, J., Faulkner, M. M., Wu, H., Li, Z., Tian, X., & Giraldo, J. P. (2020b). Nanoparticle Charge And Size Control Foliar Delivery Efficiency To Plant Cells And Organelles. *ACS Nano*, *14*(7), 7970–7986.

Ishida, H., Izumi, M., Wada, S., & Makino, A. (2014). Roles Of Autophagy In Chloroplast Recycling. *Biochimica Et Biophysica Acta*, *1837*(4), 512–521.

Izumi, M., & Nakamura, S. (2017). Partial Or Entire: Distinct Responses Of Two Types Of Chloroplast Autophagy. *Plant Signaling & Behavior*, *12*(11), E1393137.

Jarvis, P., & Soll, J. (2002). Toc, Tic, And Chloroplast Protein Import. *Biochimica Et Biophysica Acta*, *1590*(1-3), 177–189.

Jones, K., Kim, D. W., Park, J. S., & Khang, C. H. (2016). Live-Cell Fluorescence Imaging To Investigate The Dynamics Of Plant Cell Death During Infection By The Rice Blast Fungus *Magnaporthe Oryzae*. *Bmc Plant Biology*, *16*, 69.

Jung, S. (2004). Effect Of Chlorophyll Reduction In *Arabidopsis thaliana* By Methyl Jasmonate Or Norflurazon On Antioxidant Systems. *Plant Physiology And Biochemistry: Ppb / Societe Francaise De Physiologie Vegetale*, *42*(3), 225–231.

Kah, M., Tufenkji, N., & White, J. C. (2019). Nano-Enabled Strategies To Enhance Crop Nutrition And Protection. *Nature Nanotechnology*, *14*(6), 532–540.

Kalaji, H. M., Jajoo, A., Oukarroum, A., Brestic, M., Zivcak, M., Samborska, I. A., Cetner, M. D., Łukasik, I., Goltsev, V., & Ladle, R. J. (2016). Chlorophyll A Fluorescence As A Tool To Monitor Physiological Status Of Plants Under Abiotic Stress Conditions. *Acta Physiologiae Plantarum / Polish Academy Of Sciences, Committee Of Plant Physiology Genetics And Breeding*, *38*(4), 102.

Khan, W. U., Wang, D., Zhang, W., Tang, Z., Ma, X., Ding, X., Du, S., & Wang, Y. (2017). High Quantum Yield Green-Emitting Carbon Dots For Fe(Iii) Detection, Biocompatible Fluorescent Ink And Cellular Imaging. *Scientific Reports*, *7*(1), 14866.

Kitajima, M., & Butler, W. L. (1975). Quenching Of Chlorophyll Fluorescence And Primary Photochemistry In Chloroplasts By Dibromothymoquinone. *Biochimica Et*

Biophysica Acta, *376*(1), 105–115.

Koressaar, T., & Remm, M. (2007). Enhancements And Modifications Of Primer Design Program Primer3. *Bioinformatics*, *23*(10), 1289–1291.

Kranjc, E., Mazej, D., Regvar, M., Drobne, D., & Remškar, M. (2018). Foliar Surface Free Energy Affects Platinum Nanoparticle Adhesion, Uptake, And Translocation From Leaves To Roots In Arugula And Escarole. *Environmental Science: Nano*, *5*(2), 520–532.

Kubis, S. E., Lilley, K. S., & Jarvis, P. (2008). Isolation And Preparation Of Chloroplasts From *Arabidopsis thaliana* Plants. *Methods In Molecular Biology* , *425*, 171–186.

Kumar, R. A., Oldenburg, D. J., & Bendich, A. J. (2014). Changes In DNA Damage, Molecular Integrity, And Copy Number For Plastid DNA And Mitochondrial DNA During Maize Development. *Journal Of Experimental Botany*, *65*(22), 6425–6439.

Kumar Tewari, R., Kumar, P., Tewari, N., Srivastava, S., & Sharma, P. N. (2004). Macronutrient Deficiencies And Differential Antioxidant Responses—Influence On The Activity And Expression Of Superoxide Dismutase In Maize. *Plant Science: An International Journal Of Experimental Plant Biology*, *166*(3), 687–694.

Kumar, V., Sharma, M., Khare, T., & Wani, S. H. (2018). Chapter 17 - Impact Of Nanoparticles On Oxidative Stress And Responsive Antioxidative Defense In Plants. *Nanomaterials In Plants, Algae, And Microorganisms*. Academic Press, *1,* 393–406.

Kwak, S.-Y., Lew, T. T. S., Sweeney, C. J., Koman, V. B., Wong, M. H., Bohmert-Tatarev, K., Snell, K. D., Seo, J. S., Chua, N.-H., & Strano, M. S. (2019). Chloroplast-Selective Gene Delivery And Expression In Planta Using Chitosan-Complexed Single-Walled Carbon Nanotube Carriers. *Nature Nanotechnology*, *14*(5), 447–455.

Lakshmanan, M., Kodama, Y., Yoshizumi, T., Sudesh, K., & Numata, K. (2013). Rapid And Efficient Gene Delivery Into Plant Cells Using Designed Peptide Carriers. *Biomacromolecules*, *14*(1), 10–16.

Larue, C., Castillo-Michel, H., Sobanska, S., Cécillon, L., Bureau, S., Barthès, V., Ouerdane, L., Carrière, M., & Sarret, G. (2014). Foliar Exposure Of The Crop Lactuca Sativa To Silver Nanoparticles: Evidence For Internalization And Changes In Ag Speciation. *Journal Of Hazardous Materials*, *264*, 98–106.

Lee, D. W., Jung, C., & Hwang, I. (2013). Cytosolic Events Involved In Chloroplast Protein Targeting. *Biochimica Et Biophysica Acta*, *1833*(2), 245–252.

Lee, D. W., Lee, S., Oh, Y. J., & Hwang, I. (2009). Multiple Sequence Motifs In The Rubisco Small Subunit Transit Peptide Independently Contribute To Toc159-Dependent Import Of Proteins Into Chloroplasts. *Plant Physiology*, *151*(1), 129–141.

Lew, T. T. S., Wong, M. H., Kwak, S.-Y., Sinclair, R., Koman, V. B., & Strano, M. S. (2018). Rational Design Principles For The Transport And Subcellular Distribution Of Nanomaterials Into Plant Protoplasts. *Small* , *14*(44), E1802086.

Liguori, I., Russo, G., Curcio, F., Bulli, G., Aran, L., Della-Morte, D., Gargiulo, G., Testa, G., Cacciatore, F., Bonaduce, D., & Abete, P. (2018). Oxidative Stress, Aging, And Diseases. *Clinical Interventions In Aging*, *13*, 757–772.

Li, H., Huang, J., Liu, Y., Lu, F., Zhong, J., Wang, Y., & Li, S. (2019). Enhanced Rubisco Activity And Promoted Dicotyledons Growth With Degradable Carbon Dots. *Nano*.*12*, 1585–1593.

Lilley, R. M., Fitzgerald, M. P., Rienits, K. G., & Walker, D. A. (1975). Criteria Of Intactness And The Photosynthetic Activity Of Spinach Chloroplast Preparations. *The New Phytologist*, *75*(1), 1–10.

Lin, S., Reppert, J., Hu, Q., Hudson, J. S., Reid, M. L., Ratnikova, T. A., Rao, A. M., Luo, H., & Ke, P. C. (2009). Uptake, Translocation, And Transmission Of Carbon Nanomaterials In Rice Plants. *Small*, *5*(10), 1128–1132.

Li, Q., Ohulchanskyy, T. Y., Liu, R., Koynov, K., Wu, D., Best, A., Kumar, R., Bonoiu, A., & Prasad, P. N. (2010). Photoluminescent Carbon Dots As Biocompatible Nanoprobes For Targeting Cancer Cells In Vitro. *Journal Of Physical Chemistry C*, *114*(28), 12062–12068.

Li, Q., Zhang, Y., Jin, Y., Yang, Q., Du, J., & Li, Y. (2015). Fluorescent Magnetic Nanosensors For Zn 2+ And Cn- In Aqueous Solution Prepared From Adamantane-Modified Fluorescein And B-Cyclodextrin-Modified Fe3O4-SiO2 Via Host-Guest Interactions. *RSC Advances*, *5*(84), 68815–68821.

Liu, C.-J., Burghaus, U., Besenbacher, F., & Wang, Z. L. (2010). Preparation And Characterization Of Nanomaterials For Sustainable Energy Production. *ACS Nano*, *4*(10), 5517–5526.

Liu, Q., Chen, B., Wang, Q., Shi, X., Xiao, Z., Lin, J., & Fang, X. (2009). Carbon Nanotubes As Molecular Transporters For Walled Plant Cells. *Nano Letters*, *9*(3), 1007–1010.

Liu, W., Rose, J., Plantevin, S., Auffan, M., Bottero, J.-Y., & Vidaud, C. (2013). Protein Corona Formation For Nanomaterials And Proteins Of A Similar Size: Hard Or Soft Corona? *Nanoscale*, *5*(4), 1658–1668.

Liu, Y., Ren, D., Pike, S., Pallardy, S., Gassmann, W., & Zhang, S. (2007). Chloroplast-Generated Reactive Oxygen Species Are Involved In Hypersensitive Response-Like Cell Death Mediated By A Mitogen-Activated Protein Kinase Cascade. *The Plant Journal: For Cell And Molecular Biology*, *51*(6), 941–954.

Li, W., Zheng, Y., Zhang, H., Liu, Z., Su, W., Chen, S., Liu, Y., Zhuang, J., & Lei, B. (2016). Phytotoxicity, Uptake, And Translocation Of Fluorescent Carbon Dots In Mung Bean Plants. *ACS Applied Materials & Interfaces*, *8*(31), 19939–19945.

Li, Y., Pan, X., Xu, X., Wu, Y., Zhuang, J., Zhang, X., Zhang, H., Lei, B., Hu, C., & Liu, Y. (2021). Carbon Dots As Light Converter For Plant Photosynthesis: Augmenting Light Coverage And Quantum Yield Effect. *Journal Of Hazardous Materials*, *410*, 124534.

Li, Y., Xu, X., Wu, Y., Zhuang, J., Zhang, X., Zhang, H., Lei, B., Hu, C., & Liu, Y. (2020). A Review On The Effects Of Carbon Dots In Plant Systems. *Materials Chemistry Frontiers*, *4*(2), 437–448.

Lowry, G. V., Avellan, A., & Gilbertson, L. M. (2019). Opportunities And Challenges For Nanotechnology In The Agri-Tech Revolution. *Nature Nanotechnology*, *14*(6), 517–522.

Majumdar, S., Pagano, L., Wohlschlegel, J. A., Villani, M., Zappettini, A., White, J. C., & Keller, A. A. (2019). Proteomic, Gene And Metabolite Characterization Reveal The Uptake And Toxicity Mechanisms Of Cadmium Sulfide Quantum Dots In Soybean Plants. *Environmental Science: Nano*, *6*(10), 3010–3026.

Maksymiec, W., & Krupa, Z. (2006). The Effects Of Short-Term Exposition To Cd, Excess Cu Ions And Jasmonate On Oxidative Stress Appearing In *Arabidopsis thaliana*. *Environmental And Experimental Botany*, *57*(1), 187–194.

Marmiroli, M., Mussi, F., Pagano, L., Imperiale, D., Lencioni, G., Villani, M., Zappettini, A., White, J. C., & Marmiroli, N. (2020). Cadmium Sulfide Quantum Dots Impact *Arabidopsis thaliana* Physiology And Morphology. *Chemosphere*, *240*, 124856.

Maxwell, K., & Johnson, G. N. (2000). Chlorophyll Fluorescence—A Practical Guide. *Journal Of Experimental Botany*, *51*(345), 659–668.

Mba, C., Guimaraes, E. P., & Ghosh, K. (2012). Re-Orienting Crop Improvement For The Changing Climatic Conditions Of The 21st Century. *Agriculture & Food Security*, *1*(1), 1–17.

Mignolet-Spruyt, L., Xu, E., Idänheimo, N., Hoeberichts, F. A., Mühlenbock, P., Brosché, M., Van Breusegem, F., & Kangasjärvi, J. (2016). Spreading The News: Subcellular And Organellar Reactive Oxygen Species Production And Signalling. *Journal Of Experimental Botany*, *67*(13), 3831–3844.

Miralles, P., Church, T. L., & Harris, A. T. (2012). Toxicity, Uptake, And Translocation Of Engineered Nanomaterials In Vascular Plants. *Environmental Science & Technology*, *46*(17), 9224–9239.

Mondal, S., & Purkayastha, P. (2016). A-Cyclodextrin Functionalized Carbon Dots:

Pronounced Photoinduced Electron Transfer By Aggregated Nanostructures. *Journal Of Physical Chemistry C*, *120*(26), 14365–14371.

Monica, R. C., & Cremonini, R. (2009). Nanoparticles And Higher Plants. *Caryologia*, *62*(2), 161–165.

Mukherjee, S., Chakraborty, A., Mondal, S., Saha, S., Haque, A., & Paul, S. (2019). Assessment Of Common Plant Parameters As Biomarkers Of Air Pollution. *Environmental Monitoring And Assessment*, *191*(6), 400.

Nafees, M., Fahad, S., Shah, A. N., Bukhari, M. A., Maryam, Ahmed, I., Ahmad, S., & Hussain, S. (2019). Reactive Oxygen Species Signaling In Plants. In M. Hasanuzzaman, K. R. Hakeem, K. Nahar, & H. F. Alharby (Eds.), *Plant Abiotic Stress Tolerance: Agronomic, Molecular And Biotechnological Approaches*. 9(8) 681.

Nagajyoti, P. C., Lee, K. D., & Sreekanth, T. V. M. (2010). Heavy Metals, Occurrence And Toxicity For Plants: A Review. *Environmental Chemistry Letters*, *8*(3), 199–216.

Nakamura, S., Hidema, J., Sakamoto, W., Ishida, H., & Izumi, M. (2018). Selective Elimination Of Membrane-Damaged Chloroplasts Via Microautophagy. *Plant Physiology*, *177*(3), 1007–1026.

Nel, A., Xia, T., Mädler, L., & Li, N. (2006). Toxic Potential Of Materials At The Nanolevel. *Science*, *311*(5761), 622–627.

Newkirk, G. M., De Allende, P., Jinkerson, R. E., & Giraldo, J. P. (2021). Nanotechnology Approaches For Chloroplast Biotechnology Advancements. *Frontiers In Plant Science*, *12*, 691295.

Ng, K. K., Motoda, Y., Watanabe, S., Sofiman Othman, A., Kigawa, T., Kodama, Y., & Numata, K. (2016). Intracellular Delivery Of Proteins Via Fusion Peptides In Intact Plants. *Plos One*, *11*(4), E0154081.

Oldenburg, D. J., & Bendich, A. J. (2015). DNA Maintenance In Plastids And Mitochondria Of Plants. *Frontiers In Plant Science*, *6*, 883.

Park, J., Nam, J., Won, N., Jin, H., Jung, S., Jung, S., Cho, S.-H., & Kim, S. (2011). Compact And Stable Quantum Dots With Positive, Negative, Or Zwitterionic Surface: Specific Cell Interactions And Non-Specific Adsorptions By The Surface Charges. *Advanced Functional Materials*, *21*(9), 1558–1566.

Pfaffl, M. W. (2001). A New Mathematical Model For Relative Quantification In Real-Time RT-PCR. *Nucleic Acids Research*, *29*(9), e45.

Polle, A. (2001). Dissecting The Superoxide Dismutase-Ascorbate-Glutathione-Pathway In Chloroplasts By Metabolic Modeling. Computer Simulations As A Step Towards

Flux Analysis. *Plant Physiology*, *126*(1), 445–462.

Prasad, R., Kumar, V., & Prasad, K. S. (2014). Nanotechnology In Sustainable Agriculture: Present Concerns And Future Aspects. *African Journal Of Biotechnology*, *13*(6), 705–713.

Qian, Z. S., Shan, X. Y., Chai, L. J., Ma, J. J., Chen, J. R., & Feng, H. (2014). DNA Nanosensor Based On Biocompatible Graphene Quantum Dots And Carbon Nanotubes. *Biosensors & Bioelectronics*, *60*, 64–70.

Ramos-Perez, V., Cifuentes, A., Coronas, N., De Pablo, A., & Borrós, S. (2013). Modification Of Carbon Nanotubes For Gene Delivery Vectors. *Methods In Molecular Biology*, *1025*, 261–268.

Ray, D. K., Mueller, N. D., West, P. C., & Foley, J. A. (2013). Yield Trends Are Insufficient To Double Global Crop Production By 2050. *Plos One*, *8*(6), E66428.

Robinson, J. M., Smith, M. G., & Gibbs, M. (1980). Influence Of Hydrogen Peroxide Upon Carbon Dioxide Photoassimilation In The Spinach Chloroplast: I. Hydrogen Peroxide Generated By Broken Chloroplasts In An "Intact" Chloroplast Preparation Is A Causal Agent Of The Warburg Effect. *Plant Physiology*, *65*(4), 755–759.

Runk, B. R. (1983). *Chloroplast Membrane Adaptation And Repair In Response To Environmental Stress In Maize Seedlings (Zea Mays L.)*. Michigan State University. Department Of Biochemistry.

Saha, S., Roy, A., Roy, K., & Roy, M. N. (2016). Study To Explore The Mechanism To Form Inclusion Complexes Of B-Cyclodextrin With Vitamin Molecules. *Scientific Reports*, *6*, 35764.

Santana, I., Hu, P., Jeon, S.-J., Castillo, C., Tu, H., & Giraldo, J. P. (2021). Peptide-Mediated Targeting Of Nanoparticles With Chemical Cargoes To Chloroplasts In *Arabidopsis* Plants. *Bio-Protocol*, *11*(12), E4060.

Santana, I., Wu, H., Hu, P., & Giraldo, J. P. (2020). Targeted Delivery Of Nanomaterials With Chemical Cargoes In Plants Enabled By A Biorecognition Motif. *Nature Communications*, *11*(1), 2045.

Sanzari, I., Leone, A., & Ambrosone, A. (2019). Nanotechnology In Plant Science: To Make A Long Story Short. *Frontiers In Bioengineering And Biotechnology*, *7*, 120.

Servin, A. D., & White, J. C. (2016). Nanotechnology In Agriculture: Next Steps For Understanding Engineered Nanoparticle Exposure And Risk. *Nanoimpact*, *1*, 9–12.

Shen, B.-R., Zhu, C.-H., Yao, Z., Cui, L.-L., Zhang, J.-J., Yang, C.-W., He, Z.-H., & Peng, X.-X. (2017). An Optimized Transit Peptide For Effective Targeting Of Diverse Foreign Proteins Into Chloroplasts In Rice. *Scientific Reports*, *7*, 46231.

Smirnoff, N., & Arnaud, D. (2019). Hydrogen Peroxide Metabolism And Functions In Plants. *The New Phytologist*, *221*(3), 1197–1214.

Su, Y., Ashworth, V., Kim, C., Adeleye, A. S., Rolshausen, P., Roper, C., White, J., & Jassby, D. (2019). Delivery, Uptake, Fate, And Transport Of Engineered Nanoparticles In Plants: A Critical Review And Data Analysis. *Environmental Science: Nano*, *6*(8), 2311–2331.

Swift, T. A., Fagan, D., Benito-Alifonso, D., Hill, S. A., Yallop, M. L., Oliver, T. A. A., Lawson, T., Galan, M. C., & Whitney, H. M. (2021). Photosynthesis And Crop Productivity Are Enhanced By Glucose-Functionalized Carbon Dots. *The New Phytologist*, *229*(2), 783–790.

Tang, C., Qian, Z., Huang, Y., Xu, J., Ao, H., & Zhao, M. (2016). A Fluorometric Assay For Alkaline Phosphatase Activity Based On B-Cyclodextrin-Modified Carbon Quantum Dots Through Host-Guest Recognition. *Biosensors*. *83*(15), 274-280.

Tripathi, D. K., Shweta, Singh, S., Singh, S., Pandey, R., Singh, V. P., Sharma, N. C., Prasad, S. M., Dubey, N. K., & Chauhan, D. K. (2017). An Overview On Manufactured Nanoparticles In Plants: Uptake, Translocation, Accumulation And Phytotoxicity. *Plant Physiology And Biochemistry: Ppb / Societe Francaise De Physiologie Vegetale*, *110*, 2–12.

Tripathi, D., Nam, A., Oldenburg, D. J., & Bendich, A. J. (2020). Reactive Oxygen Species, Antioxidant Agents, And DNA Damage In Developing Maize Mitochondria And Plastids. *Frontiers In Plant Science*, *11*, 596.

Valavanidis, A., Vlachogianni, T., & Fiotakis, C. (2009). 8-Hydroxy-2' -Deoxyguanosine (8-Ohdg): A Critical Biomarker Of Oxidative Stress And Carcinogenesis. *Journal Of Environmental Science And Health. Part C, Environmental Carcinogenesis & Ecotoxicology Reviews*, *27*(2), 120–139.

Veljovic-Jovanovic, S., Noctor, G., & Foyer, C. H. (2002). Are Leaf Hydrogen Peroxide Concentrations Commonly Overestimated? The Potential Influence Of Artefactual Interference By Tissue Phenolics And Ascorbate. *Plant Physiology And Biochemistry: Ppb / Societe Francaise De Physiologie Vegetale*, *40*(6), 501–507.

Walker, D. A. (1965). Correlation Between Photosynthetic Activity And Membrane Integrity In Isolated Pea Chloroplasts. *Plant Physiology*, *40*(6), 1157–1161.

Walkey, C. D., & Chan, W. C. W. (2012). Understanding And Controlling The Interaction Of Nanomaterials With Proteins In A Physiological Environment. *Chemical Society Reviews*, *41*(7), 2780–2799.

Wang, J. W., Grandio, E. G., Newkirk, G. M., Demirer, G. S., Butrus, S., Giraldo, J. P., & Landry, M. P. (2019). Nanoparticle-Mediated Genetic Engineering Of Plants. *Molecular Plant*, *12*(8), 1037–1040.

Wang, J.-Z., & Dehesh, K. (2018). Er: The Silk Road Of Interorganellar Communication. *Current Opinion In Plant Biology*, *45*, 171–177.

Wang, P., Lombi, E., Zhao, F.-J., & Kopittke, P. M. (2016). Nanotechnology: A New Opportunity In Plant Sciences. *Trends In Plant Science*, *21*(8), 699–712.

Wang, T., Wang, A., Wang, R., Liu, Z., Sun, Y., Shan, G., Chen, Y., & Liu, Y. (2019). Carbon Dots With Molecular Fluorescence And Their Application As A "Turn-Off" Fluorescent Probe For Ferricyanide Detection. *Scientific Reports*, *9*(1), 10723.

Watanabe, K., Yamada, N., & Takeuchi, Y. (2006). Oxidative DNADamage In Cucumber Cotyledons Irradiated With Ultraviolet Light. *Journal Of Plant Research*, *119*(3), 239–246.

Watanabe, M., Balazadeh, S., Tohge, T., Erban, A., Giavalisco, P., Kopka, J., Mueller-Roeber, B., Fernie, A. R., & Hoefgen, R. (2013). Comprehensive Dissection Of Spatiotemporal Metabolic Shifts In Primary, Secondary, And Lipid Metabolism During Developmental Senescence In *Arabidopsis*. *Plant Physiology*, *162*(3), 1290–1310.

Weise, S. E., Weber, A. P. M., & Sharkey, T. D. (2004). Maltose Is The Major Form Of Carbon Exported From The Chloroplast At Night. *Planta*, *218*(3), 474–482.

White, J. C., & Gardea-Torresdey, J. (2018). Achieving Food Security Through The Very Small. *Nature Nanotechnology*, *13*(8), 627–629.

Willett, W., Rockström, J., Loken, B., Springmann, M., Lang, T., Vermeulen, S., Garnett, T., Tilman, D., Declerck, F., Wood, A., Jonell, M., Clark, M., Gordon, L. J., Fanzo, J., Hawkes, C., Zurayk, R., Rivera, J. A., De Vries, W., Majele Sibanda, L., … Murray, C. J. L. (2019). Food In The Anthropocene: The Eat–Lancet Commission On Healthy Diets From Sustainable Food Systems. *The Lancet*, *393*(10170), 447–492.

Wong, M. H., Misra, R. P., Giraldo, J. P., Kwak, S.-Y., Son, Y., Landry, M. P., Swan, J. W., Blankschtein, D., & Strano, M. S. (2016). Lipid Exchange Envelope Penetration (Leep) Of Nanoparticles For Plant Engineering: A Universal Localization Mechanism. *Nano Letters*, *16*(2), 1161–1172.

Yagi, Y., & Shiina, T. (2014). Recent Advances In The Study Of Chloroplast Gene Expression And Its Evolution. *Frontiers In Plant Science*, *5*, 61.

Yin, B., Whyatt, R. M., Perera, F. P., Randall, M. C., Cooper, T. B., & Santella, R. M. (1995). Determination Of 8-Hydroxydeoxyguanosine By An Immunoaffinity Chromatography-Monoclonal Antibody-Based ELISA. *Free Radical Biology & Medicine*, *18*(6), 1023–1032.

Yoshizumi, T., Oikawa, K., Chuah, J.-A., Kodama, Y., & Numata, K. (2018). Selective Gene Delivery For Integrating Exogenous DNA Into Plastid And Mitochondrial

Genomes Using Peptide-DNA Complexes. *Biomacromolecules*, *19*(5), 1582–1591.

Yu, Q., Barkan, A., & Maliga, P. (2019). Engineered RNA-Binding Protein For Transgene Activation In Non-Green Plastids. *Nature Plants*, *5*(5), 486–490.

Yu, Q., Lutz, K. A., & Maliga, P. (2017). Efficient Plastid Transformation In *Arabidopsis*. *Plant Physiology*, *175*(1), 186–193.

Zhang, H., Zhang, H., Demirer, G. S., González-Grandío, E., Fan, C., & Landry, M. P. (2020). Engineering DNA Nanostructures For Sirna Delivery In Plants. *Nature Protocols*, *15*(9), 3064–3087.

Zhang, L., & Sakamoto, W. (2015). Possible Function Of *Vipp1* In Maintaining Chloroplast Membranes. *Biochimica Et Biophysica Acta*, *1847*(9), 831–837.

Zhao, H., Oczos, J., Janowski, P., Trembecka, D., Dobrucki, J., Darzynkiewicz, Z., & Wlodkowic, D. (2010). Rationale For The Real-Time And Dynamic Cell Death Assays Using Propidium Iodide. *Cytometry. Part A: The Journal Of The International Society For Analytical Cytology*, *77*(4), 399–405.

Chapter 5: Major Contributions and Prospects

In Chapter 2 we described three different methods for *in vivo* delivery and imaging of quantum dots in plant leaves: leaf lamina infiltration, whole shoot vacuum infiltration, and root to leaf translocation. These methods provided ways to study nanoparticle uptake, transport, and distribution in plants and understand the impact of nanoparticles on plant function. The techniques demonstrated can be applied to other nanomaterials with increased biocompatibility. More importantly, this chapter lays the foundation of proper application and characterization of the materials interfaced with plants systems.

Plant cell organization controls biochemical chemical processes and gene expression between nuclear and organellar structures. Furthermore, critical compartments within the plant cell (e.g., vacuole, nucleus, cytoplasm, chloroplasts) contain their unique pH and ideal chemical milieu allowing proper functions and compartmentalization. It is also vital to maintain normal plant function during nanoparticle-plant interfacing and avoid damage to plant tissues and the cellular environment.

Engineered nanomaterials can exhibit chemical properties. Thus, future work should consider proper characterization, appropriate starting materials for nanomaterials synthesis, concentration, and buffered mediums used need to be considered carefully when interfacing nanomaterials with plants. This Chapter tested three of the best strategies to apply nanomaterials for fundamental research purposes in *Arabidopsis thaliana*. It is noteworthy that in Chapter 4, we used the fourth technology for delivering nanomaterial into plants consisting of a foliar spray formulation. This formulation

consisted of nanomaterials suspended in TES buffer with 0.1 % silwet, a surfactant commonly used in agriculture and transfection methods. The development and application of nanomaterials using the spray formulation can be dispersed evenly across the plant vegetative tissues and penetrate the cuticle layer. Furthermore, the formulation was developed to show scalable application in crops.

Chapter 3 develops nanoparticle-based methods for targeted chemical delivery in plants. Current practices for agrochemical use cannot precisely target specific subcellular compartments, leading to inefficiencies and unintended side effects that limit our ability to understand and engineer plant function. As the demand for food production rises, technologies to improve plant science and agriculture through breeding, genetic engineering, and land management strategies will follow suit. Interfacing nanomaterials with plants is becoming a novel technology to improve plant science. Thus, developing tools to enhance the efficacy of fertilizers and nutrients can aid in minimizing the negative impact on the environment and minimizing the exposure to some chemicals not intended for human exposure.

Chapter 3 of this dissertation demonstrates the rational synthesis and proof of concept for a chloroplast-targeted chemical delivery nanomaterial able to tune redox status in live plants (Figure 3.1, 4.1). The chassis of this newly developed nanomaterial is a fluorescence quantum dots (QDs) coated with a chloroplast guiding peptide sequence conserved across dicot plant taxa (Figure 3.1). The high charge and size of the quantum dot, in addition to the targeting motif, promoted penetration through plant cell walls,

membrane and import into chloroplast envelopes. The quantum dots functionalized with a chloroplast targeting peptide (Figure 3.3) showed twice as high colocalization with plant chloroplasts (74.6%) compared with control counterparts without chloroplast transit peptide (37.6%).

Furthermore, the QDs were functionalized with β-CD molecular baskets that allow loading and delivery of various biochemicals to chloroplasts (Figure 3.1, Supplementary Figure table 1, Supplementary Figure 3.1). We rationalized delivering two chemicals, methyl viologen, and ascorbic acid, to enable tunable redox states in chloroplasts through induction and reduction of superoxide anion levels.

The pioneering work in Chapter 3 demonstrates the targeted delivery of chemical cargoes through nanomaterials by leveraging the plant molecular machinery to guide nanoparticles to specific organelles, e.g., chloroplasts. This targeted approach allows the *in vivo* manipulation of plant organelle function, e.g., redox status. The tools developed in this Chapter are a critical step towards bioengineering plant functions, genetic and physiological responses without genetic modifications in non-model plant systems. The tools developed in Chapter 3 will pave the way for future studies of the delivery of nanoparticles with their cargoes into plant organelles for "smart" bioengineering strategies.

Chapter 4 of this dissertation shows proof of concept of improved chemical and plasmid delivery into chloroplast using carbon-based nanomaterials functionalized with targeting peptide motifs. There is an enormous potential for applying nanomaterials to bioengineer chloroplasts and improve crop yields. Applying nanomaterials onto plants

could increase the bioavailability of excess chemicals and foreign elements onto the surrounding ecosystem. If used to scale, these nanotechnology-based crops will be the primary route of human exposure and could become a health and environmental risk. Here, we provided biological measures and approaches towards creating safe and effective nanotechnology-based tools for smart agriculture in the future. We utilized the knowledge and engineering design highlighted in Chapters two and three to develop carbon-based nanomaterial for targeted chemical and genetic materials delivery into plants. Using two carbon-based nanomaterials designed for chemical and gene delivery platforms (carbon dot and single-walled carbon nanotube) (Figure 4.1), we demonstrate proof of concept and replicate the targeted chemical delivery platform's rational design chloroplasts demonstrated in Chapter three. The chemical cargo was delivered inside chloroplasts to a higher degree using a foliar spraying application targeted carbon dot complex. Moreover, we also provided evidence for a gene delivery platform carrying a GFP plasmid vectors design with canonical chloroplasts expression elements. We specifically designed single-walled carbon nanotube (SWCNT) nanomaterials electrostatically grafted with plasmid DNA and a targeting peptide motif (Figure 4.1, Supplemental Figure 4.2) for chloroplast genetic engineering applications.

Using the two nanomaterials (Figure 4.1), we utilized cell-based assays and measures to assess the cell, molecular, and physiology of *Arabidopsis thaliana*. Our analysis showed that targeted nanomaterial has no significant impact on cell death rates or damage to chloroplast membrane intactness at 20 and 2 mg/L of CD and SWCNT

complex concentrations, respectively. These results suggest it improved biocompatibility after 24 hr of initial treatments.

Moreover, a 2-fold increase in oxidative DNA damage was found in whole plant cell DNA after treatments with TP-β-CD and TP-pATV1-SWCNT. In contrast, the levels of isolated chloroplast DNA samples in single-walled carbon nanotube complexes (TP-pATV1-SWCNT) showed significant damage on day but not on day 5. However, targeted carbon dots (TP-β-CD) had no significant oxidative damage at days one and five.

Lastly, the result properly characterizing physiological and photosynthetic parameters pointed to a decrease or inhibition in photosynthesis. The chlorophyll content index levels significantly decreased on days one and five after treatments. The measurement of dark-adapted Photosystem II efficiency (Fv/Fm) and carbon assimilation rates at varying light levels suggest no damage to PSII complexes. Together these results demonstrate the photosynthetic measurements of dark-adapted quantum yield and carboxylation rate are reduced in photosynthesis in the carboxylation limited region (where A is saturated above 400 PAR) (Figure 4.11 A, C). However, the was no observed damage to photosystem and electron transport.

Conclusion

Agricultural breeding, genetic engineering, and land management strategies will not meet the increase in food demand needed for future food security. Sustainable food production will require radical improvements in fertilizer and nutrient use efficiency, improved breeding, and genetic engineering practices to intensify food production with high-quality outputs. One such strategy is using nanotechnology-based tools that can

enhance sustainable agriculture and maintain food security. Recent breakthroughs in nanotechnology have provided various technologies that improve upon genetic engineering platforms, agrochemical delivery, and nano-sensors, enabling farmers and plant breeders to improve crop yields and land management. Nanotechnology-based tools for agriculture rely on understanding their impact on plant health and function.

This dissertation demonstrates methods to safely interface nanomaterials into *Arabidopsis thaliana,* engineering tools that can effectively target the delivery of chemicals and genetic material into the chloroplast and assess the biological impact of engineered nanomaterials in *Arabidopsis thaliana* model systems. Significant consideration should be taken to properly characterize nanomaterials before application into biological systems. By testing for the ideal concentration and developing the nanomaterials for optimized biocompatibility, we can minimize the disruption of photosynthetic efficiency and provide standards for safe and effective nanotechnology-based tools.

Appendixes:

Supplementary Figures: Chapter 3

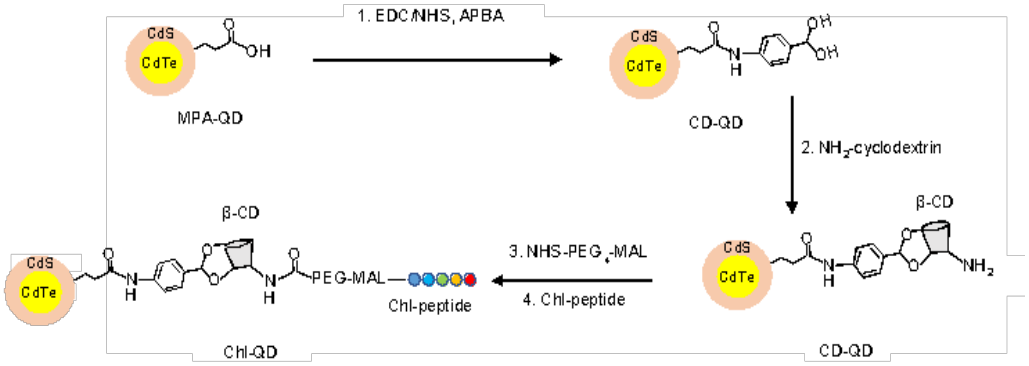

Figure S3.1: Figure diagram of the stepwise synthesis of targeted nanomaterials with biorecognition motifs. Diagram illustrates step by step synthesis of chloroplast targeting quantum dots (Chl-QD) containing β-cyclodextrin (β-CD) molecular baskets and chloroplast guiding peptides. The targeting peptide design (Chl-peptide) is based on a truncated Rubisco small subunit biorecognition motif (RbcS) that guides protein precursors to chloroplast outer membranes.

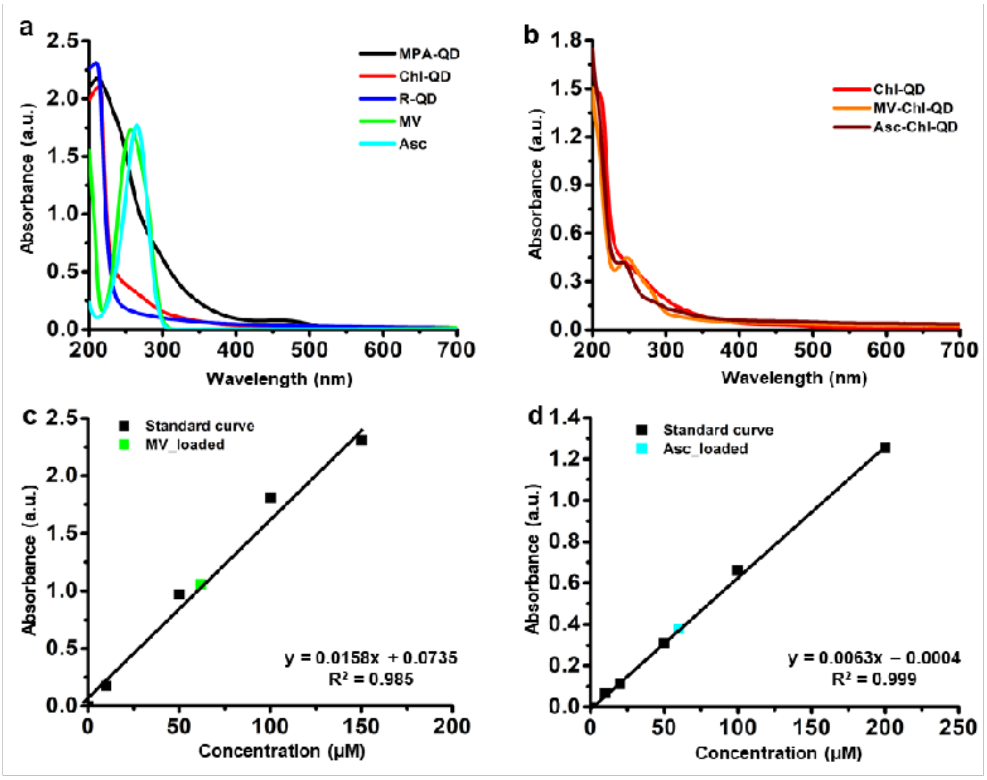

Figure 3.2: Absorption spectra of Chl-QD and loading efficiency of MV and Asc in Chl-QD. a, UV-vis absorption spectra of QDs coated with MPA (MPA- QD), targeting peptide (Chl-QD) and random peptide (R-QD), MV (methyl viologen), and Asc. (ascorbic acid). b, Absorbance spectra of Chl-QD before and after loading with MV (MV-Chl-QD) and Asc (Asc-Chl-QD). Calibration curves of c, MV, and d, Asc absorbance versus concentration were used to determine the loading efficiency of MV (green square) and Asc (cyan square) in Chl-QD.

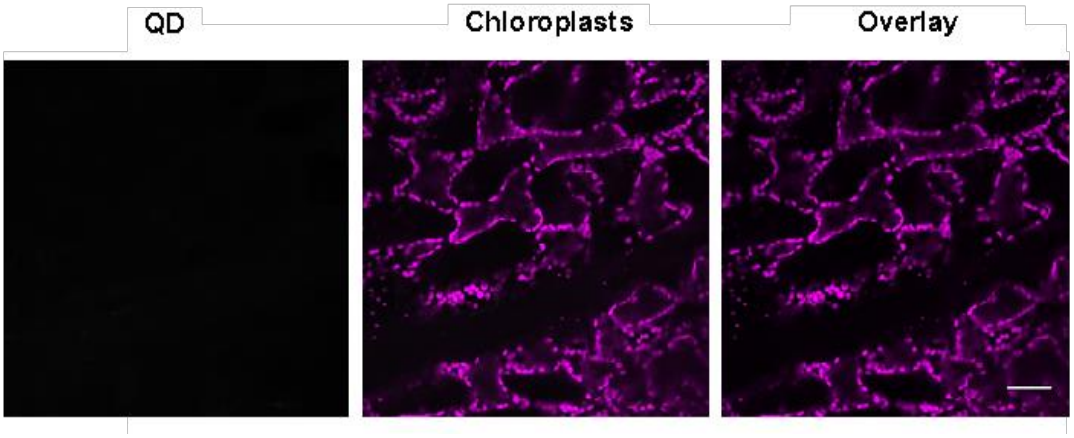

Figure S3.3: Confocal microscopy images of *Arabidopsis thaliana* leaf mesophyll cells infiltrated with TES buffer as control. Leaves infiltrated with TES buffer exhibit no fluorescence signal for QDs within the detection range for QD emission (500-550 nm). Scale bar, 50 μm.

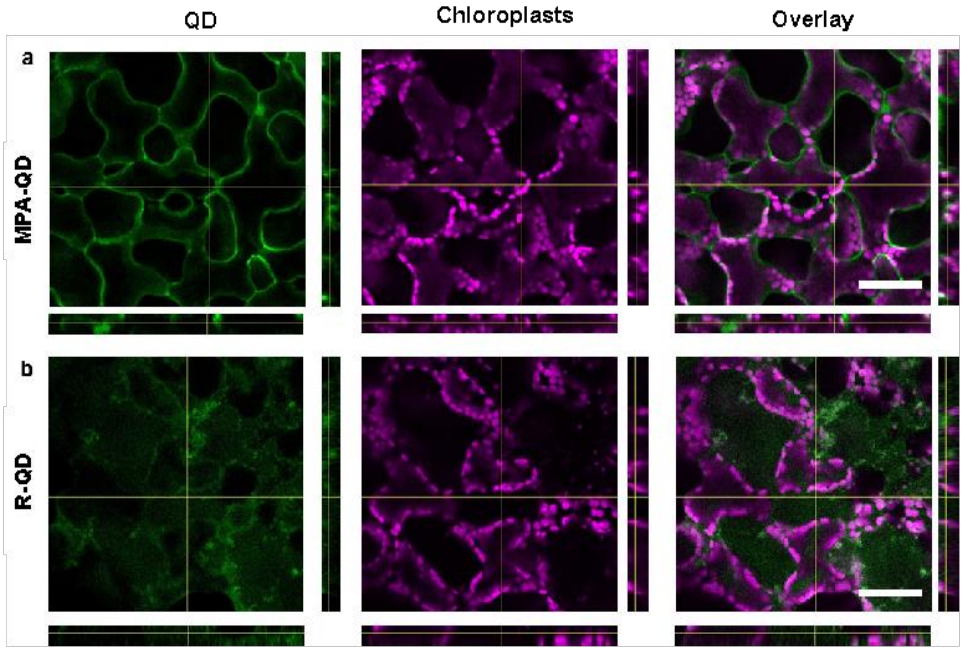

Figure S3.4: Orthogonal views of confocal microscopy images between QD and chloroplasts. Projections in the z-axis of confocal microscopy images in the x and y planes showing colocalization of nanoparticles with chloroplasts for a, QDs coated with MPA (MPA-QD) and b, random peptide (R-QD). Z-axis optical slices were taken every 2 μm up to a depth of 20 μm. Scale bar 50 μm.

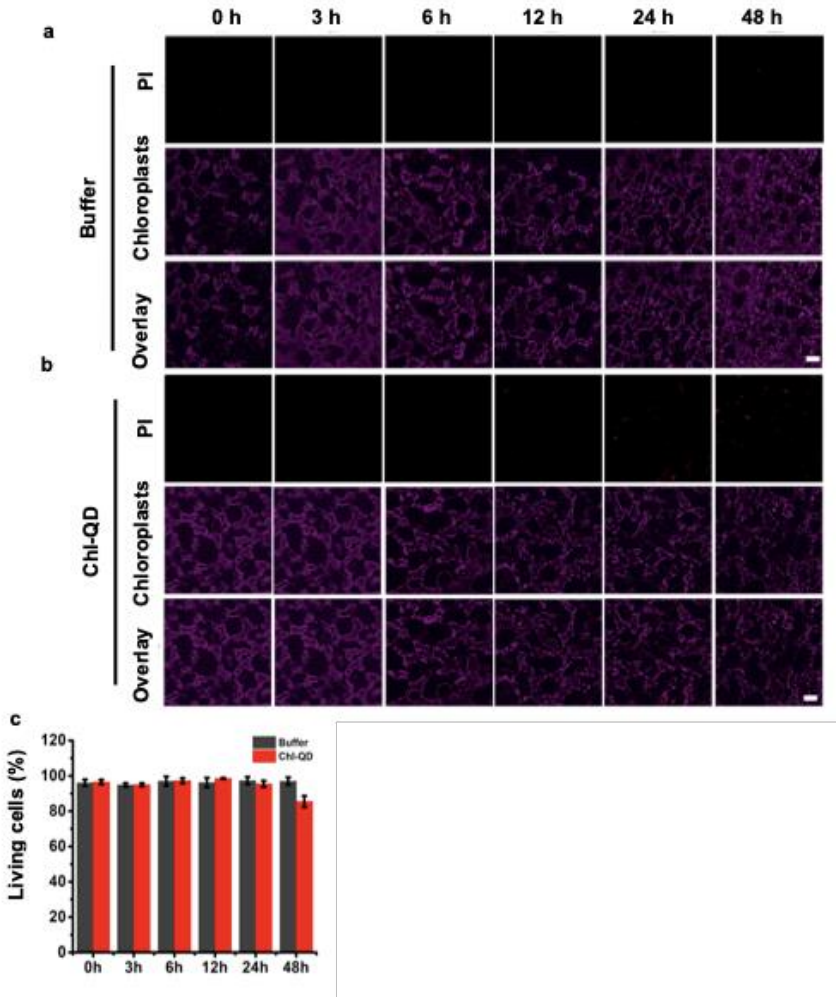

Figure S3.5: Plant cell viability assays in leaves with embedded Chl-QD. a, Confocal fluorescence microscopy images of propidium iodide (PI) stained *Arabidopsis* leaf mesophyll cells infiltrated with 10 mM TES buffer (pH 7.0) and **b,** 200 nM Chl-QD. PI only passes through damaged areas of lipid membranes in dead cells intercalating with the DNA in the nucleus. The PI fluorescence accumulation within the cell boundary was counted as dead cells. Scale bar 50 μm. **c**, The percentage of living cells in *Arabidopsis* leaves infiltrated with Chl-QD or TES buffer solution. Mean ± SD, n = 4. Error bars represent standard deviations.

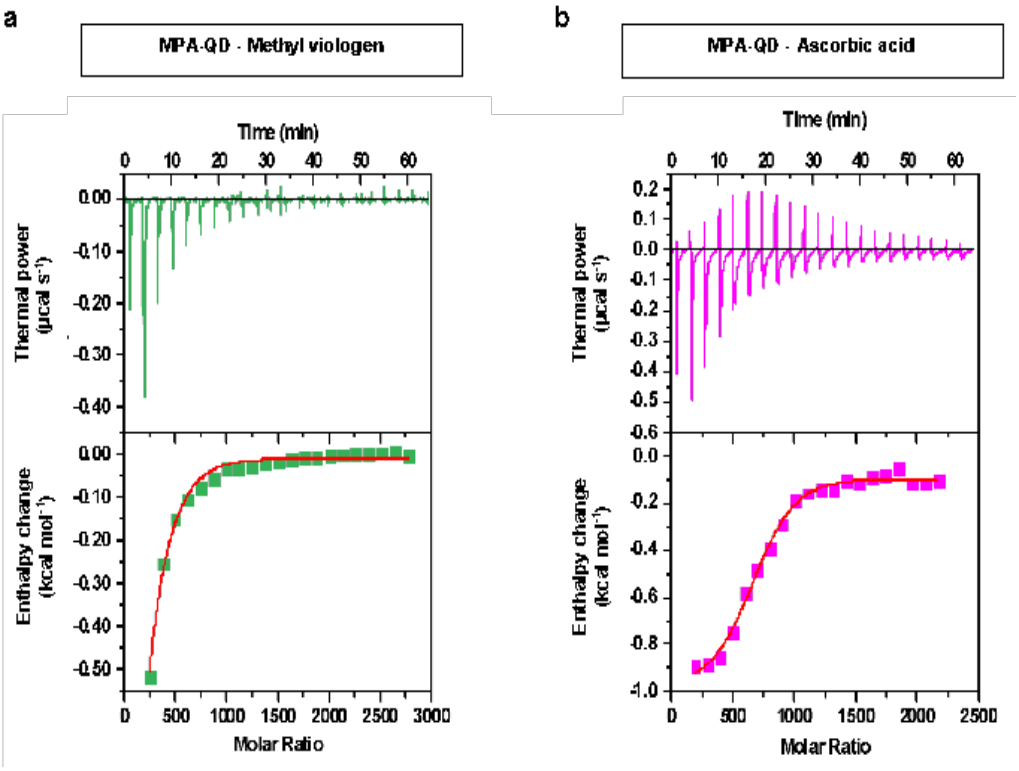

Figure S3.6 : Isothermal titration calorimetry of 3-Mercaptopropionic acid (MPA) coated quantum dots (MPA-QD) with chemical cargoes. Thermograms (top) and binding isotherms (bottom) of MPA-QD interacted with a, methyl viologen, and b, ascorbic acid**.**

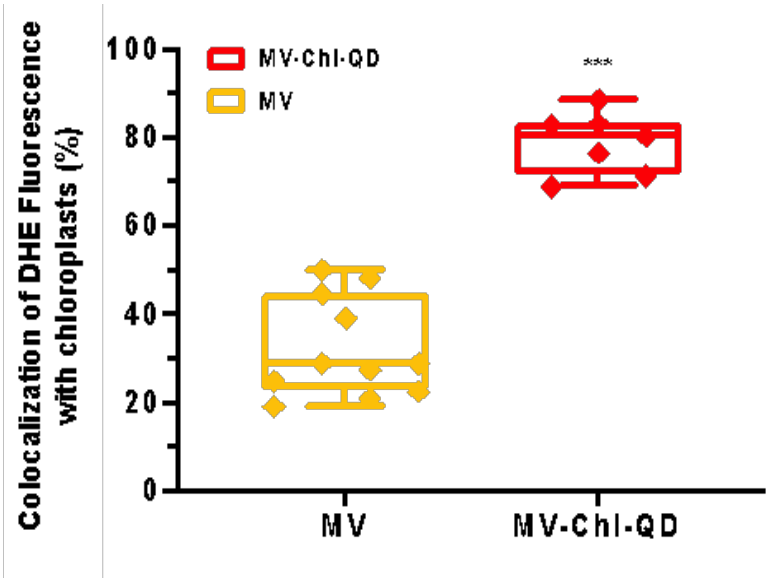

Figure S3.7: Comparison of DHE fluorescence localized within chloroplasts in leaves infused with MV chemical and MV-Chl-QD. *Arabidopsis* leaves treated with Chl-QD loaded with MV and targeted to chloroplasts have significantly higher colocalization rates of DHE (fluorescent dye for superoxide anion) with chloroplasts (78.8 ± 7.0%, Mean ± SD, n = 7) than leaves treated with MV chemical alone (32.2 ± 11.2 %, Mean ± SD, n = 11). DHE fluorescence intensities were measured after a 3 h incubation with Chl-QD and MV treated leaves. Error bars represent standard deviation and boxes represent the interquartile range from the first to the third quartile with squares as the medians and horizontal line with representative treatment color represents mean. Box plots contain diamond symbols for each data point. Statistical comparison was performed by independent samples t-test (two-tailed). *** indicates $P < 0.001$.

Supplementary Table 1: Wide range of chemicals forming inclusion complexes with cyclodextrins.		
Chemicals	**Function**	**Reference**
Allyl isothiocyanate	Antimicrobial	Li et al. 2007
Chlorpyrifos	Insecticide	Lucas-Abellán et al. 2008
Hesperidin, naringenin, naringin	Flavonoids	Ficarra et al. 2002
2-methyl-5-(1-methylethyl) (carvacrol)	Reduce intestinal parasitic infection	Shashank et al. 2018
Nicotinic acid, ascorbic acid	Vitamins and antioxidants, Plant metabolite	Garnero et al 2007, Palomar-Pardavé et al. 2011, Subhadeep et al. 2016,
Methyl viologen	Herbicide	Sivagnanam et al 1992, Ong et al 2003, Mondal et al. 2016
Dihydroxyphenylalanine	Neurotrophic factor	Palomar-Pardavé et al. 2011
Theophylline	Alkaloid treatment of respiratory diseases	Amarr et al. 1996
Amatadine	Antiviral agent	Ai et al. 2012
Beta-Carotene, carotenoids	Vitamin, plant metabolite	Kaur et al. 2016,

Nitrophenol isomers	Pharmaceutical precursor	Zhang et al. 2015
Alkaline phosphatase	Clinical disease indicator	Jia et al. 2010
Napthalene	Insecticide	Harata et al. 1975
Terfenadine	Antihistamine	Choi et al. 2001
Carvedilol	Antioxidant	Wen et al. 2004
Sulindac, Fenoprofen	Non estradiol anti-inflammatory	Diaz et al. 1999
Albendazole	Intestinal parasite treatment	Garcia et al. 2014
Cocaine	Stimulant	Nesnas et al. 2000
MCPA 4-chloro-2-methylphenoxyacetic acid	Herbicide	Garrido et al. 2014
Norflurazon	Herbicide	Villaverde et al. 2004

Figure S3.8 Supplementary video.
https://www.nature.com/articles/s41467-020-15731-w#data-availability

Supplementary Figures: Chapter 4

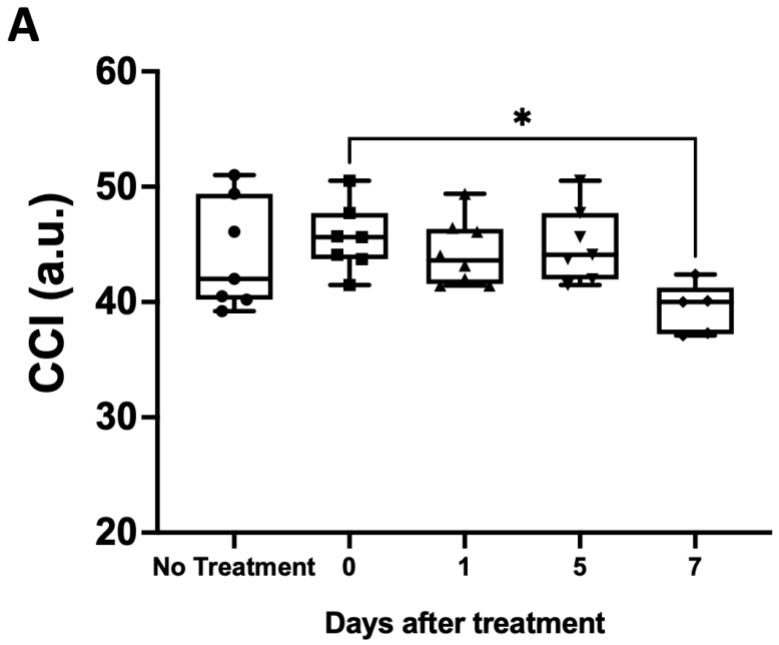

Figure. S4.1. Control measurement for chlorophyll content index **A.** CCI levels were monitored to ensure no significant change in the chlorophyll content index. 3-week-old plants were treated with a buffer and monitored for up to 7 days. At day seven significant differences in chlorophyll were detected. Statistical analysis was performed with a one-way ANOVA-based Tukey's test. n=7-12 ,*$p<0.032$.

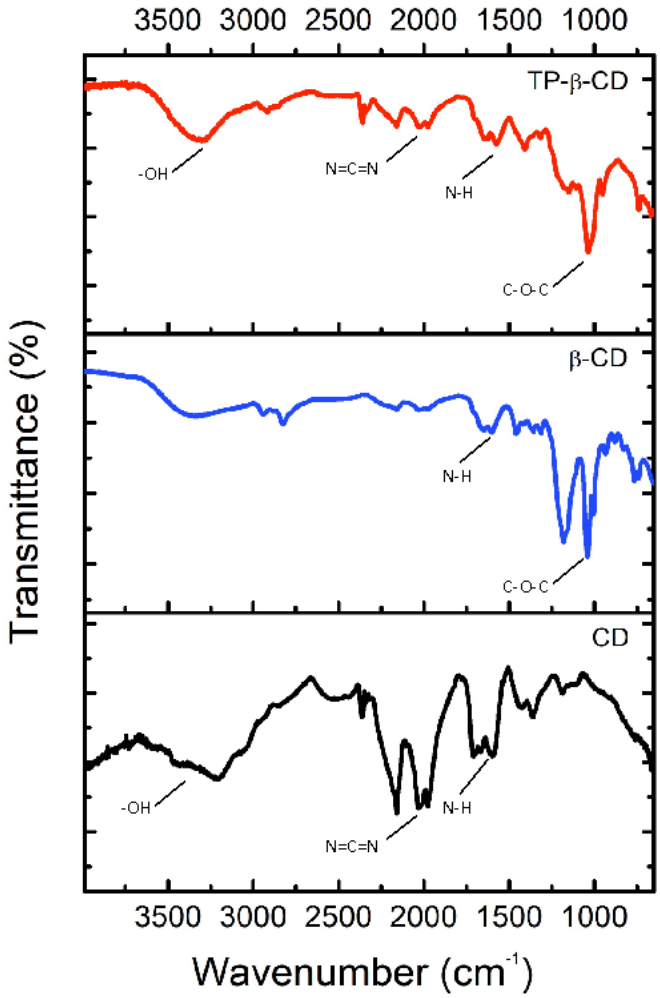

Figure S4.2. FTIR analysis spectra of carbon dots. Top panel shows spectra of core carbon dots, the middle panel shows spectra representing β-CD characteristic bonds, and the bottom panel demonstrates the spectra for TP-β-CD.

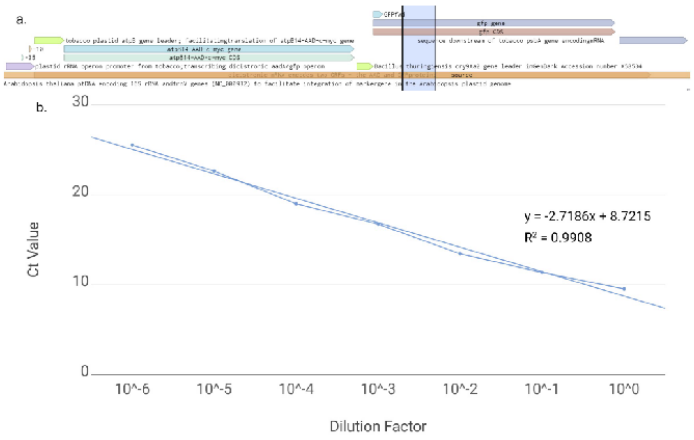

Figure. S4.3 Primer design and efficiency testing for expression analysis. Expression analysis primers were designed with Primer3 version 4.1.0 with the pATV1 sequence from Lu and colleagues (Koressaar and Remm 2007; Yu et al. 2017). Five primer sets were ordered from Integrated DNA Technologies; the primer pair, AtGFP mEA F1 = 5'-ctgtcagtggagagggtgaagg-3', AtGFP mEA R1 = 5'-caagtgttggccaaggaacagg-3', produced a 99 bp amplicon, pictured here within Benchling. b) Serial dilutions of pATV1 plasmid and *Arabidopsis thaliana* cDNA were tested with triplicate RT-qPCR reactions, and the previously mentioned primer pair was calculated with a priming efficiency of E = 1.332, where E = -1+10^(-1/slope), and y = -2.7186x + 8.7215; melt curve analysis confirmed a single amplicon was made (Pfaffl 2001). No-template controls Ct values matched the wildtype *Arabidopsis* cDNA, so off-target binding was deemed not relevant.

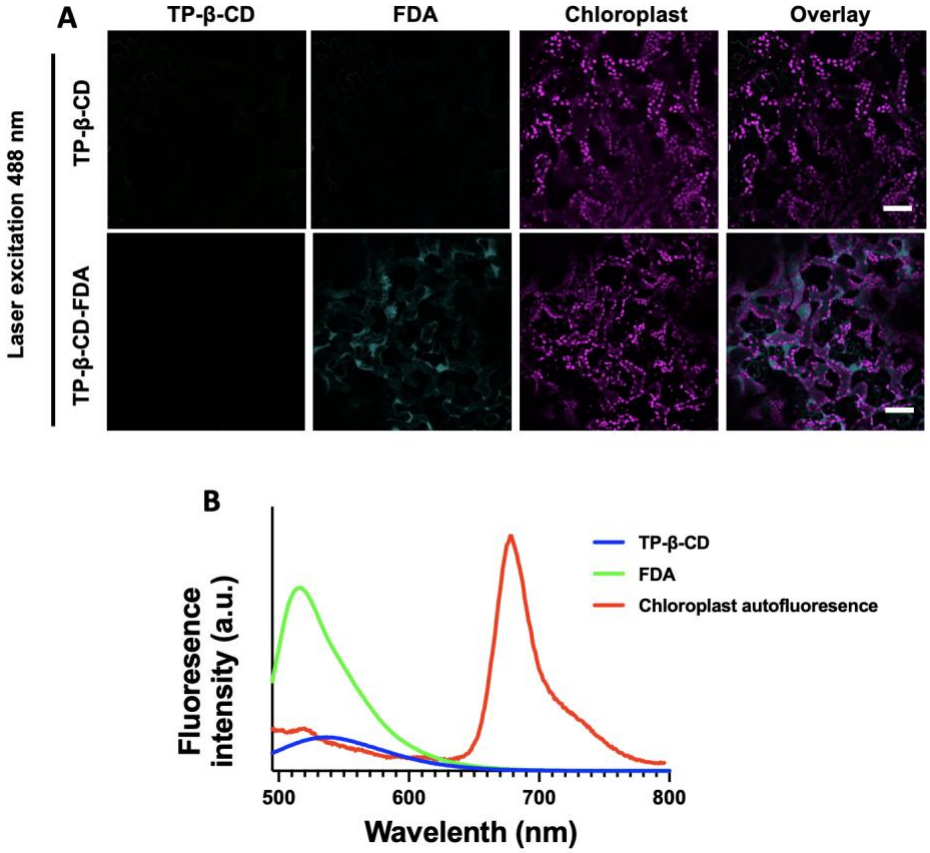

Figure. S4.4 Confocal fluorescence microscopy and fluorescence emission of TP-b-CD cargo delivery experiments. A**,** Images of plant leaves treated with only TP-β-CDs, or FDA-loaded TP-β-CD nanomaterials with laser excitation at 488 nm. Confocal images show minimal emission overlap of TP-β-CD signal with FDA signal under excitation with 488 nm. B. Plot of fluorescence emission spectra of TP-β-CDs, FDA dye, and Chloroplast autofluorescence with laser excitation at 488 nm showing significantly distinct emission detection.

Supplemental Table 1. quantitative RT-qPCR primer list		
Gene name	**Accession #**	**Sequence (5' >3')**
ACTIN 2-F	AT3G18780	CACAATGTTTGGCGGGATTGGTGA
ACTIN 2-R	AT3G18780	TGTACTTCCTTTCCGGTGGAGCAA
AtGFP mEA F1	-	CTGTCAGTGGAGAGGGTGAAGG
AtGFP mEA R1	-	CAAGTGTTGGCCAAGGAACAGG

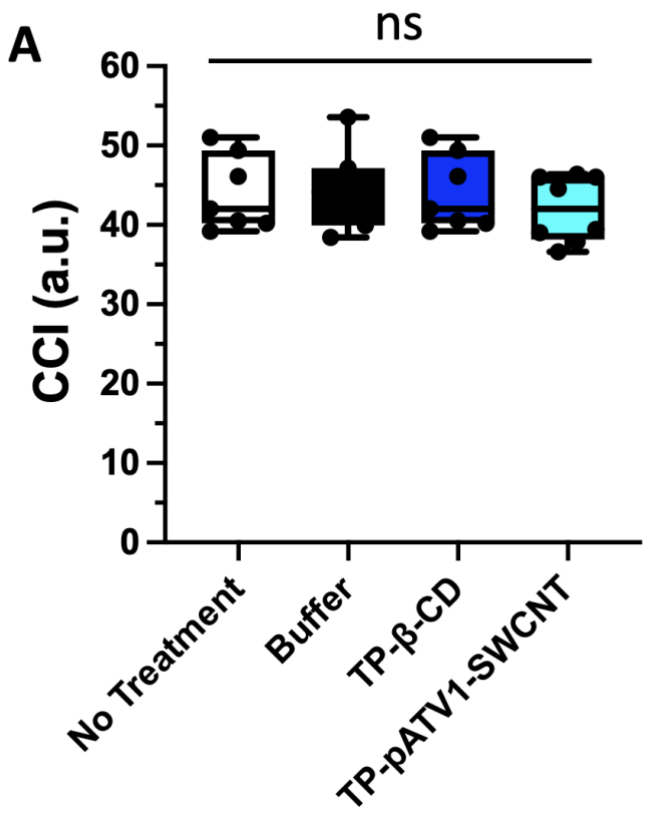

Figure. S4.5. Control measurement for chlorophyll content index A. CCI measurements comparing non-treated plants with buffer and targeted nanostructure treated plants showed no significant difference in CCI values after treatments. Not significant (ns), n=7-12.